8-2018

Complexation of Copper and Iron by Biologically Relevant Sulfur- and Selenium-Containing Small Molecules

Jaime Melissa Murphy
Clemson University, jmbean@g.clemson.edu

COMPLEXATION OF COPPER AND IRON BY BIOLOGICALLY RELEVANT SULFUR- AND SELENIUM-CONTAINING SMALL MOLECULES

A Dissertation
Presented to
the Graduate School of
Clemson University

In Partial Fulfillment
of the Requirements for the Degree
Doctor of Philosophy
Chemistry

---

by
Jaime Melissa Murphy
August 2018

Accepted by:
Julia L. Brumaghim, Committee Chair
Brian A. Powell
William T. Pennington
Andrew G. Tennyson

ABSTRACT

Misregulation of cellular copper and iron can increase labile pools of these metal ions, increasing oxidative damage and leading to neurodegeneration in Wilson's, Parkinson's, and Alzheimer's diseases. Chapter 1 of this dissertation provides an overview of the thermodynamic stability constants of Cu(II), Cu(I), Fe(II), and Fe(III) with weakly binding amino acid ligands, including sulfur- and selenium-containing amino acids and drugs such as methimazole and penicillamine. Understanding these metal-amino-acid interactions provides insight into the role of cellular amino acids as ligands for labile metals.

Stability constants of Cu(II) and Fe(II) with the sulfur- and selenium-containing amino acids methionine, selenomethionine, methylcysteine, methylselenocysteine, and penicillamine are reported in Chapter 2. Potentiometric titration data and characterization by X-ray structural analysis, infrared spectroscopy, and mass spectrometry indicate that the coordination modes and stabilities of thio- and selenoether-amino acids with Cu(II) are similar to glycine and do not involve coordination of the sulfur or selenium atom. Fe(II) stability constants with these amino acids were considerably lower than those with Cu(II), indicating that Fe(II) complexes of these amino acids likely do not form under biological conditions. Fe(II) binding to the thiol penicillamine, used to treat copper overload in Wilson's disease, is significantly more stable, suggesting potential competition with Cu(II) for penicillamine binding.

The thione methimazole is a redox-active, hyperthyroid drug that strongly coordinates copper. Reactions of methimazole with Cu(II) or Cu(I) and the effects of

oxidation state and oxygen availability on the resulting copper-coordinated products were explored (Chapter 3). Dinuclear, polymeric, and mononuclear complexes are obtained that involve redox reactions of both copper and methimazole, some of which result from sulfur elimination from the oxidized methimazole disulfide ligand. An updated mechanism is proposed for this unusual reaction.

Under air-free conditions, treating Cu(I) with methimazole disulfide results in disulfide bond cleavage to afford a copper-bound methimazole complex (Chapter 4). The analogous selenomethimazole complex forms from methimazole diselenide, and copper coordination chemistry of selenomethimazole is even more complex than that of methimazole. The remarkable diversity of copper methimazole and selenomethimazole complexes highlights the redox chemistry of metal and ligand and is highly dependent upon reaction time, solvent, and oxygen availability.

DEDICATION

I dedicate this dissertation to my husband, Philip Murphy, and my children, Colt, Ally, and Julia Murphy for their love and support. Through this process, they have shown patience and loyalty and have sacrificed for my dreams.

ACKNOWLEDGMENTS

I would like to thank my advisor, Julia L. Brumaghim, for taking a chance on a non-traditional student, whose time was limited by family expectations and extended travel time. Not only have I learned a wide variety of air-free synthetic methods and characterization techniques, she has also demonstrated the drive and commitment to excellence that has allowed her to excel in a male-dominated field.

I would also like to thank Brian Powell for his direction and advice in the field of metal stability constant determination and for the level of respect that he shows all of his students. In addition, I would like to thank Colin McMillen for his crystallography expertise, open door, and constant positive feedback.

I would like to thank my family, my church family, and my village that encouraged me to persevere and kept me grounded. Finally, I would like to thank my group members, past and present, without whom research would be a frustrating, unending process.

TABLE OF CONTENTS

Table of Contents (Continued)

Page

Table of Contents (Continued)

Page

LIST OF TABLES

List of Tables (Continued)

Page

List of Tables (Continued)

Page

LIST OF FIGURES

List of Figures (Continued)

Page

List of Figures (Continued)

Page

List of Figures (Continued)

Page

List of Figures (Continued)

Page

List of Figures (Continued)

Page

Page

List of Figures (Continued)

Page

LIST OF SCHEMES

CHAPTER ONE

STABILITY CONSTANTS OF BIOLOGICALLY RELEVANT, REDOX-ACTIVE METALS WITH AMINO ACIDS: THE CHALLENGES OF WEAKLY BINDING LIGANDS

1.1 Introduction

Metal uptake and transfer in biological systems is essential to enzyme function,[1] oxygen and electron transfer,[1] infection control,[2] and redox balance.[3] Biological mechanisms for metal transfer and redox activity are often poorly understood due to the complexities of biological environments and a limited understanding of the quantities and localization of high-affinity and weakly binding ligands present in cells. For example, mis-regulation of copper and iron homeostasis is implicated in initiation and/or progression of Parkinson's and Alzheimer's diseases,[4,5] but the role of weakly chelating biomolecules in these diseases has not been addressed. It is often assumed that non-protein-bound metal ions are coordinated to low-molecular-weight oxygen- and nitrogen-containing ligands, but the nature of these ligands and how these interactions affect cellular processes is unknown.

Determination of *in vitro* stability constants is used to predict equilibria that may occur in more complex systems[6-12] and to model speciation in biological fluids.[7] The goals of this review are to 1) examine weakly coordinating ligand interaction with copper and iron under biological conditions, with an emphasis on sulfur and selenium amino acids, 2) examine the methods and method limitations for determination of stability constants describing complexation of redox-active metal ions with weakly binding ligands, and 3) emphasize specific needs for methods development and further research on these systems.

A comprehensive discussion of stability constants for weakly binding ligands present in significant quantities in the cell is lacking and is presented in this review. The Smith and Martell database (NIST v.46)[8] is a large set of externally evaluated stability constants that involves some of the iron and copper complexes of interest to this review. However, the database is no longer being critically analyzed and curated. Specifically, this review focuses on the stability constants of amino acids with the biologically relevant, redox-active metals copper and iron. Copper and iron are of particular interest due to their availability in the cell, potential for chelation by wide variety of ligands, and known contribution to reactive oxygen species generation and oxidative damage. Ligand coordination to these metal ions can be difficult to assess, due to their variable oxidation states and coordination geometries.

This review places special emphasis on sulfur and selenium amino acids, since coordination of these ligands with copper and iron is of particular biological interest, and thiol and thioether coordination can stabilize the reduced forms of copper and iron.[6-8] A range of stability constant determination methods including potentiometric, spectrophotometric, and voltammetric analyses have been used to quantify formation of iron and copper complexes with amino acids under biologically relevant conditions. The review discusses and identifies the limitations of each method as it pertains to each metal and oxidation state and will evaluate the potential impact of amino acids on biologically relevant metal interactions by modeling of more complex systems.

1.2 Cellular Redox-Active Metal Ions and Amino Acids

Copper, iron, zinc, manganese, and cobalt are essential redox-active metal ions in biological systems that play crucial biochemical roles as cofactors in enzymes. Iron and copper of are particular interest due to their stability in multiple oxidation states which are often essential to biological processes,[9,10] but this activity makes assessing the validity of *in vitro* ligand coordination difficult. The association and distribution of copper and iron, not only within the highly selective binding pockets of proteins, but also with more weakly binding ligands such as single amino acids has implications for the uptake, transfer, and redox states of these metal ions throughout the cell.

Complex formation is dependent on amino acid concentration, metal concentration, and the thermodynamic driving forces controlling complex formation. In human plasma, free amino acid concentrations can be divided into three categories: high abundance (200-500 μM), low abundance (10-200 μM), and trace abundance (less than 10 μM).[11-13] Alanine, glutamine, glycine, leucine, lysine, proline, threonine, and valine fall into the high abundance category. With the exception of threonine, these amino acids have non-polar or positively charged side chains at pH 7, which limit their cation binding abilities to bidentate binding of the amine nitrogen and carboxylate oxygen groups. Arginine, aspartic acid, asparagine, cysteine, glutamic acid, histidine, isoleucine, serine, methionine, phenylalanine, tryptophan, and tyrosine fall into the low abundance category, and most of these have polar or negatively charged side chains at pH 7 that may allow tridentate coordination through the amine, carboxylate, and side chain groups. Trace-level amino acids include methylcysteine and the selenoamino acids, selenmethionine,

selenomethylcysteine, and selenocysteine. Methylcysteine concentrations in urine are reported to be 0.2-5 μM;[14] plasma or cellular concentrations are not reported. Selenoamino acid concentrations are also not reported, but total selenium concentration in human plasma averages 1.5-1.6 μM, with an estimated 90% incorporated into selenoprotein as selenocysteine or selenomethionine.[15] Although the abundance of selenoamino acids is extremely low, soft selenoether or selenolate groups may strongly interact with softer metals such Cu(I) and Fe(II) according to the Pearson hard-soft acid-base theory.

Penicillamine is an amino acid not naturally found in cells, but it bears close structural resemblance to cysteine. It is a highly effective copper chelator used routinely to treat Wilson's disease.[16,17] With a typical dosage of 750 mg/day, serum penicillamine levels can reach 100 μM.[18] Although it is known to bind copper, it may also influence iron homeostasis.[19,20]

Stability constant determination is discussed with Cu(I) and Cu(II) and Fe(II) and Fe(III) as separate ions due to their unique cellular roles and significantly different coordination characteristics. Each of these metal ions serves essential biological roles in electron transfer, oxygen transport, and catalysis.[21] Iron and copper are two of the most abundant transition metal ions in cells, and control of these potentially toxic ions is heavily regulated by metallochaperones and storage proteins such as ferritin.[22,23] Total copper concentrations are in the range of 10-25 μM in human serum[24] and up to 100 μM in human brain tissue.[25] Labile (non-protein-bound) copper pools are also identified in cells, primarily as Cu(I).[26] Cellular concentrations of labile copper are not quantified, but significant recent strides have been made in the development of methods to detect this

labile copper.[27-29]

Total iron concentrations are 20 to 30 μM in human serum,[30] but are approximately 300 times higher in human liver (6315 μM).[31] Jhurry and coworkers quantified labile iron concentrations in the cytosol of human cells at 30 μM and in mitochondria at 210 μM.[32] Mis-regulation of copper and iron homeostasis can lead to increased oxidative damage and protein misfolding or aggregation and is implicated in the development of neurodegenerative diseases such as Parkinson's and Alzheimer's diseases.[3,33-36] In addition, redox cycling between Cu(I) and Cu(II) that is critical for the function of most copper enzymes is often controlled by amino acid coordination and protonation state.[37-39] In conjunction with reliable and complete stability constant determination and species identification, as well as the biological concentrations of the amino acids and metal ions, the extent of biological amino-acid-metal complex formation under equilibrium conditions can be predicted. The work in this chapter was completed in collaboration with Dr. Brian A. Powell of Clemson University.

1.3 Amino Acids as Weakly Binding Ligands

Biological regulation of metal ions is dominated by strong chelation in highly specific binding pockets of proteins, often contributing to protein structural support and/or enzyme activation. It is more difficult to ascertain the role of metal-coordinating, small molecules, particularly at high metal concentrations resulting from loss of homeostasis.[26,40-44] These small, coordinating molecules may play a number of roles including: 1) cellular signaling, such as various hormones, 2) molecules required for

metabolism, such as sugars, 3) molecules needed for anabolism, such as amino acids or lipids, and 4) exogenous molecules, such as drugs, antioxidants, or toxins. Entire databases in bioinformatics and cheminformatics are committed to sorting, analyzing, and predicting chemical properties and biomolecular pathways for these types of coordinating small molecules.[45] We focus on the coordination and stability of amino-acid-metal complexes, since amino acids coordinate strongly enough to Cu(I)/Cu(II) and Fe(II)/Fe(III) to infer that these complexes may form within the cell.[46]

Potentially Bidentate Amino Acids

Because amino acids have varied potential metal-binding modes, discussion of amino acid coordination will be grouped according to their predicted denticity. Most amino acids only have the capability for bidentate coordination, through the α-carboxylate oxygen and α-amine nitrogen atoms, forming a five-membered chelate ring with the metal ion (Figure 1.1). Since glycine is the simplest amino acid and primarily binds metals with bidentate coordination, this type of bidentate metal-amino-acid coordination is often referred as glycine-like binding.[47]

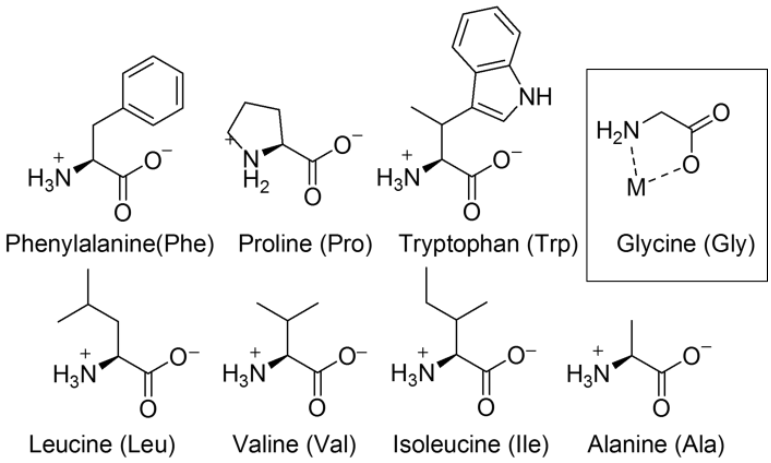

Figure 1.1. Amino acids with non-coordinating aliphatic or aromatic side chains that have the capability to coordinate metal ions in a bidentate fashion. In box: complex showing bidentate binding to a metal ion (M) through the carboxylate oxygen and amine nitrogen, using glycine as an example.

Potentially Tridentate Amino Acids

Amino acids with polar or charged side chains may have the capability to bind in a tridentate fashion (Figure 1.2), but often do not achieve full tridentate coordination. Alcohol, amine, and carboxylate groups all can potentially coordinate metals, but the influence of thermodynamic factors such as pK_a, steric strain, and entropy cost can lessen or prevent metal interactions. Predicting the likelihood of an amino acid binding in a tridentate fashion is not straightforward. For example, the polar side chains of arginine and lysine are positively charged at pH 7 (Figure 1.2), with pK_a values above 10 properties that inhibit metal binding.

Perhaps the best measure of the ability of an amino acid side chain to bind copper and iron is to consider the amino acid residues most often found in metalloprotein binding pockets. In a 2007 survey of the Protein Database, the three amino acids most commonly found in copper metalloprotein binding pockets were histidine, cysteine, and

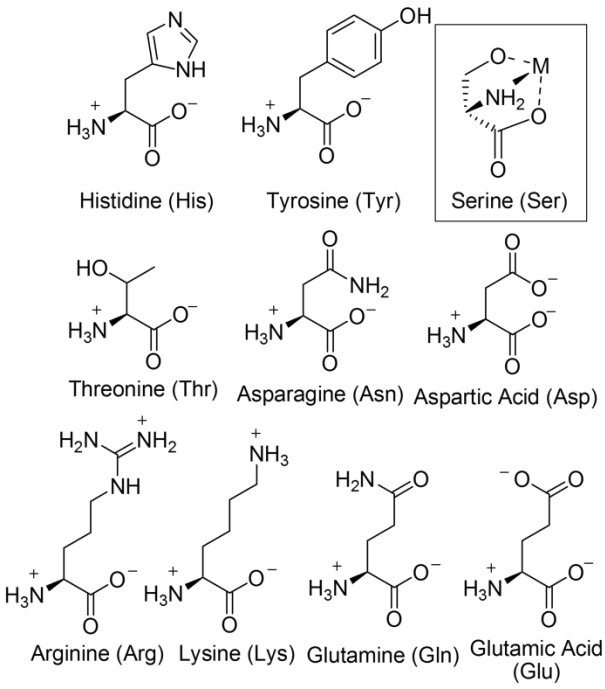

Figure 1.2. Amino acids with polar or charged side chains that have the capability to bind metals in a tridentate fashion. In box: complex showing potential tridentate binding to a metal ion (M) through the α-carboxylate oxygen and α-amine nitrogen as well as a side chain atom, using binding to the oxygen atom of the deprotonated alcohol group in serine as an example.

methionine, respectively.[48] Aspartic acid, glutamic acid, serine, threonine, glutamine, and asparagine also bind copper but much less commonly. For iron metalloproteins, histidine, glutamic acid, cysteine, aspartic acid, methionine, and tyrosine were the primary iron-binding amino acids, with serine and asparagine as minor players. Based these reports, it is reasonable to assume that these free amino acids also would potentially bind copper and iron. Higher stability constants are expected for metal-amino acid complexes with tridentate binding compared to those with only bindentate coordination, since greater chelation confers higher thermodynamic stability.

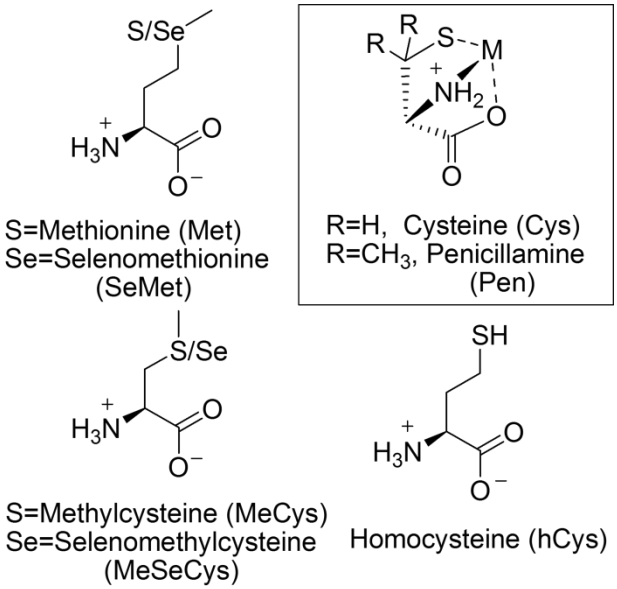

Figure 1.3. Amino acids with sulfur- or selenium-containing side chains; all have the capability to bind metals in a tridentate fashion. In box: complex showing potential tridentate binding to a metal ion (M) through the α-carboxylate oxygen and α-amine nitrogen atoms as well as a side chain atom, using deprotonated sulfur in cysteine or penicillamine as an example

Sulfur- and Selenium-Containing Amino Acids

In this review, special emphasis is given to iron and copper interactions with sulfur- and selenium-containing amino acids, including penicillamine, methylcysteine, and selenomethylcysteine (Figure 1.3). These amino acids not only show preferential binding to soft and borderline metal ions, such as Cu(I), Cu(II), and Fe(II), but they also influence redox activity of these metals.[49] Metal-sulfur and -selenium redox interactions can make it difficult to clearly interpret stability constant data for these systems, especially for thiol/selenol-containing amino acids with reduced metal ions.[50]

Because of the S/Se atom in the side chain, these amino acids can potentially act as tridentate chelators to metal ions. Although selenoamino acids are less prevalent in the cell than their sulfur analogs, metal-selenocysteine binding is required for the activity of

enzymes such as NiFeSe hydrogenases.[51] Selenoether-containing amino acids are not known to have primary metal-binding roles in metalloproteins. Selenomethionine can substitute indiscriminately for methionine when Se levels are high,[52] and has been well-studied for its ability to prevent metal-mediated oxidative damage.[53]

1.4 Comparing Apples to Apples: Defining Parameters of Stability Constant Determination

The sheer volume of stability constant data for transition metal ions with amino acids is overwhelming and has been the subject of databases[54] and extensive reviews.[47,50,55-57] Previous reviewers[50,58] noted that the wide range and seemingly inconsistent reports of these stability constants is attributable to the sensitivity of these systems to the specific conditions under which determinations are performed. Even when using the same analytical method, variables including the nature and concentration of supporting electrolyte, pH range, temperature, and solvent significantly affect the resulting stability constants. Whenever possible in this review, stability constants were chosen that represent the most consistent results, both with each other and with biological conditions. Thus, typical experimental conditions are 25-37 ˚C with 0.1-3.0 M supporting electrolyte. If limited data are available, the best or only reported metal-amino-acid stability constants are provided.

Clearly defining equilibrium constants is crucial to correctly interpreting stability constant data and identifying species formed across various analyses, especially for amino acids where charges can differ. In this review, amino acids are divided into three categories:

1) those likely to bind as bidentate ligands, composed of aliphatic or aromatic amino acids with nonpolar side chains (Figure 1.1), 2) those that can potentially bind as tridentate ligands, composed of amino acids with polar or charged side chains (Figure 1.2), and 3) sulfur- and selenium-containing amino acids (Figure 1.3). Since the sulfur and selenium-containing amino acids have greater potential for redox activity compared to other amino acids, especially upon iron or copper coordination, it is useful to treat these amino acids separately.

For all the amino acids, proton association constants can be expressed as stepwise protonation constants shown in equilibrium expressions 1 and 2.

$H^+ + L^- \rightleftharpoons HL$ protonation of $–NH_2$ group (1)

$H^+ + HL \rightleftharpoons H_2L^+$ protonation of $–COO^-$ group (2)

The equilibrium constant K_{HL} relates to the first protonation (equation 1) according to equation 3 and the equilibrium constant K_{H_2L} relates to the second protonation (equation 2) according to equation 4.

$$K_{HL} = \frac{[HL]}{[L^-][H^+]} \quad (3) \qquad K_{H_2L} = \frac{[H_2L^+]}{[HL][H^+]} \quad (4)$$

Equilibrium constants 3 and 4 apply for all amino acids that do not have side chains that can protonate or deprotonate, such as those shown in Figure 1.1 and the thioethers shown in Figure 1.3. The remaining amino acids have ionizable side chains that must be accounted for in additional equilibrium expressions.

For amino acids that are positively charged at pH 7, such as lysine, arginine, and histidine, the protonation equilibrium reactions 5, 6, and 7 apply.

$H^+ + L^- \rightleftharpoons HL$ protonation of $-NH_2$ group (5)

$H^+ + HL \rightleftharpoons H_2L^+$ protonation of side chain (6)

$H^+ + H_2L^+ \rightleftharpoons H_3L^{2+}$ protonation of $-COO^-$ group (7)

Thus, for protonation reactions of amino acids with ionizable side chains, equilibrium constants (3) and (4) apply, along with the additional equilibrium constant K_{H_3L} (8).

$$K_{H_3L} = \frac{[H_3L^{2+}]}{[H_2L^+][H^+]} \quad (8)$$

For amino acids that are negatively charged at pH = 8, including glutamic acid, aspartic acid, cysteine, homocysteine, and penicillamine, the representative equilibria are 9, 10, and 11.

$H^+ + L^{2-} \rightleftharpoons HL^-$ protonation of $-NH_2$ group (9)

$H^+ + HL^- \rightleftharpoons H_2L$ protonation of side chain (10)

$H^+ + H_2L \rightleftharpoons H_3L^+$ protonation of $-COO^-$ group (11)

The related association constants are similar to those defined in equations 3, 4, and 8, although it is important to note that the charge on each species is different.

Association constants for metal-amino-acid coordination are defined in a similar manner. Because the charge of the metal ions (M) studied varies from +1 to +3 and the charges of the amino acids (L) also vary, charges on the species are typically not indicated in these general equilibrium expressions. When discussing specific species, charges will be shown whenever possible. Equilibrium equations for mono- and bis-coordinated complexes as well as their formation constant (β) expressions are represented by equations 12 and 13, respectively. The formation constant β is related to the thermodynamic stability

of a complex, the association constant *K*, for each stepwise addition of a new ligand. At lower pH, the side chain of the amino acid may or may not be protonated, as shown in equation 14 and 12, respectively. At higher pH, some metal-amino acid systems coordinate a hydroxyl ligand, or deprotonate a coordinated water molecule, resulting in the ternary metal-ligand-hydroxide species MLOH (15).

$$M + L \rightleftharpoons ML \qquad \beta_{ML} = \frac{[ML]}{[L][M]} \qquad (12)$$

$$M + 2\,L \rightleftharpoons ML_2 \qquad \beta_{ML2} = \frac{[ML_2]}{[L]^2[M]} \qquad (13)$$

$$M + HL \rightleftharpoons MLH \qquad \beta_{MLH} = \frac{[ML]}{[H][ML]} \qquad (14)$$

$$ML + OH \rightleftharpoons MLOH \qquad \beta_{MLOH} = \frac{[ML]}{[OH][ML]} \qquad (15)$$

The thermodynamic parameter for each stepwise formation constant, *K* can then be related to the standard free energy change (ΔG°) at constant pressure (16). The total enthalpy change ΔH^0 can be determined from the temperature dependence of *K* according to the van't Hoff equation (17). Although potentiometry is commonly used to determine metal-ligand formation constants, calorimetry is often used for enthalpy determinations, since potentiometric measurements may not be stable across the full temperature range needed to calculate a free energy change. The thermodynamic parameters free energy and enthalpy are not discussed in detail in this review.

$$\Delta G^{\circ} = -RT\ln K \quad (16)$$

$$\frac{d(\ln K)}{dT} = \frac{\Delta H^{\circ}}{RT^2} \quad (17)$$

To determine stability constants for metal-amino-acid complexes, any method can be used that can actively measure the formation and elimination of the species present, and books dedicated to methods development and analysis have been published.[59-61] General problems associated with determining metal-amino-acid stability constants for all metals are thoroughly reviewed,[47,56,62-65] although these reviews are data-heavy and do not include new methods development. This review will focus specifically on the best methods for amino acid stability constant determination with Cu(I), Cu(II), Fe(II) and Fe(III), and the particular experimental limitations associated with these ions. Common methods are introduced here, and less common methods are discussed in each metal-specific section as relevant.

The three most common methods for stability constant determination are potentiometric, voltammetric, and spectrophotometric titrations. Potentiometric analyses are the most frequently used method for amino acid-metal binding constant determinations. The precision and stability of this method makes it the ideal choice of method, when conditions allow, and permits detection of minor species when coupled with the computational abilities of modeling software.[47,50,57,66] While many of these species are inconsequential under biologically relevant titration conditions for simple systems, incorporation of these species into studies of more complex systems is imperative and can

have significant effects, since their formation may influence formation of competitive species.[67]

Potentiometric analyses are not always an option, and independent analyses are helpful, and in some cases necessary, in confirming complex speciation. Voltammetric or polargraphic techniques permit measurements at a constant pH for pH-sensitive systems.[68] Often the resulting data are not as precise or as consistent as potentiometric methods, since only changes to the metal ion are typically measured. Spectrophotometric analyses work well with metal ions, ligands, and/or complexes that absorb in UV or visible wavelengths, but these methods do not indicate binding mode of multidentate interactions. Development of methods such as paper electrophoresis, involving solvent-extraction of species, is a growing area. Table 1.1 provides an overview of the most common methods and their advantages and limitations.

For amino-acid-metal complex determinations, potentiometry is the most common method utilized, because the uptake and release of protons can be measured precisely.[47,56,63-65,69-71] Electrode stability limits the analysis range, and data can be questionable at pH extremes (typically pH < 2 and pH > 12).[47,65] Although robust and precise, potentiometric analyses are limited to ligands or hydrolyzed metals with protons that associate and dissociate in the pH range investigated and can be limited by ligand and/or complex solubility across this pH range.

Table 1.1. Advantages and limitations of stability constant determination methods

Method	Advantages	Limitations
Potentiometric titration	High precision High accuracy	Ligands must protonate/deprotonate Species must be soluble across wide pH range Disproportionation issues with Cu(I)
		Curve fitting technique with no direct measurement of the metal or metal-ligand complex
Spectrophotometric titration	Can be run at narrow pH Direct probe of metal and metal-ligand complex	Either metal or ligand must be UV-vis active
Electrophoresis (paper or solution)	Simple detection Easy to identify species charges	Low precision Temperature and oxygen control more difficult Conditions differ from solution determination
Redox titration	Redox-active metals can be controlled	Species identification must be confirmed using independent methods
Solubility	Low solubility systems such as Fe(III)	Lengthy experiments due to slow equilibria between solid and solution

The IUPAC stability constant database contains a comprehensive list of all stability constant and associated thermodynamic data available for metal-amino-acid stability constant data reported up through 1989.[54] Stability constants for most of the amino acids with a variety of metals are available for a wide range of temperatures and supporting electrolyte concentrations. Various reviews present a more selective list of stability constants of metals with amino acids up until 1997.[47,50,55-57] While the database and reviews are comprehensive for the time periods indicated, they are cumbersome in the quantity of analyses given for some metals such as Cu(II) and reflect the lack of data for other metals such as Cu(I). Our analysis draws on these data and also comprehensively covers iron and copper data with amino acids up until early 2018.

1.5 The Gold Standard: Proof of Speciation

Unambiguous identification of the thermodynamically stable species present in solution is required to understand the solution equilibria of a metal-ligand complex.[59,60] For potentiometric determinations, glass electrodes are used to track the change in potential as acid/base titrations are performed. Before the advent of modeling programs, best fit analyses were determined for the most likely species formed in the given system using graphical methods documented by Bjerrnum[72,73] and Fronaeus.[74] More recently, programs such as SCOGS,[75] HYSS,[76] HYPERQUAD,[77] and MINIQUAD[78] have made modeling and model-matching much easier to perform and have allowed for more precise data analysis. As a result of computational modeling methods and perhaps a more comprehensive understanding of solution equilibria for metal-amino acid complexes, the number of

identified species in recent reports has expanded. While incorporation of additional species certainly improves model fit to the data, due to their low concentration and limited influence on metal complex formation, the existence of such species are often difficult to confirm from titration data alone. For example, minor species such as complexes with protonated, unbound side chains may not play an active role in metal binding, but they may contribute to buffering in the cell.[50,79] Thus, the gold standard for species determination should incorporate secondary methods to unambiguously identify these minor species. In this review, we describe the most consistent reported species, particularly emphasizing investigations that have demonstrated a high level of control of experimental conditions or used multiple methods of analysis to independently confirm the identified species.

1.6 Stability Constants of Non-Sulfur and -Selenium-Containing Amino Acids with Cu(II)

Cu(II) Complexes of Potentially Bidentate Amino Acids

Whether or not labile Cu(II) exists in the cell, Cu(II) plays a major role in organisms since activity and stability of Cu(II) metalloproteins depend on copper-amino acid interactions.[1] Compared to Cu(I), Fe(II), and Fe(III), Cu(II) is the most chemically well-behaved ion for analytical measurements. Most Cu(II) salts are soluble in aqueous solution and are not sensitive to air oxidation. It is not surprising, therefore, that hundreds of analyses to determine Cu(II)-amino-acid stability constants are reported[47,50,56,62-64] using a wide variety of methods: polarography,[80] spectrophotometry,[81] circular dichroism,[82] optical rotary dispersion,[83] and electrophoresis.[84,85] Although solubility of Cu(II)-amino

acid complexes with hydrophobic side chains is limited in the basic pH range, this issue is not always discussed in published reports.

Table 1.2 shows a summary of the stability constants for Cu(II) for amino acids with non-coordinating side chains that are limited to bidentate coordination through the carboxylate oxygen and amine nitrogen of the amino acid (Figure 1.1). Due to the plethora of available data for Cu(II)-amino-acid stability constants,[54] the selected stability constants in Table 1.2 are those "recommended" in previous reviews due to their data quality and reproducibility,[47,50,55-57,66] where possible. Beyond that, selected constants were 1) reported with errors, 2) determined within 25-37 ˚C, and 3) were conducted in a constant ionic strength medium (range 0.1-3 M).[86]

Analysis of Cu(II)-amino-acid stability constants with bidentate-coordinating amino acids (Figure 1.1) is fairly straightforward and consistent. Coordination is typically through the α-carboxylate oxygen and α-amine for both ML and ML_2 species and is supported by solid-state structures. The structure of $Cu(Gly)_2$, a representative bidentate-ML_2 species, is square planar with bidentate glycine ligands creating two five-membered, equatorial chelate rings around Cu(II) (Figure 1.4A).[87] The axial positions are vacant, with occasional coordination of water molecules or supporting electrolyte, such as in $Cu(Gly_2)(H_2O)$ (Figure 1.4B).[87-90]

No trend in stability constants relating to side chain hydrophobicity is observed for the aliphatic amino acids. Potential intermolecular interactions of aromatic side chains (e.g., phenylalanine) also do not impart added stability to the complexes, since all of the

Table 1.2. Stability constants for Cu(II) and Cu(I) with potentially bidentate amino acids

Ligand	ML ($\log \beta_{ML}$)[a]	ML_2 ($\log \beta_{ML2}$)[b]	Temp. (°C)	Ionic Strength (M)	Method	Ref.
Stability Constants for Cu(II)						
Alanine	8.17(3)	14.94(5)	30	0.1 KNO_3	Potentiometry	91
Glycine	8.07(2)	14.86(3)	30	0.1 $NaClO_4$	Potentiometry	92
Isoleucine	8.50(6)	15.79(8)	25	0.1 $NaNO_3$	Potentiometry	93
Leucine	8.276(1)	15.174(1)	25	0.1 KNO_3	Potentiometry	62
Phenylalanine	7.93(1)	14.83(1)	25	0.1 KNO_3	Potentiometry	62
Proline	8.60(3)[c]	15.09(7)[c]	25	0.1 $NaNO_3$	Potentiometry	94
Tryptophan	8.02(1)	15.56(1)	25	0.1 KNO_3	Potentiometry	62
Valine	8.05(2)	14.91(2)	30	0.1 $NaClO_4$	Potentiometry	95
Stability Constants for Cu(I)						
Alanine	9.6[c]		25	0.3 K_2SO_4	Redox	96
Glycine	10.0[c]		25	0.3 K_2SO_4	Redox	96

[a] $\log \beta_{ML} = [M][L]/[ML]$ [b] $\log \beta_{ML2} = [M][L]^2/[ML_2]$ [c] Authors also reported the minor species Cu(Pro)(OH) ($\log \beta = 1.29(4)$) and $[Cu(Pro)(OH)_2]^-$ ($\log \beta = -8.58(3)$).

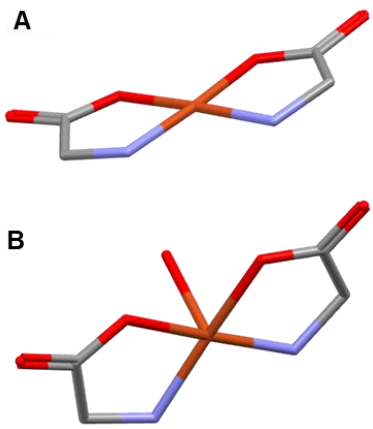

Figure 1.4. A) Crystal structure diagram for $Cu(Gly)_2$ showing carboxylate and amine coordination with square planar geometry around the central Cu(II) ion.[87] B) Crystal structure diagram of $Cu(Gly)_2(H_2O)$ also showing carboxylate and amine coordination in the equatorial position, but with a water molecule coordinated in the axial position of the square pyramidal geometry.[88,90] The Cu(II) ion is shown in orange, oxygen atoms are red, carbon atoms are grey, and nitrogen atoms are blue. Hydrogen atoms are not shown.

Cu(II) stability constants with bidentate amino acids are within one log unit of each other (Table 1.1). This stability constant uniformity indicates glycine-like ML and ML_2 complex formation for all these amino acids with Cu(II).

Minor species have also been identified for these relatively simple systems. Blais and coworkers[67] claim to have identified $[Cu(HVal)]^{2+}$ and $[Cu(HVal)(Val)]^{+}$ as well as $[Cu(HGly)]^{2+}$, $[Cu(HGly)(Gly)]^{+}$, and $[Cu(HGly)_2]^{3+}$ in their Val and Gly analyses, respectively. Because the side chains of Val and Gly cannot protonate, it can be assumed that these species arise from amine protonation and monodentate binding of the metal through the carboxylate oxygen. All of these species form below pH 3 and represent only a very small change in buffering of the system. While these species are chemically reasonable in terms of competition between a high proton concentration and Cu(II) for amino acid binding, they are formed at the accuracy limits of potentiometric measurements when formed at low pH and remain to be independently confirmed.

On the other end of the pH range, species with hydroxyl coordination, such as MLOH and ML_2OH, are reasonable and expected, especially since water is known to coordinate in the axial position in the solid state (Figure 1.4B).[87,97] However, Cu(II)-amino acid complexes typically precipitate in the alkaline range (pH > 9). Arena and coworkers note that signal drift can occur in potentiometric measurements at more basic pH when precipitation is seeding,[98] and this signal drift can be misinterpreted as new species formation.[99] Thus, distinguishing between signal drift and minor hydroxyl species formation at basic pH is a core issue in determining accurate speciation.

Analyses across methods also are consistent for Cu(II) titrations with potentially bidentate amino acids, a promising sign for methods development, particularly for the determination of stability constants for ligands that may not have the ionizable protons needed for potentiometric analysis. Paper electrophoresis is an excellent method for separating species, although it is limited in precision and may not accurately represent "solution" equilibria. For potentiometric and paper electrophoresis results for the Cu(II)-alanine system, the paper electrophoresis stability constants reported by Jokl[100] are slightly higher: 8.5 and 15.2 for the $[Cu(Ala)]^+$ and $Cu(Ala)_2$ species (no errors are reported), respectively, compared to 8.17(3) and 14.94(5) using potentiometric methods.[91] Singh's $[Cu(Val)]^+$ and $Cu(Val)_2$ electrophoresis determinations[84] are consistent with or slightly lower than potentiometrically determined values (8.02 and 14.62, respectively, compared to 8.05(2) and 14.91(2), respectively).[95] Separately, Tewari[101] reported paper electrophoresis stability constants for the Cu(II)-isoleucine system: 8.41(7) for $[Cu(Ile)]^+$ and 14.84(3) for $Cu(Ile)_2$, values consistent with or slightly lower than the potentiometric

results of 8.50(6) and 15.79(8), respectively.[93] While this is not a comprehensive list of paper electrophoresis determinations, these representative data demonstrate method viability. Indications of the charge of species due to electrophoretic movement is an advantage of electrophoresis. If the detection limits are suitable, electrophoresis may be a method worth exploring for establishing existence of minor species.

Spectrophotometric analyses also are an option for spectrophotometrically active metals such as Cu(II) or ligands with aromatic groups that absorb or fluoresce in the UV or visible spectrum. However, concentrations required for species detection in the UV-visible range can be a factor of ten higher for spectrophotometric analyses compared to the precision determination of protons in potentiometric analyses. Effects of metal-coordinating solvents or supporting electrolyte can also contribute to error in spectrophotometric methods. For example, a spectrophotometric analysis of the Cu(II)-leucine system by Bretton[102] with no supporting electrolyte results in considerably higher stability constants than those obtained by potentiometric analyses with a supporting electrolyte of 0.1 M $NaNO_3$ by Ivicic (Table 1.1).[93] Other optical methods such as circular dichroism and optical rotary dispersion have also been used to determine stability constants with Cu(II), with results similar to those from potentiometric analyses, but it can be difficult to identify minor species using these methods.[82,83] Perhaps the most compelling use of spectrophotometric methods to determine stability constants is in conjunction with potentiometric methods, since species identification can be supported by two independent methods. This combination is demonstrated by Davis[103] in determining the stability constants for Cu(II)-valine-pyridoxal complexes.

Stability constants of Cu(II) with aliphatic amino acids are one of the most widely studied of all metal-amino-acid combinations. The relative stability of this metal ion with non-redox active ligands makes the resulting data easy to interpret, as long as the method is reliable in collecting quantifiable changes to the system, whether the release of protons or spectral changes. As a result, these systems provide the best arena for development of methods to examine metal coordination with weakly binding ligands.

Cu(II) Complexes of Potentially Tridentate Amino Acids

Amino acids with polar side chains, including serine, histidine, threonine, tyrosine, aspartic acid, glutamic acid, asparagine, and glutamine, may coordinate not only through the carboxylate oxygen and amine nitrogen atoms, but also through the polar side chain atoms. Although polar, the side chains of lysine and arginine are typically positively charged in aqueous solution with pK_a values of 10.54 and 12.48,[55] respectively, and therefore are not expected to coordinate positively charged Cu(II). Methionine and cysteine also have electronegative side chains with the potential for binding Cu(II), but these sulfur-containing amino acids have unique redox properties that present potential complications for stability constant determination and are discussed separately.

Due to the thermodynamic nature of stability constants, tridentate binding to Cu(II) should be reflected in considerably higher stability constants compared to bidentate binding. With Cu(II), stability constants for asparagine, glutamine, serine, threonine, and tyrosine (Table 1.3) are not significantly different from those for the bidentate amino acids (Table 1.2), suggesting only carboxylate and amine binding. Not surprisingly, the lowest

stability constants for Cu(II) binding are observed for Lys and Arg (Table 1.3), likely indicating electrostatic repulsion between the positively charged amino acid and Cu(II). In contrast, Cu(II) stability constants of histidine (ML = 9.75, ML_2 = 17.49) and aspartic acid (ML = 8.83, ML_2 = 15.93) are considerably higher than the other tridentate amino acids (Table 1.3), indicating side chain coordination.

Tridentate coordination to Cu(II) by aspartic acid[104] and histidine are supported by solid-state structures (Figure 1.5).[105-108] Stability constants for glutamic acid (ML = 8.30, ML_2 = 15.03) are slightly elevated compared to the other potentially tridentate amino acids, suggesting weaker side-chain coordination than for His or Asp. However, the only solid-state structure to support this tridentate binding mode is the glutamate complex with cadmium, $[Cd(Glu)(H_2O)]H_2O$.[109] In general, most of the stability constants for the potentially tridentate ligands with Cu(II) do not indicate tridentate binding, and it is reasonable to assume that Cu(II) coordination by these amino acids is

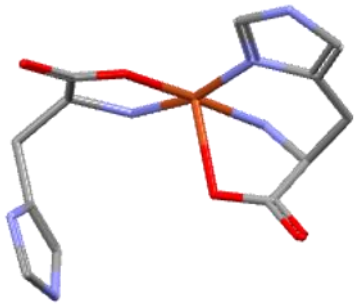

Figure 1.5. Crystal structure diagram for the $Cu(His)_2$ complex, showing both tri- and bidentate binding of histidine to the Cu(II) center. The Cu(II) ion is shown in orange, oxygen atoms are red, carbon atoms are grey, and nitrogen atoms are blue. Hydrogens are omitted for clarity.

Table 1.3. Stability constants for Cu(II) and Cu(I) with potentially tridentate amino acids

Ligand	ML ($\log \beta_{ML}$)[a]	ML_2 ($\log \beta_{ML2}$)[b]	MLOH ($\log \beta_{MLOH}$)[c]	Other Species	Temp (°C)	Ionic Strength (M)	Method	Ref.
Stability Constants for Cu(II)								
Arginine	7.555(4)	14.007(5)			25	0.1 KNO_3	Potentiometry	62
Asparagine	7.788(3)	14.142(4)	4.17(2)	MLH 10.08(3) ML_2H 17.44(3)	37	0.15 $NaClO_4$	Potentiometry	110
Aspartic acid	8.83(3)	15.93(2)	24.0(1)	MLH 12.52(2) ML_2H 19.8(3) M_2L 10.34(6) M_2L_2 19.5(1)	25	0.1 KNO_3	Potentiometry	111
Glutamine	7.71(1)	14.12(1)			25	0.1 KNO_3	Potentiometry	98
Glutamic acid	8.30(4)	15.03(3)		MLH 12.52(2) ML_2H 19.6(3) M_2L 10.41(5) M_2L_2 18.6(2)	25	0.1 KNO_3	Potentiometry	111
Histidine[d]	9.75(1)	17.49(1)	2.2(2)	MLH 13.78(1) ML_2H 23.05(1) ML_2H_2 26.29(6) ML_2OH 6.3(1)	37	0.15 NaCl	Potentiometry	112
Lysine	7.62(2)	13.94(2)		MLH 10.361(5) ML_2H 10.84(1)	25	0.1 KNO_3	Potentiometry	62
Serine	7.748(2)	14.083(5)	4.285(13)	MLH 10.030(16)	37	0.15 $NaClO_4$	Potentiometry	110
Threonine	7.98(4)	14.66(5)	4.81(3)	ML_2H_{-2} -6.0(1)	25	0.1 KNO_3	Potentiometry	107, 113, 62, 111, 114
Tyrosine	7.90(2)	15.17(3)			25	0.1 KNO_3	Potentiometry	115
Stability Constants for Cu(I)								
Histidine	12.80[d]	25.20[d]			25	0.2 KNO_3	Redox	116

[a] $\log \beta_{ML} = [M][L]/[ML]$ [b] $\log \beta_{ML2} = [M][L^2]/[ML^2]$ [c] $\log \beta_{MLOH} = [ML][OH]/[MLOH]$ [d] The protonation state for His in the ML and ML_2 species assumes the histidine has one ionizable proton.

very similar to the bidentate amino acids. Changes in side-chain protonation state, however, can complicate stability constant determination and make identifying minor species more difficult.

Challenges in Determining Cu(II)-Amino Acid Stability Constants

Determining the speciation of metal complexes with potentially tridentate amino acids is especially troublesome for modeling stability constants. These difficulties are primarily caused by reported potential minor species due to 1) inconsistency of identified species, 2) failure to independently characterize these species, and 3) absence of meaningful discussion about the relative importance or implications of the reported minor species. Thus, researchers may be adding minor species solely to optimize their model fitting to titration data, a particular issue given the unreliability of Cu(II)-amino acid titration data at pH > 9 due to precipitation. Collection of titration data is usually limited to the pH range over which all complexes remain in solution, but these pH limits are not always explained, and precipitation is rarely mentioned.

As an example, most studies describing binding constants for Cu(II)-serine complexes report only two species, ML and ML_2.[50] More recent work reports two additional species, ML_2OH and MLH.[110] The difficulties surrounding identification of additional, minor species is demonstrated by comparing the simulated titration data based on reported constants[110,117] for 1) a titration that incorporates just two primary species, $Cu(Ser)_2$ and $[Cu(Ser)]^+$, and 2) a titration that incorporates the additional minor species $[Cu(HSer)]^{2+}$ and Cu(Ser)(OH), for a total of four species (Figure 1.6). Under typical

titration conditions with a 1:2 Cu(II)-to-serine ratio, $[Cu(SerH)]^{2+}$ is present at less than 2% of total Cu and only present below pH ~4, as modeled in Figure 1.6B. Including this minor species results in no differences between the modeled two-species and four-species titration data at these concentrations at pH 4-8 (Figure 1.6A). In contrast, adding the

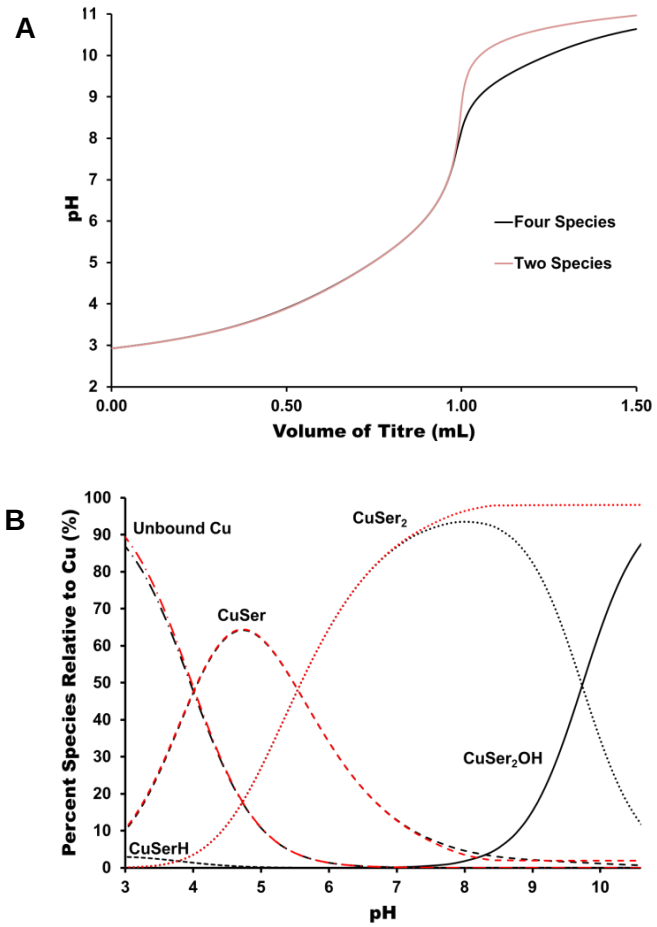

Figure 1.6. A) Simulated titration with a strong base of Cu(II) and Ser with a 1:2 metal to ligand ratio. The "two-species" (red) line shows the modeled titration with only the Cu(Ser) ($\log \beta = 7.92(1)$) and $Cu(Ser)_2$ ($\log \beta_2 = 14.57(1)$) species.[118] The "four-species" (black) line shows the modeled titration with four species, Cu(Ser) ($\log \beta = 7.57$), $Cu(Ser)_2$ ($\log \beta = 14.02$), $Cu(Ser)_2OH$ ($\log \beta = 4.29$), and Cu(Ser)H ($\log \beta = 10.03$).[110] B) A speciation diagram for the Cu(II) and Ser titration over the pH range 3-10.5 fit with two (red line) and four (black line) species.

$[Cu(Ser)_2OH]^-$ species significantly affects titration buffering above pH 8. Including this additional species may improve the model fit to experimental data; however, many Cu(II)-amino-acid complexes precipitate above neutral pH as the concentration of the ML_2 species increases, although this precipitation is often unreported, resulting in significant electrode drift and data inaccuracy. Under these conditions, the limited accuracy of the experimental data may not support including minor species to increase modeling accuracy, and in the absence of independent characterization, these species may even be artefactual.

The Cu(II) to amino ratio used in stability constant determinations also has a significant effect on complex speciation, as demonstrated with the four-species Cu(II)-Ser model titration (Figure 1.6; modeled at a 1:2 ratio) at metal-to-ligand ratios of 1:1 (Figure 1.7A) and 1:10 (Figure 1.7B). Concentrations of the two minor, potentially disputed, MLH and ML_2OH species are amplified by at least two-fold in the 1:10 simulation. These MLH and ML_2OH species are only present under very acidic or basic conditions, respectively, minimizing their impact in biological systems.

To emphasize the inconsistency in identifying minor species, one can consider the example of Cu(II)-threonine titrations. From the wide range of data available, the primary ML and ML_2 species are confirmed, and no MLH species is reported. Multiple studies identify the minor dihydroxide species, $ML_2(OH)_2$,[62,107,111,114] but the presence and contribution of this hydroxide species is disputed given the conflicting data and lack of independent characterization.

Despite their uncertainties, the Cu(II)-Ser and Cu(II)-Thr systems are straightforward compared to Cu(II)-His titration modeling, where anywhere from four to

thirteen species are identified (Table 1.2).[112,119-121] Understanding histidine-copper binding is of primary importance, since it is the most common amino acid in the binding pockets of copper metalloproteins and is the predominant non-protein-bound copper complex in blood plasma.[48,122,123] Reports of so many species, including dinuclear complexes, is indicative of inherent variability in His-Cu(II) coordination. The major species at pH 6-8

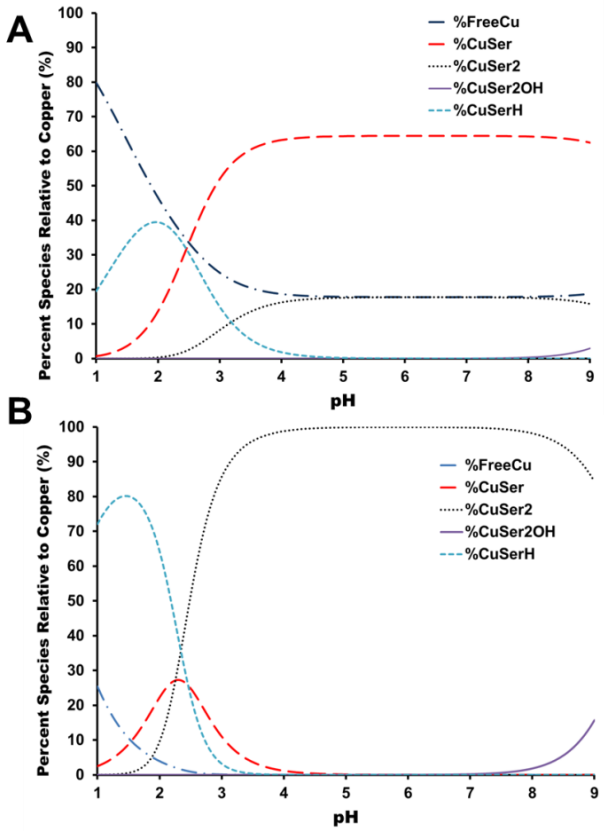

Figure 1.7. A) Modeled speciation diagrams for the Cu(II)-Ser four-species system from Figure 1.6 A) at a 1:1 Cu(II):Ser ratio and B) at a 1:10 Cu(II):Ser ratio.

are $[Cu(His)_2H]^+$ and $Cu(His)_2$; however, minor species, such as $[CuHis]^+$, are present that could influence cellular speciation.[56] Kamyabi and coworkers provided independent confirmation of $[Cu(His)]^+$, Cu(His)H, $Cu(His)_2$, $[Cu(His)_2H]^+$, and Cu(His)(OH)

complexes using spectroscopic methods.[124] The complexity and difficulties of determining Cu(II)-histidine speciation highlight core issues for stability constant determination. Even when the metal-ligand interaction is well-behaved and a variety of methods are available for analysis, confirmation of relevant species must be achieved for the data to be useful in large-scale modeling projects.

1.7 Stability Constants of Non-Sulfur and -Selenium-Containing Amino Acids with Cu(I)

Cu(I) is the least studied and the most poorly understood of the common copper and iron oxidation states in biological systems. In humans, cellular copper intake is tightly controlled through the membrane transport protein hCTR1,[125-127] which has methionine-, cysteine-, and histidine-rich amino acid sequences in the Cu(I) binding site.[6,128] Although hCTR1 and other copper transport proteins preferentially bind Cu(I) over Cu(II), Cu(I) stability constants are vastly underexamined due to the difficulties of working with this ion.

Cu(I) is highly unstable in aqueous systems and disproportionates to Cu(II) and Cu^0 in the presence of dioxygen. Cu(I) is also spectrophotometrically inactive, limiting spectrophotometric titrations to ligands that have absorbances in the UV or visible spectrum. In addition, the most commonly used Cu(I) salt, CuCl, is only sparingly soluble in aqueous systems, narrowly defining the parameters for which potentiometric methods can be utilized. Sharma and coworkers[129] used potentiometric methods to determine that Cu(I) is stabilized in aqueous systems with sufficient Cl^- support (1.0 M). Using potentiometric methods, they identified three species: CuCl, $[CuCl_2]^-$, and $[CuCl_3]^{2-}$, with

step-wise stability constants of 2.68, 5.07, and 4.78, respectively.[129] Given these difficulties with Cu(I) instability and solubility, reliable data for Cu(I) stability constants with amino acids lags far behind that of Cu(II) despite its biological importance.

Due to the significant limitations of potentiometric methods with Cu(I), stability constants have been primarily determined using redox methods. Since Cu(I) is unstable in aqueous solution, redox methods are preferred because metal oxidation state is controlled at the electrode surface. This method is dependent on predicting the potential at which half of the concentration is Cu(I) and half is Cu(II), and activity due to ionic strength is sometimes ignored in the calculations. Stability constants for Cu(I) with only three non-sulfur or -selenium amino acids are reported; Cu(I) stability constants with sulfur- and selenium-containing amino acids will be discussed separately in the *Stability constants of Cu(I) and Cu(II) with sulfur and selenium amino acids* section.

Using redox analyses, stability constants of 9.6, 10.0, and 10.4 were found for Cu(Ala), Cu(Gly), and Cu(His), respectively.[96] Since alanine and glycine have non-coordinating side chains, and stability constants for all three complexes are very similar, these data suggest that all three amino acids are binding in bidentate fashion to Cu(I). It is surprising that His would show such weak Cu(I) binding, considering the role that histidine plays in stabilizing copper in metalloproteins.[130] The only other Cu(I)-His determination identifies formation of Cu(HHis) and $[Cu(HHis)_2]^-$ species with stability constants of 12.80 and 25.20, respectively (Table 1.3),[116] where "HHis" indicates protonation of the amine or imidazole nitrogen atom, implying only bidentate binding. These Cu(I)-His results seem contradictory not only because the identified species are not the same, but because the

Cu(I) species with a potentially tridentate-binding His ligand has a significantly lower stability constant than the Cu(I) species with only a bidentate-binding His ligand. Considering the importance of Cu(I) in biological systems, the fact that methods and stability constant data for Cu(I)-amino-acid complexes are not reliable enough to compare with similar Cu(II) data highlights the extreme difficulties inherent in studying this ion. To add these difficulties, even if reliable titration methods are identified, the propensity of Cu(I) to form multinuclear species[131-133] will provide an additional challenge for these measurements.

1.8 Stability Constants of Sulfur- and Selenium-Containing Amino Acids with Copper

Similar to histidine, sulfur-containing amino acids have been credited for the stability and redox activity of a wide variety of copper metalloproteins. Both methionine and cysteine are recognized for the structural and electronic stability that they contribute to blue copper proteins.[134,135] Thiols have such a high stability with copper, that the drug penicillamine is administered in the treatment of Wilson's disease as a copper chelator.[16,17] Selenium compounds, such as selenocysteine, are crucial to the function of selenoproteins.[136-138] Selenocysteine coordinates nickel in NiFeSe hydrogenases,[139] and selenomethionine is non-specifically incorporated into proteins in place of methionine.[51] In addition, many sulfur and selenium species have been identified and extensively studied as antioxidants by *in vitro, in vivo,* and epidemiological studies,[135,140-144] in part due to their copper-binding properties. Selenium-containing supplements have been the subject of

human studies for their potential as antioxidants, although results are limited and conflicting.[53,145-148]

All of the sulfur- and selenium-containing amino acids have the potential for tridentate binding through the carboxylate oxygen, the amine nitrogen, and the S/Se atom in the side chain. Table 1.4 summarizes the available data for stability constants of Cu(II) and Cu(I) with these amino acids; unsurprisingly, data for Cu(II) are much more complete than for Cu(I).

Cu(II) Complexes of Sulfur- and Selenium-Containing Amino Acids

Thiol-containing cysteine, homocysteine, and penicillamine are redox-active in the presence of Cu(II), forming the respective disulfides and reducing Cu(II) to Cu(I).[149,150] This redox activity impacts the validity of stability constant determinations with these amino acids. Although Cu(II)-Cys stability constants have been errantly reported,[54] previous reviewers[50] have explained the misidentification of species present in these analyses, and Pinto[151] suggested that these complexes are stable at ligand:metal ratios below one. The potential for redox reactions casts a shadow over the reliability of

Table 1.4. Stability constants of Cu(II) and Cu(I) with sulfur- and selenium-containing amino acids

Ligand	ML ($\log \beta_{ML}$)[a]	ML_2 ($\log \beta_{ML2}$)[b]	Other Species	Temp (°C)	Ionic Strength (M)	Method	Ref.
Cu(II) Stability Constants							
Homocysteine	11.92(1)	13.54(2)	7.57(1) (MLOH)	25	0.1 KNO_3	Potentiometry	[151]
Methionine	7.85(2)	14.52(1)		25	0.1 KNO_3	Potentiometry	[62,152,153]
Methylcysteine	7.65[c]	14.13[c]		25	0.2 KCl	Potentiometry	[154]
Methylselenocysteine	8.2(1)	14.5(2)		25	0.1 $NaClO_4$	Potentiometry	[155]
Penicillamine	16.5[c]	21.7[c]		25	0.15 KNO_3	Potentiometry	[156]
Selenomethionine	7.77[c]	14.50[c]		25	0.1 $NaNO_3$	Potentiometry	[157]
Cu(I) Stability Constants							
Cysteine	10.164(6)	18.36(1)	20.34(2) (ML_3)	25	1.0 NaCl	Potentiometry	[158]
Methionine	9.1[c]			20	0.1 $NaClO_4$	Potentiometry	12,[159]
Penicillamine	12.41(5)		18.72(1) (MLH) 22.29(2) (M_2LH) 34.44(1) (M_2L_2H)	25	1.0 NaCl	Potentiometry	[158]

[a] $\log \beta_{ML} = [M][L]/[ML]$ [b] $\log \beta_{ML2} = [M][L^2]/[ML^2]$ [c] Error not reported

Cu(II)-thiol stability constant data and emphasizes the need for proof of speciation in these systems.

Pencillamine has the highest Cu(II) stability constants of the amino acids in Table 1.4, forming Cu(Pen) (log β = 16.5) and $[Cu(Pen)_2]^{2-}$ (log β_2 = 21.7) species.[156] The high affinity of penicillamine for Cu(II) is not surprising, since a primary use of penicillamine is as a copper chelator. Of the other sulfur and selenium amino acids examined, the thiol-containing homocysteine has a higher MLspecies stability constant (11.92(1))[151] than the others (~7.8), but the ML_2 species is slightly less stable at 13.54(2) than the ML_2 species of methionine, methylcysteine, and selenomethionine. Pinto[151] suggested that the amine and the soft thiolate of homocysteine binds borderline Cu(II) in the ML species, either in addition to the hard carboxylate oxygen or in place of it. This is reasonable, since EPR analysis of $[Cu(hCys)_2]^{2-}$ indicates tetrahedral geometry around Cu(II), with the thiolate sulfur replacing carboxylate oxygen binding.[151] The [Cu(HhCys)] species has a significantly higher stability constant than the thio- or selenoethers, potentially indicating stability afforded by tridentate binding. When sterically hindered by a second ligand coordinating in the ML_2 species, the carboxylate oxygen coordination may be lost, and the two ligands likely coordinate in a bidentate fashion through the amine nitrogen and thiolate sulfur atoms. [151]

The presence of a thioether or selenoether group does not contribute to thermodynamic stability of Cu(II) complexes, since stability constants for Cu(II) with methionine, methylcysteine, and selenomethionine are similar to those of the bidentate-coordinating Cu(II)-amino acids in Table 1.2. Solid-state structures also show no thioether

or selenoether coordination in the ML_2 complexes, including $Cu(Met)_2$,[160,161] $Cu(SeMet)_2$,[155] and $Cu(MCys)_2$,[162] but tridentate binding to Co(III)[163,164] and softer metal ions such as rhenium[165] and ruthenium[166,167] is observed.

Cu(II) Complexes of Sulfur- and Selenium-Containing Amino Acids

Stability constants for Cu(I) with sulfur and selenium amino acids are limited to two thiolates (Cys and Pen), only one thioether (Met), and no selenium-containing species (Table 1.4). This paucity of data makes evaluation difficult, as does the fact that the Cu(I)-Met results[159] have not been replicated in sixty years, and no other Cu(I) stability constants have been reported under these conditions. If these results are valid, only the $Cu^{I}(Met)$ species has a higher stability constant ($\log \beta = 9.1$) than the analogous Cu(II) species, $[Cu^{II}(Met)]^{+}$ ($\log \beta = 7.85(1)$).[62] The higher stability of the Cu(I) complex may suggest tridentate binding, or at least a different binding mode than the glycine-like coordination of the $[Cu^{II}(Met)]^{+}$ species. No X-ray diffraction structures are reported for $Cu^{I}(Met)$, but X-ray absorption spectroscopy studies supported by NMR results in aqueous solution indicate Cu(I) coordination by the thioether sulfur and the amine nitrogen atoms in a bidentate fashion.[168]

Cu(I)-Cys is one of the most thoroughly investigated Cu(I) systems, with stability constant determination attempted using at least four different methods with vastly different results. Using polargraphic methods, only the ML species was identified with a stability constant of 19.19.[169] By spectrophotometry, the stability constant for the same ML species was reported as 11.38.[170] In a review, Berthon[50] highlighted the inconsistencies between

these two reports, attributing the difference to interference by NH_3 or redox issues in the polargraphic determinations. More recently, Konigsberger[158] attempted to determine Cu(I)-Cys stability constants in a ternary system using potentiometric analyses with penicillamine. Although penacillamine addition may expand the solubility range of the system beyond pH 5.2, it adds multiple species into an already complicated model. Four different species were reported to form throughout the full pH range, including species with multiple cysteine protonation states and three dinuclear species. Polynuclear copper-thiolate complexes are well known, but suggesting the formation of multiple dinuclear species based on model fit alone is insufficient support. Adding to this complexity, kinetics analyses suggest a dinuclear, mixed-valent $Cu(II)^{/+}$-cysteine complex also may form as an intermediate between the ML and ML_2 species.[171]

Similar to Cys coordination, the Cu(I)-penicillamine system has also been extensively studied,[158,171-173] with no agreement on either the stability constants or species present (Table 1.5). Again, the tendency of Cu(I) to form dinuclear and polynuclear complexes significantly complicates species determination. Most notably, Persson and coworkers[172] determined stability constants of 39.18 and 101.5 for the $[Cu(PenH)_2]^-$ and $[Cu_5Pen_4]^{3-}$ species, respectively, high values that indicate penicillamine strongly stabilizes Cu(I).

To explore differences in speciation between Cu(I) and Cu(II) in the presence of penicillamine, a model of the speciation of copper (100 μM) with penicillamine (1000 mM) was calculated using Geochemist's Workbench[174] using the stability constants and species reported by Persson.[172] Below pH 5, Cu(I) hydrolysis species predominate

Table 1.5. Speciation and stability constants for Cu(I) with penicillamine (Pen)

Species	log β	Ionic Strength	Temp(°C)	Method	Ref.
Cu(Pen)	10.470(6)	1 M NaCl	25	Potentiometry	[158]
Cu(PenH)	18.46(1)				
Cu_2(PenH)	20.48(1)				
Cu(Pen)	12.25(2)	1 M NaCl	25	Potentiometry	[173]
Cu(PenH)	18.34(1)				
$Cu(Pen)_2$	15.44(3)				
$Cu_4(Pen)_3$	49.15(7)				
$Cu(Pen)_2H_2$	39.18	0.5 M $NaClO_4$	25	Potentiometry	[172]
$Cu_5(Pen)_4$	101.5				

(Figure 1.8A). As the pH increases and the thiolate of penicillamine deprotonates, formation of Cu(II)- and Cu(I)-Pen species increases, but the Cu(II) species are the more prevalent species, by a factor of 100. As the electrochemical potential decreases, Cu(I)-Pen species are stabilized (Figure 1.8B).

Copper binding to selenium-containing amino acids is vastly understudied compared to their sulfur analogs. Data for the Cu(II)-SeMet system are reported, with stability constants of 7.77 and 14.50 for the ML and ML_2 species, respectively. The Cu(II)-MeSeCys stability constants have been recently determined,[155] and are consistent with the other thio- and selenoether amino acids with stability constants of 8.2(1) and 14.5(2) for the ML and ML_2 species, respectively. Because these stability constants are similar to those of Cu(II) with methionine and to those for the bidentate-binding amino acids in Table 1.2, Cu(II) likely binds selenomethionine and methylselenocysteine in a glycine-like manner. No data could be found for other selenoamino acids such as selenocysteine. Selenocysteine is highly redox sensitive,[175] but stability constants with

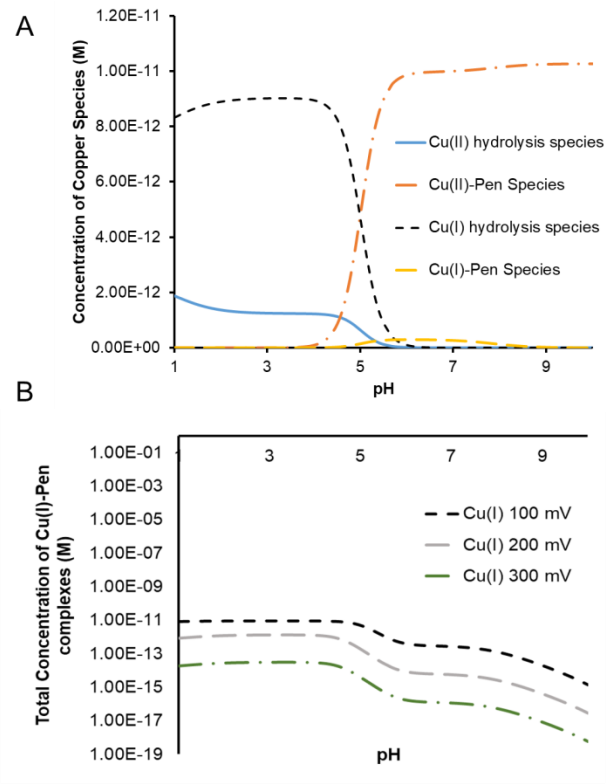

Figure 1.8. A) Speciation comparison between Cu(II) and Cu(I) complexes of penicillamine at a 10:1 ligand-to-metal ratio, showing the favorable stability of Cu(II) over Cu(I) complexes. B) As the electrochemical potential decreases, Cu(I) complexes increase in stability.

copper would contribute to the greater body of knowledge regarding selenium species incorporated into metalloproteins.

Challenges in Determining Copper Stability Constants with Sulfur- and Selenium-Containing Amino Acids

For the vast majority of Cu(II)-amino acid complexes, potentiometric analyses indicate formation of ML and ML_2 species with stability constants of approximately 8 and 14, respectively. Only histidine, glutamic acid, and penicillamine stability constants are high enough to suggest tridentate or partially tridentate Cu(II) coordination in the ML

species. In general, stability of glycine-like amino acid binding to Cu(II) is greater than to Cu(I), although increased stability constants suggest that thiols, thioethers, and selenoethers coordinate Cu(I) through the sulfur or selenium, either in addition to or in place of the carboxylate oxygen. The difficulties in controlling the redox chemistry of Cu(I) with thiols and selenols has discouraged researchers from pursuing the determination of these stability constants with Cu(I). For both Cu(I) and Cu(II), formation of a variety of multinuclear species with sulfur and selenium amino acids also significantly hinders stability constant analysis and interpretation.

1.9 Stability Constants of Non-Sulfur and -Selenium-Containing Amino Acids with Fe(II)

Labile Fe(II) pools contribute to reactive oxygen species formation and cellular oxidative stress,[176] and iron interactions with low-molecular-weight species such as amino acids may alter this behavior. Although not as robust as Cu(II) due to its tendency to form Fe(III) in the presence of oxygen, Fe(II) is fairly well-behaved in closed reaction vessels or under an inert atmosphere of nitrogen or argon. Hydrolysis constants of Fe(II) ($[FeOH]^+$ $\log \beta = -9.5$ and $Fe(OH)_2$ $\log \beta = -20.5$)[177] are low enough to be a factor only at high pH and/or high metal-to-ligand ratios. Since Fe(II) is spectrophotometrically inactive, similar to Cu(I), most stability constant measurements with this ion are performed using potentiometric methods.

Stability constants have been determined for most amino acids with Fe(II); however, a majority of these data are individual analyses, making accuracy evaluation

difficult. For some amino acids, only one stability constant for either the ML or ML_2 species is reported, with little analysis or attempts to identify minor species. Because all the Fe(II)-amino-acid stability constants were determined using potentiometric analysis, comparisons to other methods are not possible.

Fe(II) Complexes of Potentially Bidentate Amino Acids

Similar to Cu(II), Fe(II) stability constants with bidentate-coordinating amino acids all fall within one log unit of each other (3.39 to 4.13 for the ML species, and 7.1 to 8.3 for the ML_2 species; Table 1.6). Glycine, with the relatively low log β values of 4.13 and 7.65 for the ML and ML_2 species, respectively, forms the most stable Fe(II)-amino acid species.[66] Proof of speciation and details about coordination environment are scarce for these potentially bidentate Fe(II)-amino-acid complexes, since $Fe(Pro)_2$(phenanthroline) (Figure 1.9) is the only reported Fe(II) structure with any single amino acid ligand.[178] In this complex, Fe(II) is coordinated in distorted octahedral geometry, with both bidentate Pro ligands coordinating through the amine nitrogen and carboxylate oxygen atoms. Given the similarity of ML_2 stability constants for Fe(II) binding to all the potentially bidentate amino acids, it is reasonable to assume similar amine and carboxylate coordination for all the amino acids in Table 1.6.

A single study identifies ML_3 species for phenylalanine and tryptophan with log β values of 10.7(2) and ~9.5, respectively.[179] Fe(II) binding to a third amino acid must out-compete formation of the $[FeOH]^+$ and $Fe(OH)_2$ species, the latter of which has limited solubility. If all three ligands of the ML_3 species bind in a bidentate fashion, they are almost

certainly arranged in octahedral geometry around the Fe(II) center. Both Phe and Trp have aromatic side chains that would result in considerable steric encumbrance to the complex. The predictable stepwise formation constants (log K_1 = 3.74, log K_2 = 3.45, and log K_3 = 3.5) suggests there is no enthalpic penalty due to increasing coordination, and the reported potentiometric results are supported by calorimetry measurements.[179] In all cases, the stability constants for the $[FeL]^+$ and FeL_2 species are extremely weak and indicate that high ligand-to-metal concentrations are required for complex formation.

Table 1.6. Stability constants of Fe(II) and Fe(III) with potentially bidentate amino acids

Stability Constants of Fe(II)							
Ligand	**ML (log β)[a]**	**ML_2 (log β_2)[b]**	**ML_3 (log β_3)[c]**	**Temp (°C)**	**Ionic Strength (M)**	**Method**	**Ref.**
Alanine	3.54[d]			20	1.0 KCl	Potentiometry	180
Glycine	4.13[d]	7.65[d]		25	0.1 KNO_3	Potentiometry	66
Leucine	3.42[d]			20	1.0 KCl	Potentiometry	180
Phenylalanine	3.74(1)	7.19(3)	10.7(2)	25	3.0 $NaClO_4$	Potentiometry	179
Proline		8.3[d]		20	0.01[e]	Potentiometry	181
Tryptophan	3.92[d]	7.39[d]	~9.5[d]	25	3.0 $NaClO_4$	Potentiometry	179
Valine	3.39[d]			20	1.0 KCl	Potentiometry	180
Stability Constants of Fe(III)							
Alanine	10.98[d]			30	1.0 KCl	Polarography	182
Glycine	10[d]			25	1.0 $NaClO_4$	Redox	159
Leucine	9.9[d]			20	1.0 $NaClO_4$	Redox	159
Phenylalanine	10.39(4)	19.1(1)	26.0(7)	25	3.0 $NaClO_4$	Potentiometry[f]	179
Proline	10.0(3)			20	1.0 $NaClO_4$	Potentiometry	
Tryptophan	9.0[d]			20	1.0 $NaClO_4$	Redox	159
Valine	9.6[d]			20	1.0 $NaClO_4$	Redox	159

[a] $\log \beta = [M][L]/[ML]$ [b] $\log \beta_2 = [M][L^2]/[ML^2]$ [c] $\log \beta_3 = [M][L^3]/[ML^3]$ [d] No error reported by author. [e] The identity of the electrolyte was not reported; titrations were run at approximately 0.01 M ligand. [f] Data also supported by calorimetry.

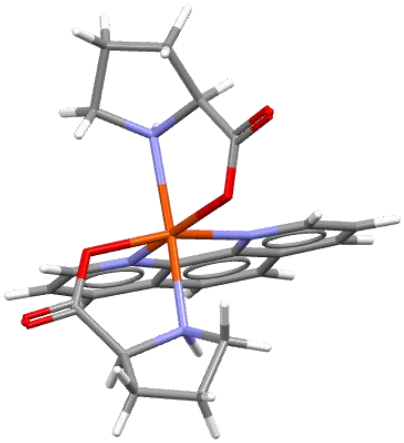

Figure 1.9. Solid-state structure of $Fe(Pro)_2$(phenanthroline),[178] showing bidentate Pro coordination through the carboxylate oxygen and the amine nitrogen atoms. Fe(II) is shown in orange, oxygen atoms are red, carbon atoms are grey, and nitrogen atoms are blue.

Fe(II) Complexes of Potentially Tridentate Amino Acids

As for the bidentate amino acids, stability constant data for potentially tridentate amino acids binding Fe(II) are incomplete. Most of the stability constants for ML (3.20-4.37) and ML_2 complexes of these amino acids are similar to those for the bidentate amino acids, consistent with glycine-like binding to Fe(II) without significant stability contributed by the polar side chain. Many of the reported constants have not been replicated or independently confirmed by other methods.

Histidine and aspartic acid have somewhat higher stability constants (5.88 and 5.34 for the ML species and 10.43 and 8.57 for the ML_2 species, respectively) than the majority of the other potentially tridentate amino acids, suggesting possible tridentate binding or Fe(II) stabilization through bridging ligands. ML_3 stability constants are determined for asparagine[183] and serine,[184] further supporting bidentate coordination of these amino acids, at a maximum. It is surprising that minor species have not been

Table 1.7. Stability constants of Fe(II) and Fe(III) with potentially tridentate amino acids

Ligand	ML ($\log \beta_{ML}$)[a]	ML_2 ($\log \beta_{ML2}$)[b]	ML_3 ($\log \beta_{ML3}$)[c]	Temp (°C)	Ionic Strength (M)	Method	Ref.
Stability Constants of Fe(II)							
Arginine	3.20[d]			20	0.01[e]	Potentiometry	99
Asparagine	4.37(3)	7.57(3)	10.26(5)	25	3.0 $NaClO_4$	Potentiometry	183
Aspartic acid	5.34[d]	8.57[d]		25	0.1[e]	Potentiometry	185
Glutamic acid	3.50[d]			20	1.0 KCl	Potentiometry	180
Histidine	5.88[d]	10.43[d]		25	3.0 $NaClO_4$	Potentiometry	186
Lysine	4.5[d]			20	0.01[e]	Potentiometry	99
Serine	4.299[d]	7.377[d]	10.299[d]	20	3.0 $NaClO_4$	Potentiometry	184
Threonine	3.69[d]	6.50[d]		40	0.2 KNO_3	Potentiometry	187
Tyrosine		7.1[d]		20	0.01[e]	Potentiometry	181
Stability Constants of Fe(III)							
Arginine	8.7(3)			20	1.0 $NaClO_4$	Potentiometry	159
Asparagine	8.6(1)			20	1.0 $NaClO_4$	Potentiometry	159
Aspartic acid	11.4(3)			20	1.0 $NaClO_4$	Potentiometry	159
Glutamic acid	13.39[d]			20	1.0 $NaClO_4$	Potentiometry	188
Histidine	4.7(4)			20	1.0 $NaClO_4$	Potentiometry	159
Serine	9.2(4)			20	1.0 $NaClO_4$	Potentiometry	159
Threonine	8.6(3)			20	1.0 $NaClO_4$	Potentiometry	159

[a] $\log \beta = [M][L]/[ML]$ [b] $\log \beta_2 = [M][L^2]/[ML^2]$ [c] $\log \beta_3 = [M][L^3]/[ML^3]$ [d]No error reported by author. [e] No supporting electrolyte was reported. Titrations were run at approximately 0.01 M ligand.

identified in the low pH range for these iron-amino acid systems, but the stability of iron hydrolysis species above pH 7 outcompetes weakly binding amino acid ligands. Fe(II) stability constants with the majority of the potentially bidentate and tridentate amino acids are fairly consistent: ML stability constants are approximately 3-4; ML_2 stability constants are approximately 7; and the few ML_3 stability constants reported are approximately 10. Extrapolating from scarce structural and supporting speciation data, it is likely that most amino acids coordinate Fe(II) in a bidentate fashion through the carboxylate oxygen and amine nitrogen atoms. Aspartic acid and histidine have somewhat higher stability constants for the ML (5.88 and 5.32, respectively) and ML_2 (10.43 and 8.57, respectively) species, suggesting that the His and Asp side chains participate significantly in coordination.

Challenges in Determining Fe(II)-Amino Acid Stability Constants

Although stability constants of divalent metals with amino acids have been the focus of a few comprehensive studies,[99,180,181,187] most Fe(II) amino acid stability constants are limited to these few studies with little speciation analysis. The majority of the published data were obtained using potentiometric titrations. Although Fe(II) salts are water soluble, Fe(II) oxidizes to Fe(III) in air, so oxygen-free conditions must be employed. This air sensitivity limits analysis techniques to methods that can be performed in a glove box or in closed cells. Fe(II) also forms hydrolysis compounds above pH 7. Although these complexes are not as stable as Fe(III) hydrolysis products, they do compete with amino acids for metal binding in the upper pH range. Fe(II) is also spectrochemically inactive,

like Cu(I), and therefore not an option for spectrophotometric techniques with non-UV-active amino acids. As a whole, these issues have limited the data availability for Fe(II) with amino acids.

Comparison of Cu(II) and Fe(II) Stability Constants of Non-Sulfur and-Selenium-Containing Amino Acids

Cu(II) and Fe(II) have the same valency and are both considered borderline Lewis acids; both also have the potential to coordinate ligands in octahedral geometry. However, stability constants of Cu(II) and Fe(II) with amino acids are significantly different, with Cu(II)-amino acid complexes significantly more stable than analogous Fe(II)-complexes. With ML constants of approximately 9 for $[CuL]^+$ species (Table 1.3) and between 3 and 4 for most of the $[FeL]^+$ complexes (Table 1.7), all of the non-sulfur- and non-selenium-containing amino acids show a higher affinity for the Cu(II) ion. A similar comparison can be made for CuL_2 and FeL_2 species with stability constants of ~14 and 7-8, respectively. With Cu(II), only His (ML log β = 9.75(1), ML_2 log β = 17.49(1)) Asp (ML log β = 8.83, ML_2 log β =15.93(2)), and Glu (ML log β = 8.30(4), ML_2 log β = 15.03(3)) have large enough stability constants to suggest the potential for tridentate coordination. With Fe(II), stability constants with His (ML log β = 5.88, ML_2 log β = 10.43) and Asp (ML log β = 5.34, ML_2 log β = 8.57) are somewhat elevated compared to bidentate-binding amino acids but are still considerably lower than stability constants with Cu(II).

Although solid-state structural data supports tridentate His coordination in $Cu(His)_2$ (Figure 1.5), no comparable Fe(II) structures exist to show tridentate amino acid

coordination. His and Asp may be tridentate ligands binding Fe(II) through the amine, carboxylate, and side-chain N or O atoms or, alternatively, adopt bidentate coordination through the N or O atom of the side chain and either the amine nitrogen or carboxylate oxygen atom. Regardless of coordination mode, the stability of Fe(II) with non-sulfur- or selenium amino acids is significantly weaker than Cu(II) and therefore less biologically significant.

1.10 Stability Constants of Non-Sulfur and –Selenium-Containing Amino Acids with Fe(III)

Most Fe(III) in the cell is sequestered in ferritin storage as ferrihydrite,[189] although Fe(III) also exists in the mitochondria.[32] Fe(III) does not generate hydroxyl radical as does Fe(II), and it is poorly soluble and therefore not readily available in the aqueous environment of a cell. Poor Fe(III) solubility, due to the stability of the hydrolysis species, also contributes to a deficit of Fe(III) stability constants with amino acids, since it restricts the use of potentiometric titrations to a very narrow pH range. The Fe(III) stability constants reported in Table 1.7 were measured below pH 5.[159]

Fe(III) Complexes of Potentially Bidentate and Tridentate Amino Acids

For most amino acids, regardless of potential denticity, Fe(III) stability constants for only the ML species have been quantified (Table 1.7) with the exception of a single study by Williams.[184] Many of these constants were determined using redox measurements

in one 1958 report by Perrin,[159] and the lack of precision inherent to the redox method is reflected in the reported values.

Stability constants for the ML species of Fe(III) and a majority of the amino acids are consistently in the 8-10 range (Tables 1.6 and 1.7). Notable exceptions to this trend are glutamic acid, with a higher ML stability constant of 13.39, and histidine, with a lower ML stability constant of 4.7(4), respectively. The considerably higher Fe(III)-Glu stability constant was determined under different experimental conditions[188] compared to most of the other amino acids, but these experimental differences would not explain such a significant disparity. The considerably lower stability constant for the $[Fe^{III}(His)]^{+}$ seems to indicate that His coordination does not greatly stabilize Fe(III). In contrast, the only solid-state structure of Fe(III) with an amino acid incorporates histidine in a tridentate coordination mode: an oxo-bridged, binuclear complex, $Fe_2(His)_2(biphenyl)_2(\mu\text{-}O)$ (Figure 1.10). Although this complex was not crystallized out of aqueous solution, it indicates that histidine is certainly capable of tridentate coordination to Fe(III).

Determining Fe(III) Stability Constants Using the Solubility Method

One method that has not been discussed thus far but has been used in environmental chemistry for determining Fe(III) stability constants is the solubility method. With this technique, insoluble metal ions are slowly dissolved by complex formation with an aqueous-phase ligand. The concentration of the soluble complex can then be determined through methods such as inductively-coupled-plasma mass spectrometry or scintillation

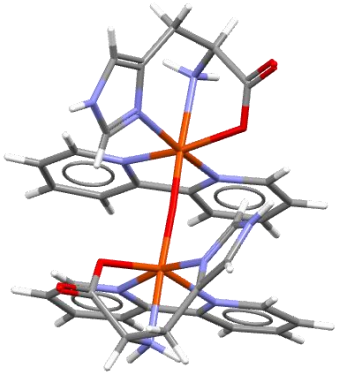

Figure 1.10. Solid-state structure of $Fe_2(His)_2(biphenyl)_2(\mu\text{-}O)$, showing tridentate coordination of histidine through a nitrogen atom of the imidazole side chain as well as the carboxylate oxygen and amine nitrogen atoms. The Fe(III) ion is shown in orange, oxygen atoms are red, carbon atoms are grey, and nitrogen atoms are blue.

techniques with radioisotopes. By varying the ratio of ligand to metal, a continuous plot can be derived to track mass transfer from solid state to aqueous solution. Due to the extreme insolubility and stability of Fe(III) hydrolysis products, the solubility method is an optimal tool for stability constant determination in this system. In this method, competition for the Fe(III) is measured through the addition of increasing concentration of ligand to a suspension of $Fe(OH)_3$. The amount of complex is then determined by the measurement of pH and Fe(III) in solution. This method is by no means the easiest or the fastest, but it may overcome the difficulties inherent in using most other methods for Fe(III) stability constant determination due to the highly insoluble Fe(III) hydrolysis species.

A model Fe(III) solubility experiment was calculated using Geochemist Workbench using low, moderate, and high amino acid stability constant values with Fe(III) as exemplified by Met, Glu, and Phe.[159,179,188] In this model, amino acid concentrations are increased until the Fe(III)-amino-acid species out-compete the insoluble iron-hydrolysis

species. In Figure 1.11A, a complex forming with a stability constant of 9.1, the same as for $[Fe(Met)]^{2+}$ and comparable to most of the other ML species reported by Perrin,[159,180] has very little ability to dissolve the solid ferric hydrolysis species to form $[Fe(Met)]^{2+}$ in aqueous solution. Increasing the stability constant by four log units to 13.39, as reported for $[Fe(Glu)]^{+}$,[188] significantly increases the amount of Fe(III) dissolved in solution (Figure 1.11B).

Utilizing the only multi-species data reported for Fe(III) complexes with non-sulfur or selenoamino acids, $[Fe(Phe)]^{2+}$, $[Fe(Phe)_2]^{+}$, and $Fe(Phe)_3$ species with stability constants of 10.39(4), 19.1(1), and 26.0(7), respectively,[179] results in a significantly higher amount of dissolved Fe(III) (Figure 1.11C) compared to that in the Fe(III)-Met and Fe(III)-Glu systems (Figures 11A and 11B). It is entirely possible that multiple species form in all of the Fe(III)-amino acid systems, but identification of these species may be hindered by low-pH precipitation of iron hydrolysis species in the potentiometric and redox titrations. Solubility titrations could provide insight into formation of additional species in these systems, although this method is limited by the aqueous solubility of the resulting Fe(III)-amino acid complexes. It is reasonable to expect, however, that even low-solubility complexes would remain in solution at the extremely low total iron concentrations found in these modeled systems (pM to nM range). Thus, solubility titrations represent a viable but almost unexplored method for Fe(III) stability constant determination.

1.11 Stability Constants of Sulfur- and Selenium-Containing Amino Acids with Iron

Sulfur-containing metalloproteins such as rubredoxins, ferredoxins, and hemerythrin play a crucial role in electron transfer through iron-sulfur interactions.[130] Despite their biological importance, Fe(II) and Fe(III) stability constant determinations with sulfur- and selenium containing amino acids are so limited, it is difficult to assess the viability of the experimental results or to identify trends.

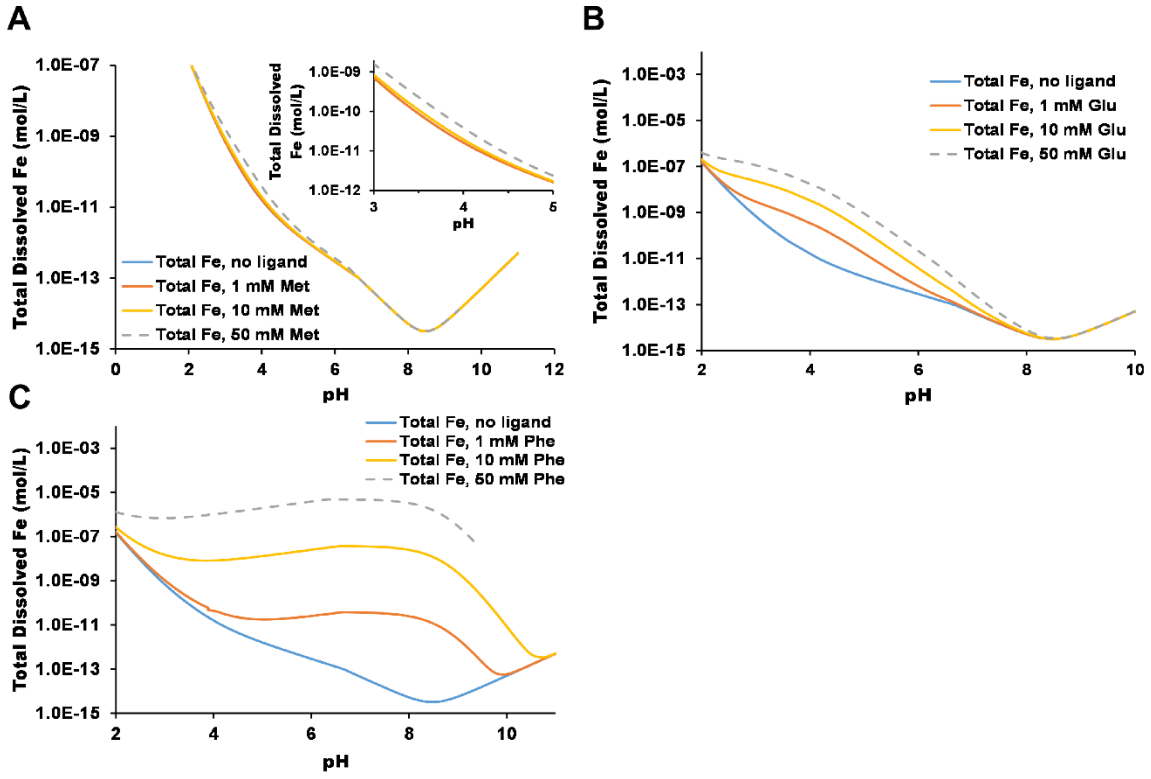

Figure 1.11. Modeled solubility method data for Fe(III) complexes with A) methionine (ML log β = 9.1),[180] B) glutamate (ML log β = 13.39),[190] and C) phenylalanine (ML log β = 10.39, ML_2 log β = 19.11, and ML_3 log β = 26).[179] Comparing graphs A and B shows the effect a change in log β by 4 log units has on ferrihydrite solubility. Comparing graphs B and C shows the significant effects of higher stability constants and multiple species on aqueous Fe(III) solubility

Fe(II) Complexes of Sulfur- and Selenium-Containing Amino Acids

In contrast to Cu(II), stability constants of thioether- and selenoether-containing amino acids with Fe(II) are extremely low: 3.2 to 3.9 for the $[FeL]^+$ species (Table 1.8). These constants are consistent with those of Fe(II)-amino-acid species with bidentate binding (Table 1.6), suggesting at most bidentate coordination and perhaps only amine or carboxylate binding. Thus, it is unlikely that the thio- or selenoether S or Se atom plays a significant role in Fe(II) coordination. Based on limited data, the selenoether-containing amino acids have slightly higher stability constants with Fe(II) than analogous thioether amino acids, although two data points (Met/SeMet and MeCys/MeSeCys) do not necessarily make a trend.

In contrast, Fe(II) stability constants with the thiol-containing amino acids Cys and Pen are significantly higher. Interestingly, these Cys and Pen stability constants are similar to those of bidentate Cu(II)-amino acid complexes (Table 1.2), potentially indicating a different coordination mode, possibly through the thiolate and amine groups, rather than tridentate binding. Studies to confirm coordination modes for these amino acids have not been performed, and there are no reported Fe(II) stability constants for selenol-containing amino acids. The lack of independent characterization of the species identified in these stability constant studies provides only a very indirect understanding of these coordination complexes.

Fe(III) Complexes of Sulfur- and Selenium-Containing Amino Acids

Only a handful of stability constant determinations with Fe(III) and sulfur amino acids have been reported, and none are reported for selenoamino acids. A variety of methods have been used for the few reported analyses, including potentiometric titrations,[181,191] paper electrophoresis,[192] and redox methods.[180] Where comparisons can be made, the data conflict. For the Fe(III)-Met system, Tewari[85] used paper electrophoresis to identify two different species $[Fe(Met)]^{2+}$ and $[Fe(Met)_2]^{+}$ with stability constants of 7.95(7) and 12.65(6), respectively (Table 1.8). In contrast, a 1958 study by Perrin and coworkers[159] reported a stability constant of 9.1 for the $[Fe(Met)]^{2+}$ species using potentiometric methods. Due to the limited competition of methionine binding with formation of Fe(III) hydrolysis products (Figure 1.11), it is not surprising that a ML_2 stability constant was not determined using this method. While paper electrophoresis is limited to low pH (1-4) to maintain solubility, this method promotes separation of species through electrophoresis, directly establishing the number of species formed.

The thiol-containing amino acids cysteine and penicillamine have Fe(III) stability constants in the 10.8-11.3 range for the $[ML]^{+}$ species, significantly higher than those with thioether-containing amino acids. Thus, it is reasonable to assume that in aqueous solution, Cys and Pen interact with Fe(III) through tridentate coordination of the thiolate sulfur, amine nitrogen, and carboxylate oxygen atoms. This binding mode is supported by the solid-state structure of $Th[Fe(Pen)_2]$, an $[Fe^{III}(Pen)_2]^{-}$ complex with a Th^{+} counterion

Table 1.8. Stability constants of Fe(II) and Fe(III) with sulfur- and selenium-containing amino acids

Ligand	ML ($\log \beta$)[a]	ML_2 ($\log \beta_2$)[b]	Temp (°C)	Ionic Strength (M)	Method	Ref.
Fe(II) Stability Constants						
Cysteine	6.69(2)	11.90(3)	20	0.1 $NaClO_4$	Potentiometry	[191]
Methionine	3.24[c]		20	1.0 KCl	Potentiometry	[159]
Methylcysteine	3.49(4)		25	0.1 NaCl	Potentiometry	[155]
Methylselenocysteine	3.84(1)		25	0.1 NaCl	Potentiometry	[155]
Penicillamine	7.58(1)	13.74(2)	20	0.1 $NaClO_4$	Potentiometry	[191]
Selenomethionine	3.51(7)		25	0.1 NaCl	Potentiometry	[155]
Fe(III) Stability Constants						
Cysteine	10.85[c]	14.49[c]	20	0.15 KNO_3	Potentiometry	[193]
Methionine	9.1[c]		20	1.0 $NaClO_4$	Redox	[159]
Methylcysteine	8.37(5)	13.92(1)	25	0.1 M KNO_3	Electrophoresis	[192]
Penicillamine	11.27[c]	16.25[c]	20	0.15 KNO_3	Potentiometry	[193]

[a] $\log \beta = [M][L]/[ML]$ [b] $\log \beta_2 = [M][L^2]/[ML^2]$ [c]No error reported.

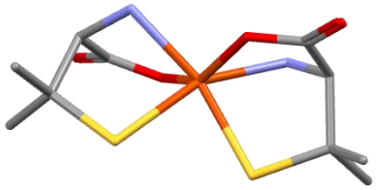

Figure 1.12. Solid-state structure for Th[Fe(Pen)$_2$]. Hydrogen atoms are omitted for clarity. The Fe(II) ion is shown in orange, oxygen atoms are red, carbon atoms are grey, nitrogen atoms are blue, and the sulfur atoms are yellow. Counterion and hydrogen atoms are omitted for clarity.

(Figure 1.12).[194] Both Pen ligands bind in tridentate fashion to Fe(III), with bond angles closer to trigonal bipyrimidal than octahedral geometry.

Challenges in Determining Iron Stability Constants with Sulfur- and Selenium-Containing Amino Acids

Determination of iron stability constants with sulfur- and selenium-containing amino acids is plagued by issues common to Fe(II) and Fe(III) titrations with any amino acid. With Fe(II), experiments must be conducted in oxygen-controlled environments, UV-visible analyses are limited to spectrochemically active ligands, and potentiometric analyses are limited above pH 7. Fe(III) stability constant determinations with weakly binding ligands are even more limited due to the high stability of Fe(III) hydroxide species.

In addition to these problems, cysteine and pencilliamine are also redox-active with Fe(III).[195,196] Although Fe(III) stability constants are reported for these amino acids, conditions must be tightly controlled and data misinterpretation is not uncommon. Sisley's[196] kinetic analysis of the interaction of redox-active metals, including iron, with

these thiol-containing amino acids is detailed and specific. Due to these significant limitations, few analyses are reported and stability constant values can vary depending on experimental methods and conditions for these sensitive systems.

Comparison of Copper and Iron Stability Constant Determinations with Sulfur- and Selenium-Containing Amino Acids

The most complete stability constant data with Cu(II), Cu(I), Fe(II), and Fe(III) exists for the thiol-containing amino acids cysteine and penicillamine. Cu(II)-penicillamine complexes are extremely stable with log β values of 16.5 and 21.7 for the ML and ML_2 species, respectively[156] (Table 1.4). The stepwise log *K* values for these constants, 16.5 for ML and 5.2 for ML_2, suggest that Pen may coordinate Cu(II) as a tridentate ligand in the ML species. The significantly lower stability increase upon adding a second Pen ligand suggests that the second ligand may have only mono- or bidentate binding. Mixed tridentate and bidentate amino acid-Cu(II) complexes are structurally characterized,[105-107] and rhenium-bound penicillamine adopts a structure where the two Pen ligands coordinate in tridentate and bidentate fashion simultaneously.[197] Fe(II)-Pen stability constants are significantly lower than the analogous Cu(II) species (7.58(1) and 13.74(2) for the ML and ML_2 species, respectively;[191] Table 1.8) but significantly higher than stability constants of other Fe(II)-amino acid complexes (except Cys). These lower stability constants are most consistent with bidentate coordination.

A comparison of stability constants for Cu(I), Fe(II), and Fe(III) with cysteine is somewhat surprising (Tables 4 and 8). Cu(I) and Fe(III) have similar ML stability constants of 10.164(6) and 10.85, respectively, but similar Fe(II) values are lower at 6.69(2).[158,191,193] This trend is slightly surprising since Cu(I) is significantly softer than Fe(III), with Fe(II) and Cu(II) falling in between. Comparing the ML_2 stability constants, the Cu(I)-Cys species has a considerably higher stability of 18.36(1), as compared to 14.49 with Fe(III) and 11.90(3) with Fe(II). Perhaps this unexpected trend can be attributed to cysteine binding all of the metal ions in a tridentate fashion, but the relative Lewis acidity of the coordinating ligand atoms is also mixed, with hard carboxylate and amine group and a relatively soft thiolate group. It should be noted that Pen stability constants exhibit the same trends, with the Cu(II) species having the greatest stability compared to the other ions.

The thioether-containing methionine is the only other sulfur- or selenium-containing amino acid with analyses reported for Cu(II), Cu(I), Fe(II), and Fe(III). Cu(II)-Met stability constants of 7.82(2) and 14.52(1) for the ML and ML_2 species, respectively, are well-supported by a variety of authors[62,152,153] and are consistent with results obtained for other amino acids with aliphatic side chains (Table 1.1). Methionine stability constants with Cu(I), Fe(II), and Fe(III) were reported in a single 1958 study by Perrin,[159] making comparisons questionable. Met binding does not provide added stability compared to amino acids with non-coordinating side chains, suggesting that the thioether sulfur atom does not bind in the ML or ML_2 species, a result supported by solid-state structures.[160,161] Assuming Perrin's results are accurate, the same trend is observed for Met as for Cys and

Pen. Methionine binding to both Cu(I) and Fe(III) has higher stability for the ML species (log β = 9.1 for both) than for the Fe(II) species (log β = 3.24).

Although Met and SeMet are also bidentate chelators of Cu(I), the soft sulfur or selenium atom coordinates Cu(I) in addition to the amine nitrogen, with no bonding of the carboxylate group. The best characterization has been obtained for the Cu(II)-Met and -SeMet complexes, where IR and X-ray diffraction data support the bidentate coordination of the amine and carboxylate groups. Differing amino acid coordination modes likely change the measured stability constants, so evaluating trends across metals is not possible.

1.12 Iron and Copper Coordination to Weakly Binding Ligands: Biological Relevance, Methods Development, and Outlook

With their similar structures and diversity of side-chain functional groups, amino acids are an ideal system for developing more accurate methods to determine metal stability constants with weakly binding ligands. The four metal ions treated in this review, Cu(II), Cu(I), Fe(II), and Fe(III) also span the range between easy to examine (Cu(II)) and extremely difficult to study due to redox activity and insoluble hydrolysis products (Cu(I) and Fe(III)). Developing methods specifically designed to work around these issues, such as solubility titrations for Fe(III) stability constant measurements, would provide a substantial advance in this field and provide a foundation for stability constant determination for metal complexes with any weakly binding ligands. In addition, accurate determination of metal-amino-acid stability constants can then be used to model

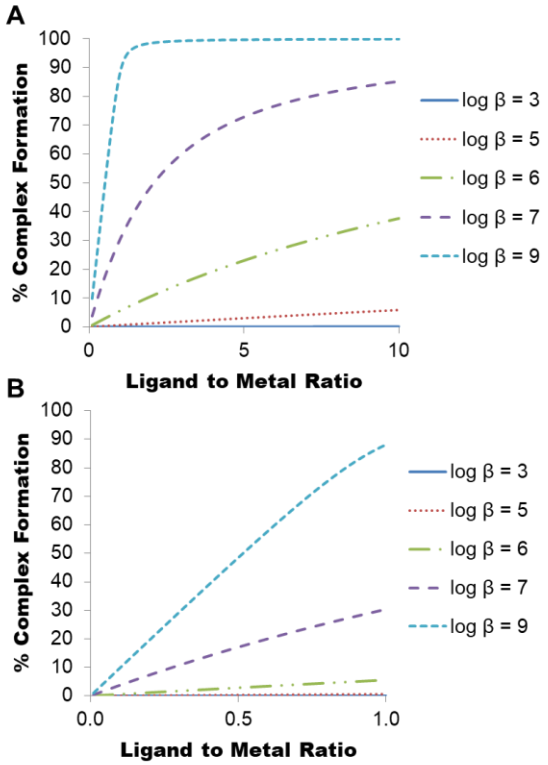

Figure 1.13. Percent complex formation of the ML species for aqueous solutions containing 10 μM metal ion and 0-100 μM amino acid. Formation constants for the amino acid (AA) of 9.2 for HAA and 11.28 for H_2AA were included to model a representative amino acid with amine and carboxylate protons.

complex biological systems and predict competition concentrations that may be relevant for maintaining metal homeostasis or in instances of metal mis-regulation.[67,79,139,158,198]

Taking into account the biological concentrations of metals and amino acids, we can use established stability constants to predict the likelihood of complex formation in binary systems. For this model, only ML species were considered with static protonation constants of 9.2 and 11.2, corresponding to the approximate stability constants for the amine and carboxylate groups of amino acids with non-protonating side chains. Figure 1.13A shows the percentage of complex formation as the amino acid ligand concentration varies from 1 μM to 500 μM, the typical range of blood amino acid concentrations (as

discussed in the *Cellular Redox-Active Metal Ions and Amino Acids* section), assuming 10 μM of available metal ion. Figure 1.13B shows complex formation for the amino acid range from 1-10 μM, where the metal (10 μM) is in excess of the ligand. Percent complex formation for these binary systems is predicted, depending on stability constants for the metal-amino-acid complexes.

Most of the Cu(II)-amino-acid complexes have [ML] stability constants of at least 7, indicating bidentate binding and resulting in approximately 40% to 70% of metal bound within a 1:1 to 1:10 ligand-to-metal ratio. For thiol-containing amino acids and histidine that have Cu(II) [ML] stability constants upward of 10, it would be expected that 90-100% of the metal ion would be coordinated to the amino acid, assuming a 1:1 or greater metal-to-amino-acid ratio. Ten-fold higher metal ion concentrations (100 μM) with the same amino acid concentration range result in decreased complex formation compared to 10 μM metal over the same stability constant range (Figure S1 in *Supplementary Data*). All of the limited number of Cu(I)-amino-acid stability constants are higher than the Cu(II) stability constants with the same amino acid, even for amino acids such as alanine and glycine that are only bidentate chelators. Thus, in the reducing cellular environment, it is reasonable to expect that available Cu(I) ions would likely be coordinated by free amino acids.

On the other end of the spectrum, the Fe(II)-amino-acid stability constants for the [ML] species are very low, approximately 3-4. With these low stability constants, even at a 10:1 ligand-to-metal ratio, less than 10% of Fe(II) would be bound (Figure 1.13). With Fe(II), only cysteine and penicillamine with stability constants of 6.69 and 7.58, respectively, would form an appreciable amount of complex. Although Fe(III)-amino-acid

complexes have high enough stability constants (8-13) to expect amino acid coordination at the modeled concentrations, amino acids could not outcompete formation of Fe(III) hydrolysis products at reasonable biological pH ranges.

From these simple models, it is evident that amino acids with higher stability constants will dominate complexation with labile metal ions. For Cu(I) and Cu(II), histidine, aspartic acid, cysteine, and penicillamine would out-compete other amino acid binding, as long as amino acid concentrations were relatively similar. For Fe(II) and Fe(III), cysteine and penicillamine coordination would dominate, neglecting Fe(III) hydrolysis.

From this overview, it is evident that there is a need for more complete analyses of the redox active metals with sulfur- and selenium-containing amino acids. Although Cu(II) has been extensively studied, the other metal ions, Cu(I), Fe(II), and Fe(III) are just as biologically relevant and data are poor. Before beginning an amino acid stability constant study, it is important to understand the advantages and disadvantages of not just the methods used, but of the metal and ligands to be studied. Cu(II) is a robust ion with high solubility in aqueous systems and its stability constants with a wide variety of amino acids and other ligands have already been thoroughly examined. Using Cu(II) is ideal for new methods development, since the breadth of data available would provide dependable comparisons. Because it is a redox-active metal, the redox activity of the ligand must be considered when selecting experimental parameters.

Cu(I) binds a variety of amino acids in metalloenzymes and also contributes to oxidative damage within the cell, if not controlled through cellular mechanisms and

complexation. Determining Cu(I) complex stabilities with available small molecules is a wide-open field with significant biological implications. Cu(I) is extremely difficult to work with due to redox activity, oxygen sensitivity, limited solubility, tendency for disproportiation, and lack of spectrochemical activity. There is much need for methods development for stability constant determination with this ion. Measuring stability in high ionic strength media may provide the best path forward for potentiometric analysis. Other methods, such as zero-current potentiometry and electrophoresis, under atmosphere-controlled conditions, are worth developing and validating.

Fe(II)- and Fe(III)-amino-acid stability constant data is also lacking. Since potentiometric analysis is not ideal due to low solubility of iron hydrolysis products, other methods need to be explored. The solubility method has the potential to open up the Fe(III) determinations, especially with mass spectrometry techniques capable of detecting and quantifying individual species.

Determining stability constants for copper and iron binding to sulfur and selenium amino acids is also critical for understanding biological systems. Sulfur amino acids are required for maintaining cellular redox balance, and modeling studies indicate that these amino acids may bind both iron and copper. Selenoamino acids and related species have been implicated in cancer prevention and as antioxidants to prevent metal-mediated oxidative damage, yet selenium speciation and interaction with biometals is thoroughly underexplored and requires more dedicated study.

"The difficulty lies not so much in developing new ideas as in escaping from old ones" (John Maynard Keynes). One of the primary difficulties with this field is that the

easiest systems have been thoroughly studied, but the more problematic ones only have single analyses or no data at all. Revisiting some of the analyses that were performed 50 years ago and using and/or developing new methods to confirm these results and continue the study of weakly binding ligands is worth exploring. Understanding and predicting the interface between metal ions and small molecules can have far reaching effects into the efficacy of drug development and oxidative-damage prevention in biological systems.

Chapter 1 reviews amino acid stability constants with the redox-active metal ions Cu(I), Cu(II), Fe(II), and Fe(III). Although reviews of metal-amino-acid complexes have been published previously, they tend to be data-heavy and make it difficult to identify the most pertinent data. In addition, few reviews have focused significant attention on sulfur- and selenium-containing amino acids. Chapter 1 is also intended to help elucidate the best methods to determine stability constants for each metal ion, based on solubility limitations and redox sensitivities.

The work in Chapter 2 focuses on the determination of stability constants for Cu(II) and Fe(II) with sulfur and selenium amino acids and identifies the species and most likely coordination modes for the complexes formed in these potentiometric titrations. $[CuL]^+$ and CuL_2 species, with stability constants of approximately 9 and 14, respectively, were determined for the amino acids glycine, methylcysteine, methionine, selenomethylcysteine, and selenomethionine. In all cases, only the amine nitrogen and the carboxylate oxygen atoms, but not the sulfur or selenium atom, are coordinated to Cu(II). For the same amino acids, the Fe(II) species $[FeL]^+$ and FeLOH were identified, with significantly lower stability constants of approximately 3 and -5, respectively.

Penicillamine, a thiol-containing amino acid, has significantly higher stability constants of approximately 7.5 and 14 for the FePen and $[Fe(Pen)]^{2-}$ species, due to direct coordination of the thiolate sulfur.

Reactions between copper and the thione methimazole, both redox-active species, are explored in Chapter 3. Cu(II) is reduced by methimazole to form Cu(I) and methimazole disulfide, and a wide variety of mono-, di-, and polynuclear copper complexes are formed with these two ligands. The effects of oxygen availability, oxidation states of the metal ion and ligand, and solvent on the reaction products is investigated. Under anaerobic conditions, the products favor direct coordination of Cu(I) with bridging and terminal methimazole ligands. In the presence of oxygen and water or methanol, sulfur extrusion from the oxidized methimazole ligand is favored. Direct coordination of methimazole disulfide to Cu(I) without sulfur extrusion occurs under air-free conditions, but this product is produced in low yield. Based on these results, a mechanism for sulfur extrusion is proposed that incorporates copper coordination, oxidation by O_2, and solvent reactivity.

In Chapter 4, the interactions of copper and methimazole explored in Chapter 3 are expanded to include the interactions of methimazole disulfides and diselenides with Cu(I). Dinuclear, mixed ligand Cu(I) complexes containing both reduced and oxidized methimazole or selenomethimazole ligands can be isolated, suggesting Cu(I)-mediated reversibility of disulfide or diselenide bond formation. When Cu(I) was treated with methimazole diselenide in air, two unusual products were crystallized from the same reaction solution. Selenium migration is observed in one complex, and reaction with the

dichloromethane solvent is observed in the other product. Methimazole and selenomethimazole show reversible redox reactivity and unique elimination and insertion reactions in the presence of copper. Sulfur- and selenium-containing amino acids and imidazole thiones and selones coordinate to softer metal ions, such as Cu(I), Cu(II), and Fe(II), and may have the potential to influence metal homeostasis, redox behavior, and biological activity of these ions.

1.13 Supplementary Data

Table 1.9. Parameters added to the visual Mintec database for Use with Geochemist Workbench to Generate the Fe(III) Solubility Models (Figure 1.11) and the Cu-penicillamine models (Figure 1.8)

Species	Reaction	log β	Reference
$[Fe(Met)]^{2+}$	$Fe(III) + Met^{-} \leftrightarrow [Fe(Met)]^{2+}$	9.1	[159]
$[Fe(Glu)]^{+}$	$Fe(III) + Glu^{2-} \leftrightarrow [Fe(Glu)]^{+}$	13.39	[188]
$[Fe(Phe)]^{2+}$	$Fe(III) + Phe^{-} \leftrightarrow [Fe(Phe)]^{2+}$	10.39	[179]
$[Fe(Phe)_2]^{+}$	$Fe(III) + 2\ Phe^{-} \leftrightarrow [Fe(Phe)_2]^{+}$	19.11	[179]
$Fe(Phe)_3$	$Fe(III) + 3\ Phe^{-} \leftrightarrow Fe(Phe)_3$	26	[179]
$[Cu(HPen)_2]^{3-}$	$Cu(I) + 2\ HPen^{2-} \leftrightarrow [Cu(HPen)_2]^{3-}$	39.18	[172]
$[Cu_5Pen_4]^{3-}$	$5\ Cu(I) + 4\ Pen^{3-} \leftrightarrow [Cu_5Pen_4]^{3-}$	101.5	[172]

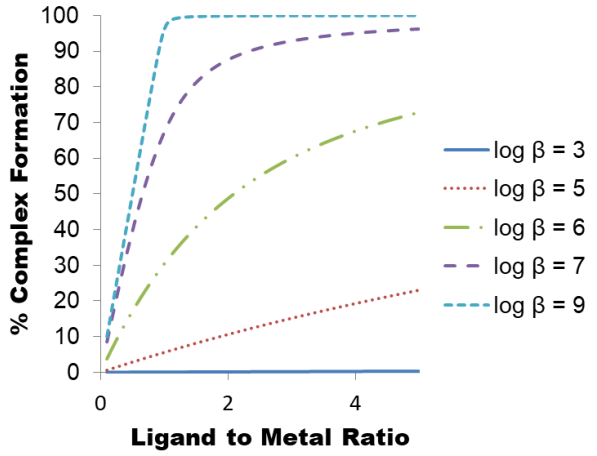

Figure 1.14. Percent complex formation for solutions containing 100 µM metal ion and 100-500 µM amino acid for the formation of the ML species. Formation constants for the amino acid (AA) of 9.2 for HAA and 11.28 for H_2AA were included in the modeling as a representative amino acid with amine and carboxylate protons.

1.14 References

(1) Andreini, C.; Bertini, I.; Cavallaro, G.; Holliday, G. L.; Thornton, J. M. *J. Biol. Inorg. Chem.* **2008**, *13*, 1205-1218.

(2) Hood, M. I.; Skaar, E. P. *Nat. Rev. Microbiol.* **2012**, *10*, 525-537.

(3) Keyer, K.; Imlay, J. A. *Proc. Natl. Acad. Sci. U. S. A.* **1996**, *93*, 13635-13640.

(4) Bolognin, S. M.; Zatta, P. *NeuroMol. Med.* **2009**, *11*, 223-238.

(5) Gillard, R.; Mason, R.; Payne, N. C.; Robertson, G. B. *J. Chem. Soc. A Inorg. Phys. Theor.* **1969**, *12*, 1864-1871.

(6) Rubino, J. T.; Riggs-Gelasco, P.; Franz, K. J. *J. Biol. Inorg. Chem.* **2010**, *15*, 1033-1049.

(7) Okada, M.; Miura, T. *J. Inorg. Biochem.* **2016**, *159*, 45-49.

(8) Sun, W.-Y.; Ueyama, N.; Nakamura, A. *Biopolymers* **1998**, *46*, 1-10.

(9) Roat-Malone, R. M. *Bioinorganic Chemistry*; John Wiley & Sons, Inc.: Hoboken, New Jersey, 2002.

(10) Jurado, R. L. *Clin. Infec. Dis.* **1997**, *25*, 888-895.

(11) Metcoff, J. *J. Am. Coll. Nutr.* **1986**, *5*, 107-120.

(12) Fukuda, K.; Nishi, Y.; Usui, T. *J. Pediatr. Gastroenterol. Nutr.* **1984**, *3*, 432-439.

(13) Stegink, L. D.; Filer, L. J.; Brummel, M. C.; Baker, G. L.; Krause, W. L.; Bell, E. F.; Ziegler, E. E. *Am. J. Clin. Nutr.* **1991**, *53*, 670-675.

(14) Rubino, F. M.; Pitton, M.; Di Fabio, D.; Meroni, G.; Santaniello, E.; Caneva, E.; Pappini, M.; Colombi, A. *Biomed. Chromatogr.* **2011**, *25*, 330-343.

(15) Burk, R. F.; Norsworthy, B. K.; Hill, K. E.; Motley, A. K.; Byrne, D. W. *Cancer Epidemiol. Biomarkers Prev.* **2006**, *15*, 804-810.

(16) Sarkar, B. *Chem. Rev.* **1999**, *99*, 2535-2544.

(17) Brewer, G. J.; Askari, F. K. *J. Hepatol.* **2005**, *42*, S13-S21.

(18) Muijsers, A. O.; van de Stadt, R. J.; Henrichs, A. M. A.; Ament, H. J. W.; van der Korst, J. K. *Arthritis Rheumatol.* **1984**, *27*, 1362-1369.

(19) Medici, V.; Di Leo, V.; Lamboglia, F.; Bowlus, C. L.; Tseng, S. C.; D'Inca, R.; Irato, P.; Burra, P.; Martines, D.; Sturniolo, G. C. *Scand. J. Gastroenterol.* **2007**, *42*, 1495-1500.

(20) Lyle, W. H.; Pearcy, D. F.; Hui, M. *Proc. R. Soc. Med.* **1977**, *70*, 48-49.

(21) Lippard, S. J.; Berg, J. M. *Principles of Bioinorganic Chemistry*; University Science Books: Mill Valley, 1994.

(22) Meneghini, R. *Free Radic. Biol. Med.* **1997**, *23*, 783-792.

(23) Mzhel'skaya, T. I. *Bull. Exp. Biol. Med.* **2000**, *130*, 719-727.

(24) Stockel, J.; Safar, J.; Wallace, A. C.; Cohen, F. E.; Prusiner, S. B. *Biochemistry* **1998**, *37*, 7185-7193.

(25) Gaggelli, E.; Kozlowski, H.; Valensin, D.; Valensin, G. *Chem. Rev.* **2006**, *106*, 1995-2044.

(26) Yang, L.; McRae, R.; Henary, M. M.; Patel, R.; Lai, B.; Vogt, S.; Fahrni, C. J. *Proc. Natl. Acad. Sci. USA* **2005**, *102*, 11179-11184.

(27) Au-Yeung, H. Y.; Chan, C. Y.; Tong, K. Y.; Yu, Z. H. *J. Inorg. Biochem.* **2017**, *177*, 300-312.

(28) Cotruvo, J. A., Jr.; Aron, A. T.; Ramos-Torres, K. M.; Chang, C. J. *Chem. Soc. Rev.* **2015**, *44*, 4400-4414.

(29) Verwilst, P.; Sunwoo, K.; Kim, J. S. *Chem. Commun.* **2015**, *51*, 5556-55571.

(30) Que, L. J.; Ho, R. Y. N. *Chem. Rev.* **1996**, *96*, 2607-2624.

(31) Griesmann, G. E.; Hartmann, A. C.; Farris, F. F. *Int. J. Environ. Health Res.* **2009**, *19*, 231-238.

(32) Jhurry, N. D.; Chakrabarti, M.; McCormick, S. P.; Holmes-Hampton, G. P.; Lindahl, P. A. *Biochemistry* **2012**, *51*, 5276-5284.

(33) Bellingham, S. A.; Guo, B.; Hill, A. F. *Biol. Cell* **2015**, *107*, 389-418.

(34) Mital, M.; Wezynfeld, N. E.; Fraczyk, T.; Wiloch, M. Z.; Wawrzyniak, U. E.; Bonna, A.; Tumpach, C.; Barnham, K. J.; Haigh, C. L.; Bal, W.; Drew, S. C. *Angew. Chem. Int. Ed. Engl.* **2015**, *54*, 10460-10464.

(35) Kawahara, A.; Tsukada, J.; Yamaguchi, T.; Katsuragi, T.; Higashi, T. *Biomark Res.* **2015**, *3*, 10.

(36) Robert, A.; Liu, Y.; Nguyen, M.; Meunier, B. *Acc. Chem. Res.* **2015**, *48*, 1332-1339.

(37) Jeuken, L. J.; Ubbink, M.; Bitter, J. H.; van Vliet, P.; Meyer-Klaucke, W.; Canters, G. W. *J. Mol. Biol.* **2000**, *299*, 737-755.

(38) Jeuken, L. C.; Camba, R.; Armstrong, F. A.; Canters, G. W. *J. Biol. Inorg. Chem.* **2002**, *7*, 94-100.

(39) Ambundo, E. A.; Ochrymowycz, L. A.; Rorabacher, D. B. *Inorg. Chem.* **2001**, *40*, 5133-5138.

(40) Ala, A.; Walker, A. P.; Ashkan, K.; Dooley, J. S.; Schilsky, M. L. *Lancet* **2007**, *369*, 397-408.

(41) Leone, N.; Courbon, D.; Ducimetiere, P.; Zureik, M. *Epidemiology* **2006**, *17*, 310-314.

(42) Ando, K.; Ogawa, K.; Misaki, S.; Kikugawa, K. *Free Radic. Res.* **2002**, *36*, 1079-1084.

(43) Rae, T. D.; Schmidt, P. J.; Pufahl, R. A.; Culotta, V. C.; O'Halloran, T. V. *Science* **1999**, *284*, 805-808.

(44) Prus, E.; Fibach, E. *Br. J. Haematol.* **2008**, *142*, 301-307.

(45) Wishart, D. S. *PLoS Comput. Biol.* **2012**, *8*, e1002805.

(46) Hallman, P. S.; Perrin, D. D.; Watt, A. E. *Biochem. J.* **1971**, *121*, 549-555.

(47) Kiss, T. S., I.; Gergely, A. *Pure Appl. Chem.* **1991**, *63*, 597-638.

(48) Dokmanic, I.; Sikic, M.; Tomic, S. *Acta Crystallogr., Section D.* **2008**, *64*, 257-263.

(49) Rigo, A.; Corazza, A.; di Paolo, M. L.; Rossetto, M.; Ugolini, R.; Scarpa, M. *J Inorg Biochem* **2004**, *98*, 1495-1501.

(50) Berthon, G. *Pure Appl. Chem.* **1995**, *67*, 1117-1240.

(51) Marques, M. C.; Tapia, C.; Gutierrez-Sanz, O.; Ramos, A. R.; Keller, K. L.; Wall, J. D.; De Lacey, A. L.; Matias, P. M.; Pereira, I. A. C. *Nat. Chem. Biol.* **2017**, *13*, 544-550.

(52) Suzuki, K. T. *J. Health Sci.* **2005**, *51*, 107-114.

(53) Battin, E. E.; Zimmerman, M. T.; Ramoutar, R. R.; Quarles, C. E.; Brumaghim, J. L. *Metallomics* **2011**, *3*, 503-512.

(54) Martell, W. R. S., R. K. *Critical Stability Constants, Standard Reference Database 46, Version 6.30*; National Institute of Standards: Gaithersburg, MD, 2001.

(55) Yamauchi, O.; Odani, A. *Pure Appl. Chem.* **1996**, *68*, 469-496.

(56) Pettit, L. D. *Pure Appl. Chem.* **1984**, *56*, 247-292.

(57) Sovago, I.; Kiss, T.; Gergely, A. *Pure Appl. Chem.* **1993**, *65*, 1029-1080.

(58) Beck, M. T. *Pure Appl. Chem.* **1977**, *49*, 127-135.

(59) Rossotti, F.; Rossotti, H. *The Determination of Stability Constants*; McGraw-Hill: New York, 1961.

(60) Beck, M. T.; Nagypal, I. *Chemistry of Complex Equilibria*; Ellis Horwood Ltd.: Chichester, 1989.

(61) Beck, M. T. *Chemistry of Complex Equilibria*; Akademiai Kiado: Budapest, 1969.

(62) Brookes, G.; Pettit, L. D. *J. Chem. Soc. Dalton Trans.* **1977**, *19*, 1918-1924.

(63) Anderegg, G. *Pure Appl. Chem.* **1982**, *54*, 2693-2758.

(64) Nancollas, G. H.; Tomson, M. B. *Pure Appl. Chem.* **1982**, *54*, 2675-2692.

(65) Braibanti, A.; Ostacoli, G.; Paoletti, P.; Pettit, L. D.; Sammartano, S. *Pure Appl. Chem.* **1987**, *59*, 1721-1728.

(66) Gergely, A. *Acta Chim. Acad. Sci. Hung.* **1969**, *59*, 309-318.

(67) Berthon, G.; Blais, M. J.; Piktas, M.; Houngbossa, K. *J. Inorg. Biochem.* **1984**, *20*, 113-130.

(68) Rao, A. L. J.; Singh, M.; Sanjiv, S. *Rev. Anal. Chem.* **1986**, *8*, 283-311.

(69) Stary, J.; Liljenzin, J. O. *Pure Appl. Chem.* **1982**, *54*, 2557-2592.

(70) Tuck, D. G. *Pure Appl. Chem.* **1983**, *55*, 1477-1528.

(71) Paoletti, P. *Pure Appl. Chem.* **1987**, *56*, 491.

(72) Bjernum *Metal Maine Formation in Aqueous Solutions*; Haas & Sons: Copenhagen, 1941.

(73) Calvin, M.; Wilson, K. W. *J. Am. Chem. Soc.* **1945**, *67*, 2003-2007.

(74) Fronaeus, S. *Acta Chem. Scand.* **1950**, *4*, 72-87.

(75) Sayce, I. G. *Talanta* **1968**, *15*, 1397-1411.

(76) Alderighi, L.; Gans., I.; Peters, D.; Sabatini, A.; Vacca, A. *Coord. Chem. Rev.* **1999**, *184*, 311-318.

(77) Gans, P.; Sabatini, A.; Vacca, A. *Talanta* **1996**, *43*, 1739-1753.

(78) Sabatini, A.; Vacca, A.; Gans, P. *Talanta* **1974**, *21*, 53-77.

(79) Tran-Ho, L. C.; May, P. M.; Hefter, G. T. *J. Inorg. Biochem.* **1997**, *68*, 225-231.

(80) Shah, S. K.; Gupta, C. M. *Talanta* **1980**, *27*, 823-824.

(81) Mercier, R. C.; Bonnet, M.; Paris, M. *Bull. Soc. Chim. France* **1965**, *10*, 2926-2932.

(82) Bonniol, A.; Vieles, P. *J. Chim. Phys.* **1968**, *65*, 414-420.

(83) Ramel, M. M.; Paris, M. R. *Bull. Soc. Chim. France* **1967**, *4*, 1359-1367.

(84) Singh, S.; Yadava, H. L.; Yadava, P. C.; Yadava, K. L. *Bull. Soc. Chim. France* **1984**, *11*, 349-352.

(85) Tewari, B. B. *Rev. Inorg. Chem.* **2003**, *23*, 349-357.

(86) Debye, P.; Huckel, E. *Phys. Z.* **1923**, *24*, 185-206.

(87) Tomita, K. *Bull. Soc. Chim. Jpn.* **1961**, *34*, 297-300.

(88) Konar, S.; Gagnon, K.; Clearfield, A.; Thompson, C.; Hartle, J.; Ericson, C.; Nelson, C. *J. Coord. Chem.* **2010**, *63*, 3335-3347.

(89) Davies, H.; Park, J.; Gillard, R. D. *Inorg. Chim. Acta* **2003**, *356*, 69-84.

(90) Casari, B. M.; Mahmoudkhani, A. H.; Langer, V. *Acta Crystallogr.* **2004**, *E60*, m1949-m1951.

(91) Arena, G.; Cali, R.; Cucinotta, V.; Musumeci, S.; Rizzarelli, E.; Sammartano, S. *J. Chem. Soc. Dalton Trans.* **1983**, *1983*, 1271-1278.

(92) Arbad, B. R.; Shelke, D. N.; Jahagirdar, D. V. *Inorg. Chim. Acta* **1980**, *46*, L17-L19.

(93) Ivicic, N.; Simeon, V. *J. Inorg. Nucl. Chem.* **1981**, *43*, 2581-2584.

(94) Shoukry, A. A. *J. Solution Chem.* **2011**, *40*, 1796-1818.

(95) Arbad, B. R.; Shelke, D. N.; Jahagirdar, D. V. *Inorg. Chim. Acta* **1980**, *46*, L17-L19.

(96) James, B. R.; Williams, R. *J. Chem. Soc.* **1961**, 2007-2019.

(97) Wojciechowska, A.; Gagor, A.; Jezierska, J.; Duczmal, M. *RSC Adv.* **2014**, *4*, 63150-63161.

(98) Arena, G.; Conato, C.; Contino, A.; Pulidori, F.; Purrello, R.; Remelli, M.; Tabbi, G. *Ann.Chim.***1998**, *88*, 1-12.

(99) Albert, A. *Biochem. J.* **1952**, *50*, 690-697.

(100) Jokl, V. *J. Chromatogr.* **1964**, *14*, 71-78.

(101) Tewari, B. B. *J. Mex. Chem. Soc.* **2008**, *52*, 219-223.

(102) Bretton, P. *J. Chim. Phys.* **1958**, *55*, 61-72.

(103) Davis, L.; Roddy, F.; Metzler, D. E. *J. Am. Chem. Soc.* **1961**, *83*, 127.

(104) Antolini, L.; Battaglia, L. P.; Bonamartini, C. A.; Marcotrgiano, G.; Menabue, L.; Pellacani, G. C.; Saladini, M.; Sola, M. *Inorg. Chem.* **1986**, *26*, 2901-2904.

(105) Ono, T. S., H.; Sasada, Y.; Sakurai, T.; Yamauchi, O.; Nakahara, A. *Bull. Soc. Chim. Jpn* **1979**, *52*, 2229-2234.

(106) Deschamps, P.; Kulkarni, P. P.; Sarkar, B. *Inorg. Chem.* **2004**, *43*, 3338-3340.

(107) Freeman, H. C.; Guss, J. M.; Healy, R. P.; Martin, C. E.; Nockolds, C. E.; Sarkar, B. *J. Chem. Soc. D* **1969**, 225-226.

(108) Abdel-Rahman, L. H.; Battaglia, L. P.; Sgarabotto, P.; Mahmoud, M. R. *J. Chem. Cryst.* **1994**, *24*, 567-571.

(109) Soylu, H.; Ulku, D.; Morrow, J. C. *Z. Kristallogr., Kristallgeom., Kristallphys., Kristllchem.* **1974**, *140*, 281-288.

(110) Brumas, V.; Alliey, N.; Berthon, G. *J. Inorg. Biochem.* **1993**, *52*, 287-296.

(111) Daniele, P.; Amico, P.; Ostacoli, G. *Ann. Chim.* **1984**, *74*, 105-116.

(112) Brumas, V.; Brumas, B.; Berthon, G. *J. Inorg. Biochem.* **1995**, *57*, 191-207.

(113) Pettit, L. D.; Swash, J. *J. Chem. Soc. Dalton Trans.* **1976**, *23*, 2416-2419.

(114) Lin, H.; Gu, Z.; Chen, X.; Chen, Y. *Thermochim. Acta* **1988**, *123*, 201-212.

(115) Barr, M. L.; Baumgartner, E.; Kustin, K. *J. Coord. Chem.* **1973**, *2*, 263-270.

(116) Zuberbuhler, A. *Helv. Chim. Acta.* **1970**, *53*, 669-675.

(117) Lin, H.-K.; Gu, Z.-Z.; Chen, X.-M.; Chen, Y.-T. *Thermochim. Acta* **1988**, *123*, 201-212.

(118) I, T. P.; Nancollas, G. *Inorg. Chem.* **1972**, *11*, 2414-2425.

(119) Shtyrlin, V. G.; Zyavkina, Y. I.; Gilyazetdinov, E. M.; Bukharov, M. S.; Krutikov, A. A.; Garipov, R. R.; Mukhtarov, A. S.; Zakharov, A. V. *Dalton Trans.* **2012**, *41*, 1216-1228.

(120) Gorboletova, G. G.; Metlin, A. A. *Russ. J. Phys. Chem.* **2015**, *A89*, 218-223.

(121) Doran, M. A.; Chaberek, S.; Martell, A. E. *J. Am. Chem. Soc.* **1964**, *86*.

(122) Sarkar, B.; Kruck, T. P. *Can. J. Chem.* **1967**, *45*, 2046-2049.

(123) Neumann, P. Z.; Sass-Kortsak, A. *J. Clin. Invest.* **1967**, *46*, 646-658.

(124) Abbaspour, A.; Kamyabi, M. A. *Anal. Chim. Acta* **2004**, *512*, 257-269.

(125) Yang, L.; Huang, Z.; Li, F. *J. Pept. Sci.* **2012**, *18*, 449-455.

(126) Voskoboinik, I.; Camakaris, J. *J. Bioenerg. Biomembr.* **2002**, *34*, 363-371.

(127) Lutsenko, S.; Efremov, R. G.; Tsivkovskii, R.; Walker, J. M. *J. Bioenerg. Biomembr.* **2002**, *34*, 351-362.

(128) Rubino, J. T.; Chenkin, M. P.; Keller, M.; Riggs-Gelasco, P.; Franz, K. J. *Metallomics* **2011**, *3*, 61-73.

(129) Sharma, V. K.; Millero, F. J. *J. Solution Chem.* **1990**, *19*, 375-390.

(130) Liu, J.; Chakraborty, S.; Hosseinzadeh, P.; Yu, Y.; Tian, S.; Petrik, I.; Bhagi, A.; Lu, Y. *Chem. Rev.* **2014**, *114*, 4366-4469.

(131) Ford, P. C.; Cariati, E.; Bourassa, J. *Chem. Rev.* **1999**, *99*, 3625-3647.

(132) Pickering, I. J.; George, G. N.; Dameron, C. T.; Kurtz, B.; Winge, D. R.; Dance, I. G. *J. Am. Chem. Soc.* **1993**, *15*, 9498-9505.

(133) Heaton, D. N.; George, G. N.; Garrison, G.; Winge, D. R. *Biochemistry* **2001**, *40*, 743-751.

(134) Ryde, U.; Olsson, M.; Pierloot, K. *Theor. Comput. Chem.* **2001**, *9*, 1-55.

(135) Tapiero, H.; Townsend, D. M.; Tew, K. D. *Biomed. Pharmacother.* **2003**, *57*, 386-398.

(136) Glass, R. S.; Singh, W. P.; Jung, W.; Veres, Z.; Scholz, T. D.; Stadtman, T. C. *Biochemistry* **1993**, *32*, 12555-12559.

(137) Ohta, Y.; Suzuki, K. T. *Toxicol. Appl. Pharmacol.* **2008**, *226*, 169-177.

(138) Lacourciere, G. M.; Stadtman, T. C. *Biofactors* **2001**, *14*, 69-74.

(139) Weekley, C. M.; Harris, H. H. *Chem. Soc. Rev.* **2013**, *42*, 8870-8894.

(140) Battin, E. E.; Brumaghim, J. L. *J. Inorg. Biochem.* **2008**, *102*, 3036-3042.

(141) Atmaca, G. *Yonsei Med. J.* **2004**, *45*, 776-788.

(142) Ip, C.; Ganther, H. E. *Carcinogenesis* **1992**, *13*, 1167-1170.

(143) Pezzini, A.; Del Zotto, E.; Padovani, A. *Curr. Med. Chem.* **2007**, *14*, 249-263.

(144) Zimmerman, M. T.; Bayse, C. A.; Ramoutar, R.; Brumaghim, J. L. *J. Inorg. Biochem.* **2015**, *145*, 30-40.

(145) Clark, L. C.; Dalkin, B.; Krongrad, A.; Combs, G. F., Jr.; Turnbull, B. W.; Slate, E. H.; Witherington, R.; Herlong, J. H.; Janosko, E.; Carpenter, D.; Borosso, C.; Falk, S.; Rounder, J. *Br. J. Urol.* **1998**, *81*, 730-734.

(146) Combs, G. F., Jr. *Br. J. Cancer* **2004**, *91*, 195-199.

(147) Lippman, S. M.; Klein, E. A.; Goodman, P. J.; Lucia, M. S.; Thompson, I. M.; Ford, L. G.; Parnes, H. L.; Minasian, L. M.; Gaziano, J. M.; Hartline, J. A.; Parsons, J. K.; Bearden, J. D., 3rd; Crawford, E. D.; Goodman, G. E.; Claudio, J.; Winquist, E.; Cook, E. D.; Karp, D. D.; Walther, P.; Lieber, M. M.; Kristal, A. R.; Darke, A. K.; Arnold, K. B.; Ganz, P. A.; Santella, R. M.; Albanes, D.; Taylor, P. R.; Probstfield, J. L.; Jagpal, T. J.; Crowley, J. J.; Meyskens, F. L., Jr.; Baker, L. H.; Coltman, C. A., Jr. *JAMA* **2009**, *301*, 39-51.

(148) Reid, M. E.; Duffield-Lillico, A. J.; Slate, E.; Natarajan, N.; Turnbull, B.; Jacobs, E.; Combs, G. F., Jr.; Alberts, D. S.; Clark, L. C.; Marshall, J. R. *Nutr. Cancer* **2008**, *60*, 155-163.

(149) Anderson, C. H.; Holwerda, R. A. *J. Inorg. Biochem.* **1985**, *23*, 29-41.

(150) Perrin, D. D.; Sayce, I. G. *J. Chem. Soc. A Inorg. Phys. Theor.* **1968**, *1*, 53-57.

(151) Pinto, L. D.; Puppin, P.; Behring, V. M.; Alves, O.; Rey, N.; Felcman, J. *Inorg. Chim. Acta* **2012**, *386*, 60-67.

(152) Lenz, G.; Martell, A. *Biochemistry* **1964**, *3*, 745-750.

(153) Israeli, M.; Pettit, L. D. *J. Inorg. Nucl. Chem.* **1975**, *37*, 999-1003.

(154) Sovago, I.; Petocz, G. *J. Chem. Soc., Dalton Trans.* **1987**, *7*, 1717-1720.

(155) Murphy, J. M.; Williams, T.; McMillen, C.; Powell, B. A.; Brumaghim, J. L. *Manuscript in preparation*.

(156) Kuchinkas, E. J.; Rosen, Y. *Arch. Biochem. Biophys.* **1962**, *97*, 370-372.

(157) Zainal, H.; Wolf, W. *Transition Met. Chem.* **1995**, *20*, 225-227.

(158) Konigsberger, L.-C.; Konigsberger, E.; Hefter, G.; May, P. M. *Dalton Trans.* **2015**, *44*, 20413-20425.

(159) Perrin, D. D. *J. Chem. Soc.* **1958**, 3125-3128.

(160) Ou, C.; Powers, D.; Thich, J.; Felthouse, T.; Hendrickson, D.; Potenza, J.; Schugar, H. *Inorg. Chem.* **1978**, *17*, 34-40.

(161) Veidis, M.; Palenik, G. *J. Chem. Soc. D* **1969**, *21*, 1277-1278.

(162) Dubler, E.; Cathomas, N.; Jameson, G. B. *Inorg. Chim. Acta* **1986**, *123*, 99-104.

(163) Hambley, T. W. *Acta. Crystallogr. Sect. B* **1988**, *44*, 601-609.

(164) De Meester, P.; Hodgson, D. J. *J. Chem. Soc., Dalton Trans.* **1976**, *7*, 618-621.

(165) Tessier, C.; Rochon, F. D.; Beauchamp, A. L. *Inorg. Chem.* **2004**, *43*, 7463-7473.

(166) Sheldrick, W. S.; Exner, R. *J. Organomet. Chem.* **1990**, *386*, 375-387.

(167) Balakaeva, T. A.; Churakov, A. V.; Ezernitskaya, M. G.; Kuz'mina, L. G.; Lokshin, B. V.; Efimenko, I. A. *Koord. Khim.* **1999**, *25*, 579-583.

(168) Wang, H. C.; Riahi, M.; Pothen, J.; Bayse, C. A.; Riggs-Gelasco, P.; Brumaghim, J. L. *Inorg. Chem.* **2011**, *50*, 10893-10900.

(169) Stricks, W.; Kolthoff, I. M. *J. Am. Chem. Soc.* **1951**, *73*, 1723-1727.

(170) Bagiyan, G. A.; Koroleva, I. K.; Soroka, N. V. *Zh. Neorg. Khim.* **1978**, *23*, 2422-2429.

(171) Mezyk, S. P.; Armstrong, D. A. *Can. J. Chem.* **1989**, *67*, 736-745.

(172) Oesterberg, R.; Ligaarden, R.; Persson, D. *J. Inorg. Biochem.* **1979**, *10*, 341-355.

(173) Hefter, G.; May, P. M.; Sipos, P. *Chem. Commun.* **1993**, 1704-1706.

(174) Bethke, C. *Geochemical and Biogeochemical Reaction Modeling*; Cambridge Press: Cambridge, 2008.

(175) Stadtman, T. C. *Annu. Rev. Biochem.* **1996**, *65*, 83-100.

(176) Dixon, S. J.; Stockwell, B. R. *Nat. Chem. Biol.* **2014**, *10*, 9-17.

(177) Wells, C. F.; Salam, M. A. *Nature* **1965**, *205*, 690-692.

(178) Magill, C. P.; Floriani, C.; Chiesi-Villa, A.; Rizzoli, C. *Inorg. Chem.* **1994**, *33*, 1928-1933.

(179) Williams, D. R.; Yeo, P. A. *J. Chem. Soc., Dalton Trans.* **1972**, *18*, 1988-1990.

(180) Perrin, D. D. *J. Chem. Soc.* **1959**, 290-296.

(181) Albert, A. *Biochem. J.* **1950**, *47*, 531-538.

(182) Kapoor, R. C.; Mathur, K. C. *J. Polarogr.* **1967**, *13*, 86-88.

(183) Baxter, A.; Williams, D. *J. Chem. Soc. Dalton Trans.* **1974**, *11*, 1117-1120.

(184) Williams, D. R. *J. Chem. Soc. Dalton Trans.* **1973**, 1064-1066.

(185) Gowda, R.; Venkatappa, M. *J. Electrochem. Soc. India* **1981**, *30*, 336-340.

(186) Williams, D. R. *J. Chem. Soc. A Inorg. Phys. Theor.* **1970**, *9*, 1550-1555.

(187) Raju, E. V.; Mathur, H. B. *J. Inorg. Nucl. Chem.* **1968**, *30*, 2181-2188.

(188) Djurdjevic, P.; Jelic, R. *Trans. Met. Chem.* **1997**, *22*, 284-293.

(189) Linder, M. C. *Nutrients* **2013**, *5*, 4022-4050.

(190) Girdhar, H. L.; Parveen, S.; Puri, M. K. *Indian J. Chem., Sect. A: Inorg., Bio-inorg., Phys., Theor. Anal. Chem.* **1976**, *14A*, 1021-1022.

(191) Doornbos, D. A.; Faber, J. S. *Pharm. Weekbl.* **1964**, *99*, 289-309.

(192) Tewari, B. B. *J. Chromatogr. A* **2002**, *962*, 233-237.

(193) Zucconi, T. D.; Janaeur, G. E.; Donahe, S.; Lewkowicz, C. *J. Pharm. Sci.* **1979**, *68*, 426-432.

(194) Muller, A.; Straube, M.; Krickemeyer, E.; Bogge, H. *Die Naturwissenschaften* **1992**, *79*, 323-325.

(195) Michaelis, L.; Guzman Barron, E. S. *J. Biol. Chem.* **1929**, *83*, 191-210.

(196) Sisley, M. J. *Inorg. Chem.* **1995**, *34*, 6015-6023.

(197) Leibnitz, P.; Reck, G.; Pietzsch, H.; Spies, H. *Forschungszentrum Rossendorf* **2001**, *FZR-311*, 1-311.

(198) Harris, W. R.; Sammons, R. D.; Grabiak, R. C. *J. Inorg. Biochem.* **2012**, *116*, 140-150.

CHAPTER TWO

STABILITY CONSTANT DETERMINATION OF SULFUR AND SELENIUM AMINO ACIDS WITH Cu(II) AND Fe(II)

2.1 Introduction

Despite the ubiquity and importance of amino acids in biological systems, very little is understood about coordination of labile (non-protein-bound) metal ions by free amino acids. Determining aqueous stability constants for metal ions with biologically relevant ligands, including amino acids, is one way in which more complex systems such as biological fluids or ocean water can be modeled. Fifty years ago, Hallman and coworkers simulated plasma speciation of Cu(II) and Zn^{2+} with seventeen amino acids,[1] but subsequent reviews and analysis of this plasma speciation model revealed deficiencies in the underlying stability constant data, since the importance of minor species and redox interactions were neglected.[2,3] More recently, amino acid stability constant data and speciation modeling have been used to help explain copper and zinc deficiencies that occur with total parenternal nutrition,[4] trace element speciation in phloem sap[5] and xylem fluid,[6] and copper speciation in the eye.[7] Developing more accurate Cu(I) speciation models with penicillamine, cysteine, and glutathione resulted in a better understanding of metallic copper precipitation in the lens and cornea in patients with Wilson's disease.[7] Development of these complex models relies heavily on the accuracy of measured metal-amino-acid stability constants, a particular issue with potentially redox-active sulfur- and selenium-containing amino acids.

Amino acid interactions with copper and iron may also play a crucial role in preventing oxidative damage and diseases that arise due to oxidative stress. Loss of metal homeostasis, mitochondrial malfunction, and the resulting oxidative stress is linked to neurodegenerative disease development, but the mechanistic details that cause this oxidative damage is poorly understood.[8-10] Labile copper and iron produce reactive oxygen species (ROS) such as hydroxyl radical that can damage nucleic acids, proteins, and lipids, and this oxidative damage is catalytic in cells (Figure 2.1).[11-13] Antioxidants capable of disrupting catalytic ROS generation through metal chelation may lessen the oxidative damage leading to Alzheimer's, Parkinson's, Huntington's, and Wilson's diseases.[14] To ascertain whether amino acid binding to copper and iron may affect their ability to generate ROS, several factors must be determined: the amino acids and other small molecules most likely to interact with labile metal ions, metal ion and amino acid concentrations in the system, and stability constants for the metal-amino-acid complexes.

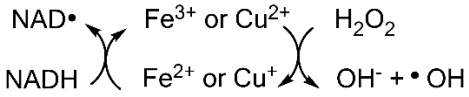

Figure 2.1. Catalytic hydroxyl radical generation by iron and copper in cells.

Naturally occurring and biomimetic sulfur and selenium amino acids with thioether/selenoether and thiol/selenol groups are of significant interest due to their abundance in the active sites of metalloenzymes, their presence in biofluids, and their affinity for binding softer metal ions, such as Cu(I), Cu(II), and Fe(II). A variety of sulfur and selenium amino acids are present naturally (Figure 2.2), including methionine (Met),

cysteine (Cys), methylcysteine (MeCys), homocysteine (hCys), selenomethionine (SeMet), selenocysteine (SeCys), and methylselenocysteine (MeSeCys). One of the most prevalent sulfur amino acids,[15] cysteine, has reported concentrations of 256 ± 15 μM in human plasma[16] and 180 ± 20 μM in muscle tissue.[17] Methionine has somewhat lower concentrations of 69 ± 15 μM[16] and 110 ± 20 μM[17] in plasma and muscle tissue, respectively. Normal levels of homocysteine (hCys) in plasma are in the 5 – 18 μM range,[18] and elevated hCys levels are an established risk factor for cardiovascular diseases, cognitive impairment, and chronic renal failure.[19-22] Methylcysteine is not typically used for protein synthesis, but is occasionally incorporated into proteins.[23] MeCys concentrations are not quantified in plasma or cells, but are found at concentrations of 0.2-5 μM in human urine.[24] Although not a natural amino acid, penicillamine (Pen; Figure 2.2) is structurally similar to cysteine and is used to chelate and remove excess copper in Wilson's disease.[25,26] When supplemented at 750 mg/day, penicillamine levels can reach 100 μM in human serum.[27]

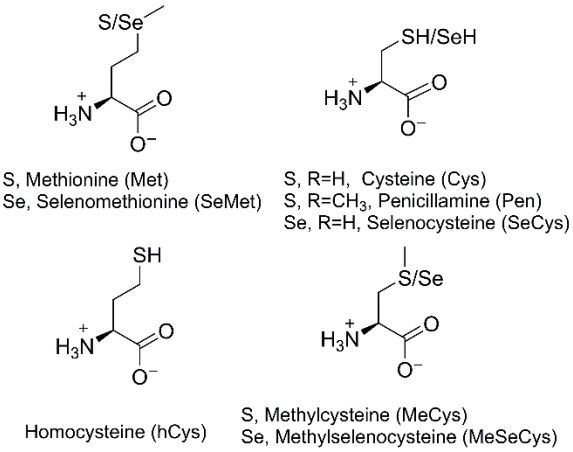

Figure 2.2. Structures of common sulfur- and selenium-containing amino acids.

Biological concentrations of selenium-containing amino acids are not determined, although total selenium concentration in human plasma averages 1.5-1.6 μM with 90% incorporated into selenoproteins as SeCys or SeMet.[28] In humans, total selenium concentration is unlikely to exceed 10 μM due to selenium toxicity.[29] SeCys is the most prevalent selenium amino acid in mammalian selenoproteins,[30] but it is difficult to study in solution because its low pK_a (~5) results in dimerization to form the oxidized diselenide species, selenocystine, at physiological pH.[31] In contrast, MeSeCys is the most abundant selenium metabolite in plants.[32] Although selenoamino acids are required for selenoprotein activity[33,34] and can prevent ROS damage,[35-37] their interaction with metal ions is not as widely studied as their sulfur-containing analogs.

Labile iron is typically found in low concentrations but increases when the cell is under oxidative stress.[38] In *Escherichia coli,* the concentration can rise from 20 μM under normal conditions up to 320 μM when stressed,[39] increasing cellular damage. Labile iron pools of up to 10 μM are present in human lymphocytes.[40] Iron accumulation in certain regions of the brain[41-43] is implicated in the pathology of Parkinson's disease.[44,45] Cellular labile copper pools have been identified but not precisely measured,[46,47] and total copper has been reported as high as 100 μM in brain tissue.[48,49] Labile copper causes increased protein aggregation in Alzheimer's disease, which may be a direct result of oxidative protein damage.[9,49,50]

Many researchers have examined the antioxidant activity of sulfur- and selenium-amino acids,[51-56] and Brumaghim, et al.[37,57] established metal binding as a primary antioxidant mechanism for sulfur- and selenium-amino acid prevention of *in vitro* metal-

mediated oxidative DNA damage. Structural analyses and density functional theory determinations established that the HOMO orbital energies of copper-amino-acid complexes predict the observed antioxidant activity.[58,59] However, it is not clear if the stabilities of these amino-acid-metal complexes also correlate with DNA damage prevention ability. Such an analysis is critically hampered by the lack of stability constants for these amino acids with Cu(II) and Fe(II). To test this hypothesis, we determined stability constants for Cu(II) and Fe(II) with sulfur- and selenium-amino acids by potentiometric titration. In addition, metal binding modes of these amino acids with Cu(II) a predicted based on speciation trends, infrared (IR) spectroscopy, mass spectrometry, and solid-state structural determination. We use these measured stability constants and reported metal ion and amino acid concentrations, to discuss the likelihood of metal-amino-acid complex formation in biological systems. This work was a collaborative work. Andrea Gaertner completed the IC_{50} gel electrophoresis analysis of copper and iron with penicillamine. Tyler Williams performed the ESI-MS analyses of Cu(II) and Fe(II) with methionine in solution. Colin D. McMillen determined the XRD determination of $Cu(SeMet)_2$. Brian A. Powell provided expertise in the advisement of potentiometric titrations and stability constant determination.

2.2 Results and Discussion

Stability constants measure the thermodynamic likelihood of metal complex formation (Equations 1 and 2) and are directly related to the Gibbs free energy of a system (Equation 3). A positive log β indicates favorable thermodynamic stability for complex

formation. In this study, potentiometric titrations for multiple metal:ligand molar ratios at 25 °C and pH 3-9 were used to determine stability constants of sulfur and selenium amino acids (L) with Cu(II) and Fe(II) (M), where x is the stoichiometric number of complexing ligands.

$$M + x\,L \rightleftharpoons ML_x \quad (1)$$

$$\beta_{ML} = \frac{[ML_X]}{[M][L]^X} \quad (2)$$

$$\Delta G = -2.30RT\log\beta_{ML} \quad (3)$$

Amino Acid Protonation Constant Determination

Protonation constants for Gly, Met, SeMet, MeCys, and MeSeCys were determined prior to titrations with metal ions. Although several of these amino acids have established protonation constants, precise determinations of these values under the exact conditions of temperature, ionic strength, and ionic salt used for the Cu(II) and Fe(II) titrations were required to ensure consistency and accuracy across all measurements (Table 2.1). The data agree well with previously reported values, with minor variations due slightly different analysis conditions, such as the solution composition or concentration. Speciation diagrams for glycine and the thio- and selenoether amino acids, such as the example speciation diagram for Met (Figure 2.3), indicate that three separate species (L^-, LH, and LH_2^+) form from pH 3 to 11, with the zwitterionic LH species as the primary species at pH 7.

Table 2.1. Amino acid protonation constants; amine protonation is represented by K_1 and carboxylate protonation by K_2.

Amino Acid	log K_1[a]	log K_2[b]	Temp (˚C)	Ionic Strength	Reference
Gly	9.67(2)	2.28(5)	25	0.1 M $NaClO_4$	This work
Gly	9.62	2.43	25	0.2 M $NaClO_4$	[60]
Met	9.196(5)	2.09(1)	25	0.1 M $NaClO_4$	This work
Met	9.12	2.22	25	0.2 M KCl	[61]
SeMet	9.29(2)	2.05(1)	25	0.1 M $NaClO_4$	This work
SeMet	9.15	2.37	25	0.1 M $NaNO_3$	[62]
MeCys	8.79(2)	2.02(5)	25	0.1 M $NaClO_4$	This work
MeCys	8.72	2.2	25	0.2 M KCl	[61]
MeSeCys	8.86(2)	2.3(2)	25	0.1 M $NaClO_4$	This work

[a] log K_1= $[L^-][H^+]/[HL]$ [b] log K_2 = $[HL][H^+]/[H_2L^+]$

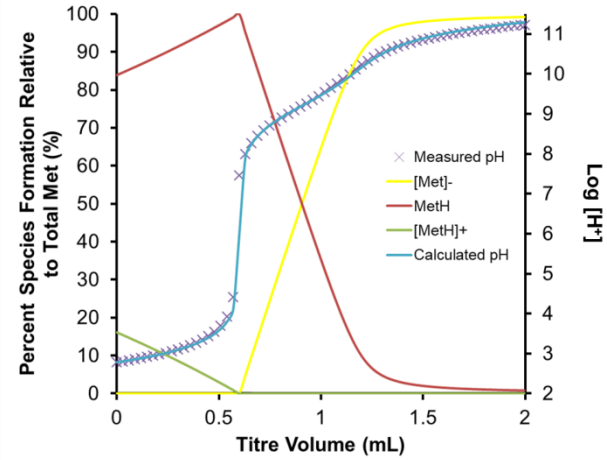

Figure 2.3. Representative titration and speciation diagrams for the potentiometric titration of the fully protonated amino acids (LH_2 with Met shown in this example; 0.1 M NaOH, I = 0.1 M $NaClO_4$, 25˚C). The solid blue line represents the modeled titration data with points indicating measured data (pH on the right y-axis); formation of Met^-, MetH, and $MetH_2^+$ species are indicated as shown in the legend.

Glycine has the highest log K_1 values compared to the thio- and selenoether amino acids, indicating the amine proton is less likely to dissociate. These data represent the first reported protonation constants for methylselenocysteine. Structurally similar MeCys and MeSeCys have the lowest log K_1 values, indicating amine deprotonation at lower pH. MeCys and MeSeCys protonation constants are also in close agreement, 8.79(2) and 2.02(5) for log K_1 and 8.86(2) and 2.3(2) for log K_2, respectively, indicating that selenium substitution for sulfur has no significant effect on amine or carboxylate protonation. The carboxylate dissociation constant (log K_2) is similar for all amino acids (2.02 to 2.3), and thus the carboxylate group is deprotonated at biologically relevant pH values.

Cu(II)-Amino Acid Stability Constants

Cu(II) stability constants with the sulfur-containing amino acids have been widely studied,[1,3,4,61,63-74] due to their bioavailability and their role in metal coordination in metalloproteins. Two species are identified, $[CuL]^+$ and CuL_2, where L^- represents the amino acid with both amine and carboxylate groups deprotonated. For Met, SeMet, MeCys, and MeSeCys, the S/Se atom in the side chain can potentially bind Cu(II) in addition to the amine N and carboxylate O atoms, resulting in a tridentate species. Such tridentate binding occurs for Cu(II)-amino acid complexes such as $Cu(His)_2$ (His = L-histidine),[75] and $[Cu(Asp)(phen)(H_2O)]$ (Asp = aspartic acid; phen = 1,10-phenanthroline).[76] Glycine is well known to bind Cu(II) in a bidentate fashion[77] but cannot bind through the side chain to become a tridentate chelator; therefore, it was included in this study as a bidentate-binding control. If the thio- or selenoether S/Se atom participates in tridentate binding to Cu(II), higher stability constants are expected compared to those of the Cu(II)-glycine system.

Cu(II) stability constants were determined for Gly, Met, SeMet, MeCys, and MeSeCys at 25˚C with a constant ionic strength of 0.1 M $NaClO_4$ to provide a self-consistent data set. Titrations were performed in triplicate at metal-to-ligand ratios of 1:2 and 1:5, and stability constants describing metal-ligand binding are provided in Table 2.2. For all the Cu(II) titrations, precipitation occurred above pH 8, except for the Cu(II)-SeMet system in which precipitation began at pH 5. A representative speciation graph for the Cu(II)-Met titrations at a 1:2 Cu:amino acid ratio is provided in Figure 2.4.

Only two species are present at pH 7, $[CuMet]^+$ and $Cu(Met)_2$ (Figure 2.4), and the $Cu(Met)_2$ species reaches a maximum concentration around pH 8, approximately the pH that precipitation occurs. When the full data set (pH 2-10) was included in the modeling, incorporation of a third species, Cu(Met)(OH), produced a better fit (Figure 2.9); however, this species was excluded from the analysis because its log β value was extremely low. Since this putative Cu(Met)(OH) species forms at pH 8 and above, it is more likely that deviation in the fit reflects the instability of the system as Cu(II) and Met^- are depleted due to precipitation, rather than the presence of a new species. The precipitate was confirmed as $Cu(Met)_2$ by IR analysis (see *Proof of Speciation for Cu(II) Complexes* section). All the thio- and selenoether amino acids as well as glycine form the same $[CuL]^+$ and CuL_2 species.

Table 2.2. Stability constants for Cu(II)- amino acid complexes determined by potentiometric titration

Amino Acid	ML ($\log \beta$)[a]	ML_2 ($\log \beta_2$)[b]	MLOH ($\log \beta_{-1}$)[c]	Temp (°C)	Ionic Strength (M)	Reference
Cu(II) Stability Constants						
Gly	8.11	14.96		25	0.1	[78]
	8.26(1)	15.10(5)		25	0.1 $NaClO_4$	This work
Met	7.85(2)	14.52(1)		25	0.1 KNO_3	[67,69,79]
	7.96(5)	14.65(7)		25	0.1 $NaClO_4$	This work
MeCys	7.65[d]	14.13[d]		25	0.2 KCl	[80]
	8.05(5)	14.47(5)		25	0.1 $NaClO_4$	This work
SeMet	7.77[d]	14.50[d]		25	0.1 $NaNO_3$	[62]
	8.02(2)	14.63(2)		25	0.1 $NaClO_4$	This work
MeSeCys	8.2(1)	14.5(2)		25	0.1 $NaClO_4$	This work
hCys	11.92(1)	13.54(2)[e]	7.57(1)	25	0.1 KNO_3	[81]
Pen	16.5[d]	21.7[d]		25	0.15 KNO_3	[82]
Fe(II) Stability Constants						
Gly	4.13[d]	7.65[d]		25	0.1 KNO_3	[83]
	4.04(5)		-4.24(2)	25	0.1 $NaClO_4$	This work
Met	3.24[d]			20	1.0 KCl	[84]
	3.51(3)		-4.9(1)	25	0.1 $NaClO_4$	This work
MeCys	3.49(4)		-5.7(1)	25	0.1 $NaClO_4$	This work
SeMet	3.51(7)		-5.3(3)	25	0.1 $NaClO_4$	This work
MeSeCys	3.84(1)		-5.08(2)	25	0.1 $NaClO_4$	This work
Cys	6.69(2)	11.90(3)		20	0.1 $NaClO_4$	[85]
Pen	7.58(1)	13.74(2)		20	0.1 $NaClO_4$	[85]
	7.48(7)	13.91(7)		25	0.1 $NaClO_4$	This work

[a] $\log \beta = [M][L]/[ML]$ [b] $\log \beta_2 = [M][L^2]/[ML^2]$ [c] $\log \beta_{-1} = [ML][OH]/[MLOH]$ [d] No error reported.
[e] Reported as the $[MHL]$ species, not the $[ML_2]$ species.

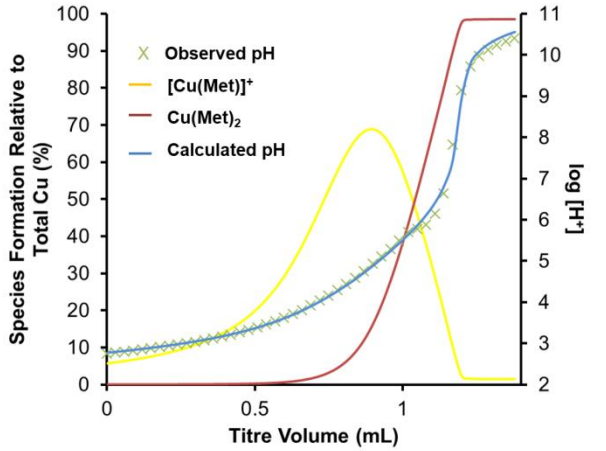

Figure 2.4. Representative titration and speciation diagram for the potentiometric titration of Cu(II) and methionine in a 1:2 metal-to-ligand ratio (0.1 M NaOH, I = 0.1 M $NaClO_4$, 25°C. The solid blue line represents the modeled titration and points represent the measured data. Formation of $[Cu(Met)]^+$ and $Cu(Met)_2$ species are indicated as shown in the legend.

Proof of Speciation for Cu(II) Complexes

Speciation in the Cu(II)-thio- and selenoether amino acid systems was confirmed using a variety of solution and solid-state analyses. For the soluble Cu(II)-Met species, electrospray ionization mass spectrometry (ESI-MS) confirmed the presence of $[Cu(Met)]^+$ (212 *m*/*z*). The Cu(Met)(OH) (230 *m*/*z*) species was also identified; however, the samples were prepared at pH 5, well below the pH where modelling indicates possible formation of this species. Thus, this species is most likely arises from water coordination of the $[Cu(Met)]^+$ species. Since Gly, Met, SeMet, MeCys, and MeSeCys all have Cu(II) stability constants within 0.5 log units, the resulting species are assumed to bind Cu(II) similarly.

Above pH 8, the Cu(II)-amino-acid complexes precipitated, and IR spectroscopy was used to confirm CuL_2 formation of the species and to compare with reported spectra (Table 2.3).[62,86-88] For $Cu(Met)_2$ and $Cu(SeMet)_2$, broad N-H stretching absorption bands at 3077 and 3080 cm^{-1} for Met and SeMet, respectively, split into three distinct stretching

vibrations for the corresponding Cu(II) complexes: 3300, 3241, and 3120 cm^{-1} for the Met complex and 3281, 3233, and 3132 cm^{-1} for the SeMet analog. This N-H splitting confirms participation of the amine nitrogen in Cu(II) binding, since the environment of the amine protons change slightly to compensate for the loss of freedom due to the proximity of the copper ion.[62] Amine binding is further supported by a N-H deformation band that appears at 1569 cm^{-1} for Met and 1570 cm^{-1} for SeMet. Carboxylate oxygen binding is also indicated by the shift of the asymmetric C-O stretch from approximately 1610 cm^{-1} to 1622 and 1616 cm^{-1} for the Met and SeMet complexes, respectively.[62,87] M-N and/or M-O bond formation is also indicated by the presence of one or two absorbances in the 440-600 cm^{-1} region.

IR results for MeCys and MeSeCys are consistent with the trends observed with the aforementioned Met and SeMet, although the C=O stretch observed at approximately 1620 cm^{-1} for the other complexes was shifted to 1640 cm^{-1} for the MeSeCys and no discernible NH_2 deformation was observed. Trends observed in the IR spectrum of $Cu(MeSeCys)_2$ can help confirm that the same structural confirmations are being formed in the binding of the $[MeSeCys]^-$ ligand to the Cu(II) as has been shown with the other thio- and selenoether amino acids. The stability constants indicate similar coordination for all of the thio- and seleno-ether amino acids.

Table 2.3. IR data for metal-amino-acid complex precipitates in potentiometric titrations (pH > 8; NR = not reported)

Vibration	**$Cu(Met)_2$**[86] (cm^{-1})	**$Cu(Met)_2$**[a] (cm^{-1})	**$Cu(MeCys)_2$**[87] (cm^{-1})	**$Cu(MeCys)_2$**[a] (cm^{-1})	**$Cu(SeMet)_2$**[a] (cm^{-1})	**$Cu(MeSeCys)_2$**[a] (cm^{-1})	**$Fe(Met)_2$**[a] (cm^{-1})
NH_2 stretching	3390 3230 3130	3300 3241 3120	3300 3230 2990	3299 3232 3110	3281 3233 3132	3322 3221 3130	3410 3360 3289
C=O stretch	1620	1622	1620	1618	1616	1640	1598
NH_2 deformation	1580	1569	1570	1571	1570	1571	1562
C-N vibration	NR	1337	NR	1340	1399	1335	1330
M-N and/or M-O stretch	NR	578	NR	576	497	521	568

[a] This work

Amine nitrogen and carboxylate oxygen coordination to Cu(II) is strongly supported by the solid-state structure of $Cu(SeMet)_2$ (Figure 2.5 and Table 2.4), the first structure for a Cu(II)-seleno amino acid complex. In $Cu(SeMet)_2$, each SeMet ligand coordinates the copper ion through bidentate binding of nitrogen and oxygen atoms in the equatorial position, resulting in an overall distorted square planar geometry (τ_4 = 0.043) around Cu(II) (Cu-N = 1.980(6) and 1.992(6) Å; Cu-O = 1.950(5) and 1.954(5) Å). This is similar to the thioether complexes $Cu(Met)_2$ (Cu-N = 1.97(1) and 2.01(1) Å; Cu-O = 1.944(8) and 1.970(8) Å)[86,89] and $Cu(MeCys)_2$ (Cu-N = 1.994 and 2.000 Å; Cu-O = 1.936(1) and 1.951(1) Å).[87] All other bond lengths and angles are comparable to those in the $Cu(Met)_2$ structure reported by Ou and coworkers,[86] with the exception of a slight lengthening in the carbon-chalcogen bonds, averaging 1.950(9) for the C-Se bonds in the present study compared to 1.80(2) Å for the C-S bonds in $Cu(Met)_2$. This lengthening also results in a slightly longer *c*-axis of the selenoether complex (16.082(1) Å) compared to the thioether complex (15.563(8) Å).

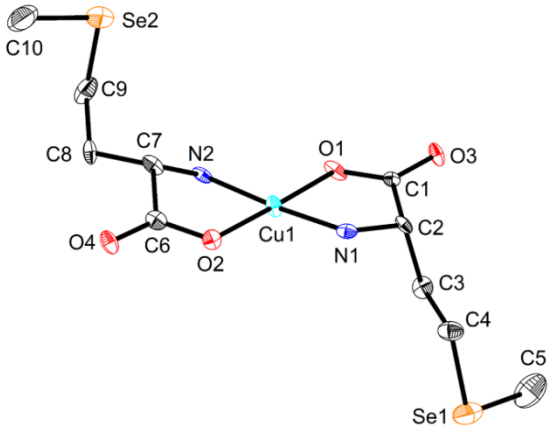

Figure 2.5. Structure of $Cu(SeMet)_2$ shown with 70% probability ellipsoids for $Cu(SeMet)_2$. Hydrogen atoms are omitted for clarity.

Table 2.4. Selected bond lengths (Å) and angles (°) for $Cu(SeMet)_2$

$Cu(L\text{-}SMet)_2$	**Bond lengths (Å)**		**Angles (°)**
Cu1-N1	1.992(6)	O2-Cu1-O1	178.3(2)
Cu1-N2	1.980(6)	O2-Cu1-N2	84.4(2)
Cu1-O1	1.954(5)	O1-Cu1-N2	94.8(2)
Cu1-O2	1.950(5)	O2-Cu1-N1	96.2(2)
Cu1-O4[a]	2.640(4)	O1-Cu1-N1	84.4(2)
Cu1-O3 [a]	2.687(4)	N2-Cu1-N1	175.5(2)
C4-Se1	1.952(7)	C4-Se1-C5	98.4(3)
C5-Se1	1.953(9)	C10-Se2-C9	98.5(4)
C9-Se2	1.958(7)		
C10-Se2	1.939(9)		

[a] Cu1-O3 and Cu1-O4 represent the carboxylate-bridged, apical bond distances in the packing diagram (Figure 2.8).

Carboxylate oxygen atoms from neighboring molecules form axial bonds to the Cu centers with extended copper-oxygen bond lengths of 2.640(4) and 2.687(4) Å, significantly longer than the equatorial carbon-oxygen bonds of 1.950(5) and 1.954(5) Å. These apical interactions result in the formation of sheets in the *ab*-plane (Figure 2.10). Hydrophobic intermolecular interactions of the Se-CH_3 side chains isolate neighboring sheets from one another along the *c*-axis. The structures of $Cu(Met)_2$ and $Cu(MeCys)_2$ also crystallize in space group $P2_1$ and feature similar long range motifs directed by the axial interactions of Cu(II) with carboxylate groups (though in the case of $Cu(MeCys)_2$, the sheets occur in the *bc*-plane, and the β angle is expanded somewhat to 97.55(2)°.[86,87,89]

Similar elongated Cu-carboxylate axial interactions are observed in Cu(II)-glycine-based structures;[90,91] however, some Cu(II)-glycine structures instead incorporate one[92-95] or two[77] water molecules in the axial positions. This water coordination in the solid state suggests that Cu(II) would likely be hydrated in solution, especially for $[Cu(Met)]^+$ and similar amino acid species with open coordination sites around the central metal ion. Water coordination at pH < 7 also suggests formation of species with hydroxide ligands at pH >

7, although these species may not be readily identifiable in titrations due to complex precipitation.

Structure-Stability Analysis for Cu(II)

Cu(II)-MeSeCys stability constants are reported for the first time as 8.2(1) and14.5(2) for the $[Cu(MeSeCys)]^+$ and $Cu(MeSeCys)_2$ species, respectively (Table 2.2). The higher error for these MeSeCys titrations relative to other thio- and selenoether amino acid values is likely due to interactions of the soft selenoether species with the electrode. To mitigate this issue, MeSeCys titrations were back-titrated to demonstrate reversibility. Cu(II)-MeSeCys stability constants are within 0.5 log units of those for the other thioether and selenoether amino acids, suggesting similar binding modes.

Stability constants of Cu(II) with Met, SeMet, and MeCys are within 0.2 log units for the $[ML]^+$ species (7.96(5) to 8.05(5) and ML_2 species (14.47(5) to 14.65(7)), although they are slightly higher than other reported results (Table 2.2), indicating little difference in Gly, Met, MeCys, and SeMet thermodynamic stability upon Cu(II) binding. Small variations in these values are likely due to differences in supporting electrolyte or in time allowed for the titrations to reach equilibrium. The greater relative stability of Cu(II) binding to Gly compared to thioether and selenoether amino acids corroborates the solid-state results that show no Cu(II)-S/Se interactions and suggests that the thio- and selenoether side chains slightly destabilize these complexes in solution.

Cu(II) complexes of thiol-containing amino acids are more stable than their thio- and selenoether counterparts (Table 2.2). In contrast to the thio- and selenoether functional

groups, thiols have ionizable protons and thiol-containing amino acids have four possible protonation states: $[H_3L]^+$, $[H_2L]$, $[HL]^-$, and L^{2-}. To date, no selenol copper stability constants have been reported, likely due to the low pK_a of selenols (~5) and the resulting tendency to form diselenide species.[31] In potentiometric titrations with Cu(II), both homocysteine (hCys) and penicillamine (Pen) form CuL species (Table 2.2),[81,82] and Rosen and Kuchinkas[82] also identified a $[Cu(Pen)_2]^{2-}$ species.

Other reported Cu(II) complexes of thiol-containing amino acids are not consistent; Pinto and coworkers[81] identified $[Cu(HhCys)]^+$ and [Cu(hCys)(OH)] species in a potentiometric titration of a 1:1 Cu(II) to hCys (to prevent Cu(II)oxidation of hCys) and identified $Cu(hCys)_2$ as a precipitate at higher ligand-to-metal ratios. Based on our model simulations using the stability constant values reported by Pinto, *et al.*,[81] the Cu(hCys)(OH) species is the dominant species above pH 4, with no evidence for formation of the $[Cu(HhCys)]^+$ species under the given experimental conditions. Solid-state analysis of $Cu(hCys)_2$ by IR and EPR spectroscopy indicated bidentate Cu(II) coordination of the amine and thiolate groups, with no binding of the carboxylate group.

In contrast, tridentate Cu(II) coordination in the solid state is reported for penicillamine, and in a unique polymeric structure supported by a gold-bis(diphenylphosphino)alkane linker, Cu(II) coordinates two penicillamine ligands, one in a tridentate fashion through the amine, carboxylate, and thiolate groups, and one in a bidentate fashion through only the amine and thiolate.[96] Higher stability constants for the thiol-containing amino acids with Cu(II) indicate increased stability compared to thioether and selenoether amino acids and glycine, either due to increased stability of an amine and

side-chain thiolate coordination or tridentate chelation of the copper by the carboxylate, amine, and thiolate groups.

Fe(II)-Amino Acid Stability Constants

Even though iron is the most abundant transition metal ion in the biological system, stability constant data for Fe(II) with sulfur and selenium amino acids is much more limited than for Cu(II). Since Fe(II) is more difficult to work with due to its tendency to oxidize in air, titrations must be performed under nitrogen or argon to exclude oxygen during analysis. In addition to oxygen sensitivity, Fe(II)-amino acid complexes precipitate above pH ~8, limiting the analysis window for potentiometric titrations. Likely because of these limitations, Met is the only thio- or selenoether amino acid with reported Fe(II) stability constants,[63,97] and data from these 1950s papers are inconsistent. Perrin[97] reports a stability constant of 3.42 for a $[Fe(Met)]^+$ species; however, Albert[63] reports formation of a $Fe(Met)_2$ species with a stability constant of 6.7. In neither study were the identified species investigated using alternative methods.

To address the paucity of Fe(II) stability constant data with sulfur and selenium amino acids, potentiometric titrations of Fe(II) with Met, MeCys, SeMet, MeSeCys, and penicillamine (Pen) at a 1:2 and 1:5 metal to ligand ratio were performed in a nitrogen-atmosphere glovebox. Similar to the Cu(II) studies, glycine titrations with Fe(II) were performed for comparison. Because precipitation is observed above pH 8, with the exception of the Fe(II)-Pen system that shows no precipitation up to pH 10, titrations were restricted to a maximum of pH 8. These titrations indicate formation of $[FeL]^+$ and

Fe(L)(OH) complexes with Gly, Met, SeMet, MeCys, and MeSeCys (Figure 2.6A and Table 2.2). In contrast, Fe(II) titrations with thiol-containing Pen indicate formation of Fe(Pen) and $[Fe(Pen)_2]^{2-}$ species (Figure 2.6B) in excellent agreement with previous analyses.[85]

Stability constants for the 1:1 $[Fe(Gly)]^+$ and $[Fe(Met)]^+$ agree with previously reported data (Table 2.2).[83,84,97-99] For Gly titrations, Gergely[83] also identifies a $Fe(Gly)_2$

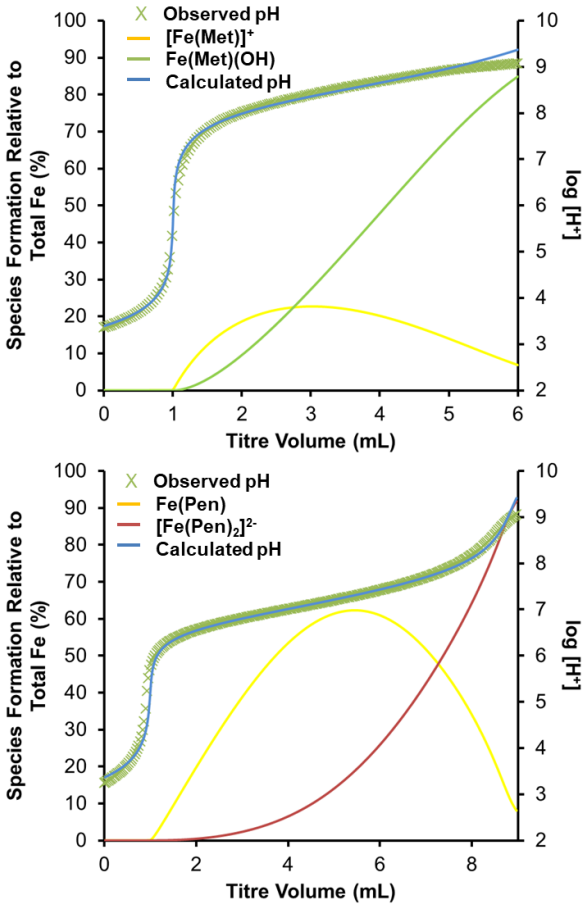

Figure 2.6. Representative titrations (0.1 M NaOH, I = 0.1 M NaCl, 25˚C) and speciation diagrams for the titration of A) Fe(II) and methionine in a 1:2 ratio and B) Fe(II) and penicillamine in a 1:2 ratio. The solid blue line represents the modeled titration, and points represent the measured data. Formation of Fe(II)-amino-acid species are indicated as shown in the legend.

species with a log β of 7.65, whereas Micskei[99] identifies two additional species, $Fe(Gly)_2$ with a log β of 6.65(1) and $[Fe(Gly)_3]^-$ with a log β of 8.87(1). Under our titration conditions, these $Fe(Gly)_2$ and $[Fe(Gly)_3]^-$ species are not present; instead, a Fe(Gly)(OH) species is observed with a stability constant of -4.24(2). In Met titrations, a similar Fe(Met)(OH) species is also identified, but the $Fe(Met)_2$ species reported by Albert is not.[63] Due to a lack of reported detail, it is unclear how these titrations differ from the analysis by Albert, although the authors of these studies included data above the pH at which precipitation begins to occur, perhaps skewing the fit of their models.

Stability constants for the 1:1 species of Fe(II) with MeCys, SeMet, and MeSeCys were determined to be 3.49(4), 3.51(7), and 3.84(1), respectively (Table 2.2), representing the first stability constant determinations for Fe(II) with these amino acids. These $[FeL]^+$ stability constants are similar to those for $[Fe(Gly)]^+$ (3.73(1)) and $[Fe(Met)]^+$ (4.13).[83,84] As noted for the Cu(II) titrations, the $[Fe(Gly)]^+$ stability constant is slightly higher than those for any of the thio- or selenoether amino acids, likely indicating no Fe(II)-S/Se binding. In contrast to previous reports, presence of the Fe(L)(OH) species (L = Met, SeMet, MeCys, MeSeCys) is identified in the best fit model for these systems, with this species growing in above pH 4 as hydroxide becomes more readily available.

For Fe(II) titrations with the thiol-containing penicillamine, the [FePen] and $[Fe(Pen)_2]^{2-}$ species are present, with stability constants of 7.48(7) and 13.91(7), respectively, closely matching results reported by Doornbas[85] in 1964 (Table 2.2). The lack of precipitation in this system up to pH 10 is due to strong Fe(II)-thiolate interactions as well as the greater charge of $[Fe(Pen)_2]^{2-}$ that makes it more soluble in aqueous solution

than the $[Fe(L)]^+$ species formed with the thio- and selenoether amino acids. These speciation differences in the Fe(II)-Pen and Fe(II)-Met systems are obvious when comparing their respective titration data (Figure 2.6) . In fact, Fe(II)-Pen complexes are slightly more stable than Fe(II)-Cys complexes (Table 2.2).

Proof of Speciation for Fe(II) Complexes

Proof of speciation using mass spectrometry was more difficult for the representative Fe(II)-Met system than for the analogous Cu(II)-Met system, likely due to the weaker stability constants determined for the Fe(II) species. By ESI-MS only the Fe(III) species, $[Fe(Met)_2]^+$ (m/z = 353), is observed due to Fe(II) oxidation during injection and analysis. Precipitate formed during Fe(II)-Met titrations was analyzed using IR spectroscopy to determine amino acid binding modes as a representative sample of the Fe(II)-thioether and –selenoether interactions. As discussed in detail for the Cu(II)-amino acid complexes, shifts in both the N-H and C=O stretches for $Fe(Met)_2$ (Table 2.3) compared to unbound Met indicate Fe(II) coordination through both the amine nitrogen and the carboxylate oxygen atoms, similar to the IR spectrum of the fully characterized $Cu(Met)_2$. In addition, the absence of a broad absorption in the 3500-3700 cm^{-1} range indicates that no hydroxide or water is coordinated. The Fe(II)-Pen species were not confirmed by IR, because they do not precipitate in aqueous solution. The formation of the complex as the thiol is deprotonated is consistent with coordination via the amine and the thiol, as discussed by Doornbos and Faber.[85]

The only single crystal structure for Fe(II) with any amino acid is $Fe(Pro)_2(phen)$ (Pro = L-proline; phen = 1,10-phenanthroline,[100]) which binds Fe(II) through the amine N and carboxylate O atoms. The only stability constant reported for the Fe(II)-Pro system is for the ML_2 complex (log β = 8.3), determined by Albert[63] in 1950. This low stability constant indicates extremely weak Fe(II) coordination, similar to those observed for the thio- and seleno-ethers, but does indicate that bidentate binding of thio- and selenoether amino acids is likely. As all of the FeL_2 stability constants with the thio- and selenoether amino acids were similarly low and approximately the same as the $Fe(Pro)_2$ stability constant, it is reasonable to assume that the coordination environments are similar. The lack of reported solid-state structures for Fe(II)-amino-acid complexes is indicative of weak coordination and difficulty in working with oxygen-sensitive Fe(II) complexes.

Structure-Stability Analysis for Fe(II)

Fe(II)-amino acid stability constants for the $[FeL]^+$ species with the thio- and selenoether amino acids are within 0.5 pH units of each other (3.49(4) to 3.84(1); Table 2.2), and stability constants for the Fe(L)(OH) complexes are in the range -4.9(1) to -5.7(1), slightly less accurate due to precipitation at pH 8. The $[Fe(Gly)]^+$ stability constant is slightly higher (4.04(5)) than those of the thio- and selenoether amino acids, indicating that the sulfur and selenium atoms of these amino acids do not contribute to complex stability.

In contrast, the thiol-containing Pen exhibits stronger binding to Fe(II), with Fe(Pen) and $[Fe(Pen)_2]^{2-}$ stability constants of 7.48(7) and 13.91(7), respectively, similar to Cu(II) stability constants with the thio- and selenoether amino acids, but much higher

than the stability constant for $[Fe(Gly)]^+$ (Table 2.2). Similarities in the stability constants for the Fe(II)-Pen and Cu(II)-Met systems suggest bidentate coordination, although Pen likely binds through the thiolate sulfur, replacing either the amine nitrogen or the carboxylate oxygen. Stability constants for Cu(II) with penicillamine have been reported as 16.5 and 21.7 for the Cu(Pen) and $[Cu(Pen)_2]^{2-}$ species, respectively (Table 2.2). This significant increase in stability compared to Fe(II)-Pen complexes strongly suggests tridentate Cu(II) coordination of the thiolate, amine, and carboxylate groups, a trait critical for its use as a biological Cu(II) chelator to treat Wilson's disease.

Greater binding stability for Cu(II) over Fe(II) coordination was determined for all the sulfur and selenium amino acids in Table 2.2. Stability constants of approximately 8 for the $[CuL]^+$ species and approximately 4 for the $[FeL]^+$ species, indicates a much lower affinity of the amino acid for Fe(II) in comparison to Cu(II). This may be due to differences in electronic environment and/or preferred coordination geometries around these two divalent metal ions. The extremely low $[FeL]^+$ stability constants indicate unlikely complex formation in a competitive environment of other biomolecules with much higher stability constants.

Cu(II)/Fe(II) Competition for Sulfur- and Selenium-Containing Amino Acids at Biological Concentrations

The sulfur- and selenium- containing amino acids form significantly more stable complexes with Cu(II) than with Fe(II), as discussed previously. However, iron is considered to be the most abundant transition metal ion in the biological system, with labile

pools believed to be as high as 10 μM.[40] Copper is the third most abundant transition metal ion, although discrete determination of copper pools has not been accurately determined.[47,101] Although the stability of the Fe(II) complexes is considerably weaker, the higher concentrations available may allow Fe(II) to compete for the available amino acids, especially with the thiol amino acids.

Penicillamine is routinely used as a chelating agent in the treatment of Wilson's disease[25,26] and has been used in the treatment of copper and lead poisoning.[102] As such, it is not surprising that the stability constants for Cu(II) and penicillamine are significantly higher (ML=16.5 and ML_2=21.7, Table 2.2) than those reported for the thio- and selenoether amino acids (ML=7.6-8.1 and ML_2=14.5-14.7). The stability constants for the Fe(Pen) (7.6) and $[Fe(Pen)_2]^{2-}$ (13.7) also indicate much weaker coordination than those for Cu(II), but if more Fe(II) is available, these complexes may form in significant quantities. The penicillamine may be effective for removing excess copper, but may also interfere with iron homeostasis.

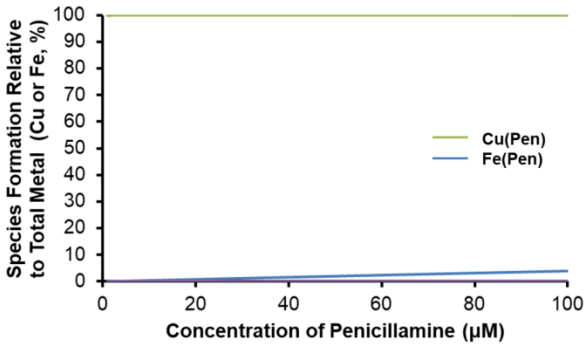

Figure 2.7. The simulated speciation graph for the modeled solution of 1 μM Cu(II), 10 μM Fe(II), and 1-100 μM Pen incorporating the stability constants for Cu(Pen), Fe(Pen), $[Cu(Pen)_2]^{2-}$, and $[Fe(Pen)_2]^{2-}$ species, with less than 1% formation was observed for the $[Cu(Pen)_2]^{2-}$, and $[Fe(Pen)_2]^{2-}$ species.

To demonstrate the preference of penicillamine for the Cu(II) ion over the Fe(II) ion, a model solution was studied that incorporated 1 μM Cu(II), 10 μM Fe(II), and 1-100 μM Pen at pH=7. These concentrations were chosen based on approximate labile concentrations for iron[40] and reported concentrations for penicillamine for patients being treated for Wilson's disease.[27] Although exact labile concentrations for Cu(II) have not been reported,[47,101] the concentration of 1 μM was chosen to examine the effect of a ten-fold difference between copper and iron. The model can be seen in Figure 2.7.

From the model seen in Figure 2.7 at pH 7, the formation of the Cu(Pen) species is unaffected by the availability of excess Fe(II). If the total concentrations are considered, the Pen ligand is initially equimolar to the Cu(II) and ten times less concentrated than the Fe(II). From these ratios, 99.8% of the Cu(II) (or 0.998 μM) is coordinated to the penicillamine. As the penicillamine concentration rises with excess available for coordination, limited Fe(II) coordination is observed, even when the pencillamine is ten times more concentrated than the Fe(II). A maximum of 3.93% of the Fe(II) (or 0.393 μM) is coordinated by penicillamine in this simulation. The $[Cu(Pen)_2]^{2-}$ and $[Fe(Pen)_2]^{2-}$ species are only observed in trace amounts (<0.1 μM, not seen in Figure 2.7) at pH 7 and do not seem to be a contributing species in this model. From this model, limited coordination of labile Fe(II) is observed when the penicillamine is in 10x excess which may affect iron homeostasis, but the Fe(II) would not outcompete or inhibit Cu(II) complexation.

Correlation of Stability Constants with Amino Acid Antioxidant Ability and Biological Speciation

Iron- and copper-mediated DNA damage can lead to oxidative stress and cell death, and sulfur and selenium compounds have been widely examined for their ability to inhibit DNA damage by Fe(II) or Cu(II)-mediated hydroxyl radical generation (Figure 2.1). *In vitro* gel electrophoresis studies quantified the concentration of thio- and selenoether amino acids required to inhibit 50% of the DNA damage (IC_{50} values) caused by Fe(II) or Cu(I) and hydrogen peroxide (Table 2.5). Brumaghim and coworkers[37,57,103] established that this antioxidant behavior was due to metal-amino-acid coordination, although they did not attempt to correlate DNA damage prevention with stability constants.

Table 2.5. Inhibitory concentrations for metal-mediated DNA damage prevention by amino acids.

Amino Acid	Cu(I) IC_{50} (μM)	Fe(II) IC_{50} (μM)	Reference
Gly	22.4 ± 0.1	None	[48]
Met	11.8 ± 1.3	None	[57]
SeMet	25.1 ± 0.1	None	[37]
MeCys	9.6 ± 1.0	None	[57]
MeSeCys	8.64 ± 0.02	None	[37]
Pen	26.9 ± 0.1	591±1	This work

To investigate potential correlations between metal-amino-acid binding and DNA damage prevention, we examined the relationship between the IC_{50} data (Table 2.5) and stability constants for the $[CuL]^+$ and CuL_2 species with Gly, Met, SeMet, MeCys, and MeSeCys. Data for the Cu(II)-Pen system were excluded from this analysis due to the differences in metal binding modes. Although stability of the ML species and inhibition of metal-mediated DNA damage are not correlated (R^2 = 0.045; Figure 2.8B), a weak correlation exists between stability constants for the ML_2 species and DNA damage

prevention (R^2 = 0.4742; Figure 2.8A). This limited correlation indicates that the stronger the Cu(II)-amino-acid binding, the less effective the amino acid is at preventing metal-mediated DNA damage.

These DNA damage inhibition assays use Cu(I)/H_2O_2 to generate damaging hydroxyl radical, and Cu(I) complexes are not expected to have the same stability constants as Cu(II). A comparison of Cu(I) stability constants with IC_{50} values would be ideal, but only Cu(I) stability constants with and Cys,[7] Pen,[7] and Met[84] are reported, due to the difficulty of working with Cu(I) in aqueous systems. Cu^{I}(Met) has a higher log β than $[Cu^{II}(Met)]^{+}$ species, 9.1 vs. 7.65, respectively, so Met is more stable binding Cu(I) than Cu(II), but data are too limited to establish trends.

Perhaps the most relevant general trend of complex stability with DNA damage prevention can be elucidated from the poor stability of the Fe(II)-thioether and -selenoether complexes. Thio- and selenoether amino acids do not inhibit DNA damage by Fe(II) (Table 2.5), but the more strongly binding Pen does. Although quantifiable trends cannot be determined due to lack of IC_{50} values with Fe(II), it is possible that thio- and selenoether ligands do not coordinate Fe(II) strongly enough to prevent iron-mediated DNA damage.

Based on the stability constants of Cu(II) with Met, SeMet, MeCys, MeSeCys, and Gly, the models indicate approximately 100% coordination by at least one ligand at biological pH (Figure 2.3). For the Fe(II) stability determinations with the same amino acids, only the Fe(II)-Pen system shows appreciable coordination at biological pH (Figure 2.6). These low stability constants reflect the fact that very little Fe(II) is coordinated up to

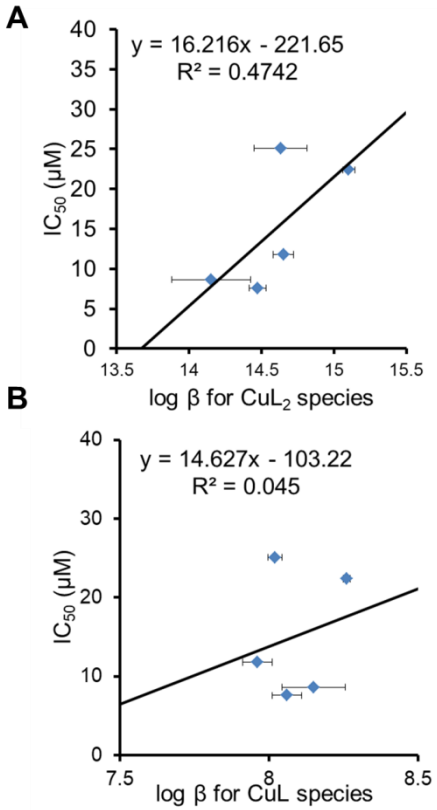

Figure 2.8. Graphs of A) stability constants of the CuL_2 species and B) stability constants of the CuL species vs. 50% inhibitory concentrations for oxidative DNA damage (IC_{50} values) for the amino acid antioxidants (L) in Table 2.5. Solid lines show the best-fit linear trend line for the data with the equations given.

pH 7, although a small change in pH to 8 results in >80% coordination of Fe(II) as $[ML]^+$ or MLOH species. The Fe-penicillamine system indicates a much higher stability with >90% coordination at pH 7, indicating probable coordination of the thiolate group to Fe(II). Thus, sulfur and selenium amino acid binding may affect the biological chemistry of Cu(II) significantly more than Fe(II).

2.3 Conclusions

Stability constants were determined for Cu(II) with the thio- and selenoamino acids, methylcysteine, methionine, methylselenocysteine, and selenomethionine, and stability constants for the $[Cu(MeSeCys)]^+$ and $Cu(MeSeCys)_2$ species were reported for the first time. Identity of these Cu(II)-amino acid species were independently confirmed by IR spectroscopy, ESI-MS, and/or solid-state structural analysis, including the first Cu(II) structure with a selenium-containing amino acid, $Cu(SeMet)_2$. Cu(II) binds these amino acids through the amine nitrogen and carboxylate oxygen atoms, and the thioether or selenoether moiety does not coordinate or increase complex stability. Based on the Cu(II) stability constants with these amino acids ($\log \beta = 8.0$ to 8.2 for the $[ML]^+$ species), all of the available Cu(II) is coordinated at pH 7 in as the $[ML]^+$ and $[ML_2]$ species, suggesting that these complexes may potentially form in biological systems.

Stability constants of Fe(II) with methylcysteine, methylselenocysteine, and selenomethionine also were determined for the first time. Fe(II) stability constants are consistently lower than the Cu(II) constants for all sulfur and selenium amino acids tested, including penicillamine. The $[FeL]^+$ species was identified for all of the thio- and seleno-ether amino acids, consistent with previous reports for the Fe(II)-methionine system; however, including a secondary [FeLOH] species provided a better match of the model to the collected data. The low stability constants for the $[FeL]^+$ species of the thioether and selenoether amino acids ($\log \beta = 3$-4) indicate much weaker binding than with Cu(II). As with Cu(II), the similarity of the stability constants for Fe(II) with glycine and all of the thio- and selenoamino acids indicates that the sulfur and selenium atoms do not interact

with the metal ion. Of the sulfur- and selenoamino acids, only penicillamine is likely to form complexes with the Fe(II) at pH 7.

In general, the higher stability constants of Cu(II) with the thio- and selenoether amino acids indicates that amino acid binding to Cu(II) at pH 7 may inhibit copper generation of hydroxyl radical, resulting in the weak correlation identified between Cu(II) stability constant and DNA damage prevention abilities of these amino acids. With the thio- and seleno-ether amino acids, the very weakly coordinated Fe(II) is more available than the stronger-binding Cu(II) for redox cycling to generate hydroxyl radical. Although sulfur- and selenium-containing amino acids are considered relatively weakly binding ligands, they may have large-scale implications for the biological availability and reactivity of redox-active metals such as Cu(II) and Fe(II).

2.4 Experimental Methods

Materials and Instrumentation

Concentrations of stock solutions of copper(II) nitrate trihydrate solutions and iron(II) sulfate heptahydrate were confirmed by ICP-OES. Infrared spectra were recorded using a Magna 550 IR spectrometer in the range 4000-450 cm^{-1} as Nujol mulls on KBr plates. IR absorption abbreviations are vs, very strong; s, strong; m, medium; w, weak; sh, shoulder.

ESI-MS analysis was carried out with a Thermo Scientific (San Jose, CA) TSQ Quantum Access MAX triple quadrupole mass spectrometer. Sample solutions were prepared in 50/50 mixture by volume of MeOH/H_2O and $NaClO_4$ (10 mM) at pH of 5.

Samples were prepared by mixing Cu(II) or Fe(II) (2 mM) with of the amino acid (4 mM) and introduced to the ESI source by direct infusion. A scan containing 5 micro scans was taken every 0.5 seconds across a 10 to 1000 Da range. For each sample, 100 scans were collected and averaged to obtain a final spectrum. TSQ Tune software (Thermo Scientific) was used for data acquisition. ESI-MS data are shown in Figures 2.11-2.12, and both mass/charge ratio and isotopic distribution match simulated envelope intensities.

Potentiometric Titrations

Titrations were performed using an 836 Titrando equipped with a 800 Dosino autotitrater. A Thermo Sure-flow Ag/AgCl electrode with 0.1 M NaCl filling solution was used to monitor potential of the solution during titration. Amino acid protonation constants were determined by direct titration of 30 mL of a 2.0 mM solution of each amino acid in $NaClO_4$ (0.1 M) to maintain a constant ionic strength. After bubbling with CO_2-scrubbed Ar, the solutions were titrated with CO_2-free, NIST standardized 0.1002 M NaOH using the 836 Titrando equipped with the 800 Dosino to autotitrate.

Cu(II) stability constants with the indicated amino acids were determined using aqueous solutions of $Cu(NO_3)_2 \cdot 3H_2O$ (1.0 mM) and each amino acid (2.0 mM or 3.0 mM) in 1:2 and 1:3 ratios of Cu:ligand and a constant ionic strength of 0.1 M $NaClO_4$. The electrode was calibrated for the system utilizing NIST-standarized 0.1001 M HCl and NIST-standarized 0.1002 M NaOH and the GLEE program[104] to determine standard reduction potentials in 0.1 M $NaClO_4$. For all titrations, 0.1001 M HCl was added to the metal-amino acid solution to bring the solution pH down to 2-3. Copper solutions were

bubbled with argon for 15 min and maintained at a constant temperature of 25.0˚C with a jacketed cell under a constant stream of argon to minimize CO_2 contamination of the reaction solutions. The solutions were then titrated as described above for the pure amino acid system. Potentials were measured at 25˚C until precipitation was visible.

Fe(II) stability constants were determined by titrating aqueous solutions of $FeSO_4 \cdot 7H_2O$ (1.0 mM) in 1:2 and 1:3 metal to ligand ratios with solutions of each amino acid (2.0 mM or 3.0 mM) at a constant ionic strength of 0.1 M NaCl in a dry, nitrogen-atmosphere glovebox. All solutions were prepared and titrations were performed in the glovebox. Temperature was maintained at 25.0˚C with a jacketed cell and water circulator. Iron solutions were then titrated with NIST standardized 0.0100 M NaOH utilizing the 836 Titrando and 800 Dosino autotitrator. Precipitation was observed above pH 8 during iron titrations, except with penicillamine. The iron titrations were back-titrated from pH 10 to 3 to demonstrate reversibility and to improve stability of the electrode over multiple analyses. For all amino acid, Cu(II), and Fe(II) titrations, data were collected in triplicate with reported standard deviations. Potentiometric titration data were analyzed and model-matched using HYPERQUAD2013.[104]

Synthesis of $Cu(SeMet)_2$

A solution of L-selenomethionine (117.7 mg, 0.6 mmol) in water was added to a solution of $Cu(NO_3)_2 \cdot 3H_2O$ (72.5 mg, 0.3 mmol) in water. NaOH (0.1 M) was added dropwise until the solution reached pH 6.0. The solution was evaporated in air over three weeks, resulting in light-blue crystals as well as powder precipitate. Yield:106 mg, 78%.

IR (cm^{-1}): 3299 w, 3232 w, 3110 s, 1618 vs, 1571 sh, 1462 w, 1340 w, 1304 w, 1138 s, 1083 w, 1246 w, 1160 s, 818 w, 722 w, 671 s, 638 w, 576 s. ESI-MS (*m*/*z*): 251 $[Cu(C_5H_{11}NO_2Se)]^+$, 274 $[Cu(C_5H_{11}NO_2Se)(OH)]^+$, 456 $[Cu(C_5H_{11}NO_2Se)_2H]^+$. Anal. Calc. for $C_{10}H_{20}CuN_2Se_2O_4$: C, 26.47; H, 4.44; N, 6.17. Found: C, 26.03; H, 4.66; N, 6.86.

X-ray crystallography

Single crystals for X-ray diffraction were obtained through slow evaporation of a 1:2 metal to ligand solution in water at pH 6, yielding blue, plate-like crystals. A single crystal was mounted on a low background loop and quenched to 100 K in a cold nitrogen stream. Data were collected at this temperature using a Bruker D8 Venture diffractometer with Mo Kα radiation (λ = 0.71073 Å) and a Photon 100 CMOS detector; crystallographic data are summarized in Table 2.6. A total of 10345 reflections were collected (3012 independent) using phi and omega scans. Data collection, processing (SAINT), and scaling (SADABS) were performed using the Apex 3 software package.[105] The monoclinic space group $P2_1$ was determined from the systematic absences. The structure was solved using intrinsic phasing (SHELXT) and refined using full matrix least squares techniques (SHELXL) using the SHELXTL software suite.[106] All non-hydrogen atoms were refined anisotropically, and hydrogen atoms were then placed in geometrically optimized positions using appropriate riding models. The presence of two hydrogen atoms on the amine nitrogen atoms was confirmed on the difference electron density map prior to hydrogen atom assignment at these positions. The proper absolute structure was confirmed by a Flack parameter of 0.06(2).

Table 2.6. Summary of crystallographic data for $Cu(SeMet)_2$.

	$Cu(SeMet)_2$
Chemical formula	$C_{10}H_{20}CuN_2O_4Se_2$
F.W. (g mol^{-1})	453.74
Temperature, K	100(2)
Wavelength, Å	0.71073
Crystal system	Monoclinic
Space group	$P2_1$
a, Å	9.4131(7)
b, Å	4.9660(4)
c, Å	16.0824(11)
β, °	90.897(2)
V, $Å^3$	751.7(1)
Z	2
D, g cm^{-3}	2.005
Absorption coefficient, mm^{-1}	6.305
Crystal size, mm^3	0.021 × 0.124 × 0.268
F(000)	446
2θ range, °	2.16 to 26.38
Collected reflections	10345
Unique reflections	3012
R_{int}	0.0542
Final *R* (obs. data)[α], R_1; wR_2	0.0382; 0.0700
Final *R* (all data)[α], R_1; wR_2	0.0497; 0.0733
Flack parameter	0.06(2)
Largest diff. peak/hole (e/$Å^3$)	0.506/-0.575

Plasmid DNA transfection, amplification, and purification.

Plasmid DNA (pBSSK) was purified from DH1 E. *coli* competent cells using a ZyppyTM Plasmid Miniprep Kit (400 preps, Fisher). Plasmid was dialyzed against 130 mM NaCl for 24 h at 4°C to ensure all Tris-EDTA buffer and metal contaminates were removed, and plasmid concentration was determined by UV-vis spectroscopy at a wavelength of 260 nm. Absorbance ratios of $A_{250}/A_{260} \geq 0.95$ and $A_{260}/A_{280} \geq 1.8$ were determined for DNA used in all experiments. Plasmid purity was determined through digestion of plasmid (0.1 pmol) with Sac 1 and KpN1 in a 10x Fast Digest Buffer (Thermo

Scientific) at 37°C for 90 minutes. Digested plasmids were compared to an undigested plasmid sample and a 1 kb molecular weight marker using gel electrophoresis.

DNA damage gel electrophoresis experiments

For the DNA damage assays with copper, deionized water, MOPS buffer (10 mM, pH 7.0), NaCl (130 mM), ethanol (100%), 10 mM), $CuSO_4 \cdot 5H_2O$, ascorbic acid (7.5 µM, to reduce Cu(II) to Cu(I)), and penicillamine were combined in an acid-washed (1 M HCl for ~ 1 h) and dried microcentrifuge tube and allowed to stand for 5 min at room temperature. Plasmid (pBSSK, 0.1 pmol in 130 mmol NaCl) was then added to the reaction mixture and allowed to stand for 5 min at room temperature. H_2O_2 (50 µM) was added and allowed to react at room temperature for 30 min. EDTA (50 µM) was added after 30 min to quench the reaction. For the Fe(II) DNA damage experiments, the 2 µM $FeSO_4 \cdot 7H_2O$ and MES buffer (10 mM, pH 6.0) were used. All concentrations are final concentrations in a 10 µM volume. Samples were loaded into a 1% agarose gel in a TAE running buffer (50×); damaged and undamaged plasmid was separated by electrophoresis (140 V for 60 min). Gels were stained using ethidium bromide and imaged using UV light. The amounts of nicked (damaged) and circular (undamaged) were analyzed using UViProMW software (Jencons Scientific Inc.). Intensity of circular plasmid was multiplied by 1.24, due to the lower binding affinity of ethidium bromide to supercoiled plasmid.[107,108] Intensities of the nicked and supercoiled DNA bands were normalized for each lane so that % nicked + % supercoiled = 100%. Plots of percent inhibition of DNA damage versus log concentration of amino acid were fit to a variable-slope, sigmoidal dose-response curve using SigmaPlot

(v. 9.01, Systat Software, Inc., San Jose, CA). IC_{50} value errors represent standard deviations of the values obtained from fits of three separate experiments. Data and IC_{50} plots for all gel electrophoresis experiments are provided in Tables 2.7-2.8 and Figures 2.11-2.12.

2.5 Supplementary Data

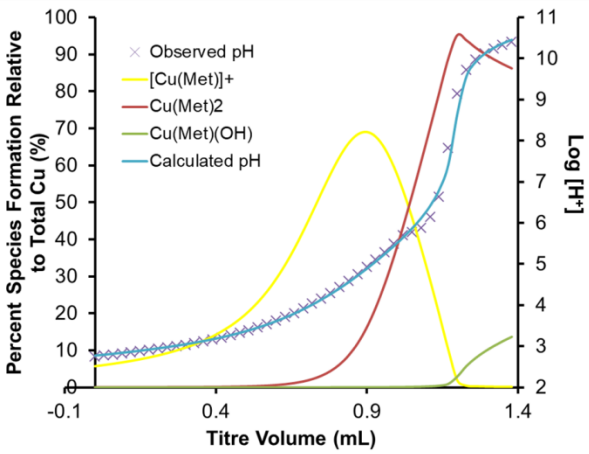

Figure 2.9 Representative titration (0.1 M NaOH, I = 0.1 M $NaClO_4$, 25˚C) and speciation diagram for the potentiometric titration of Cu(II) and methionine in a 1:2 ratio. The solid blue line represents the modeled titration with the measured data points overlayed; formation of $[Cu(Met)]^+$, $Cu(Met)_2$, and Cu(Met)(OH) species are indicated as shown in the legend.

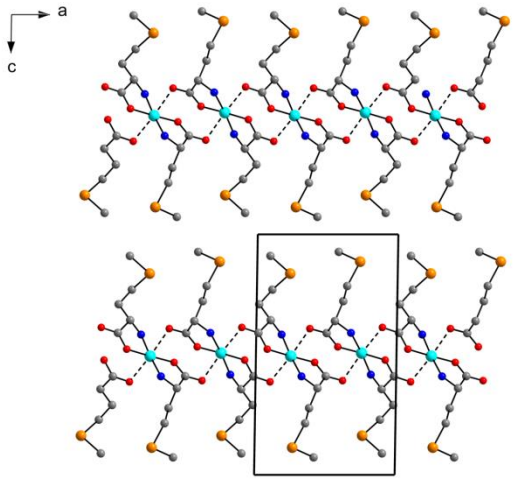

Figure 2.10 Crystal packing diagram for $Cu(SeMet)_2$. The long range intermolecular interactions of the carboxylate oxygens (red) with the copper ions (turquoise) in the axial positions are designated by dashed bonds.

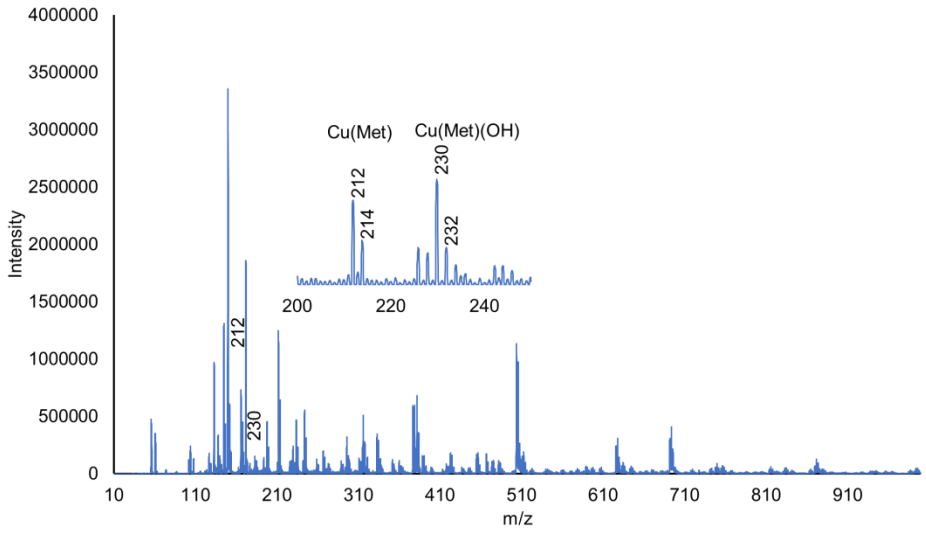

Figure 2.11ESI-MS data for $Cu(NO_3)_2$ (2 mM) and methionine (4 mM) with 0.01 M $NaClO_4$ in methanol/water at pH 5. The inset shows the isotopic distribution that confirms the identify of $[Cu(Met)]^+$ and $[Cu(Met)(OH)]^+$ species.

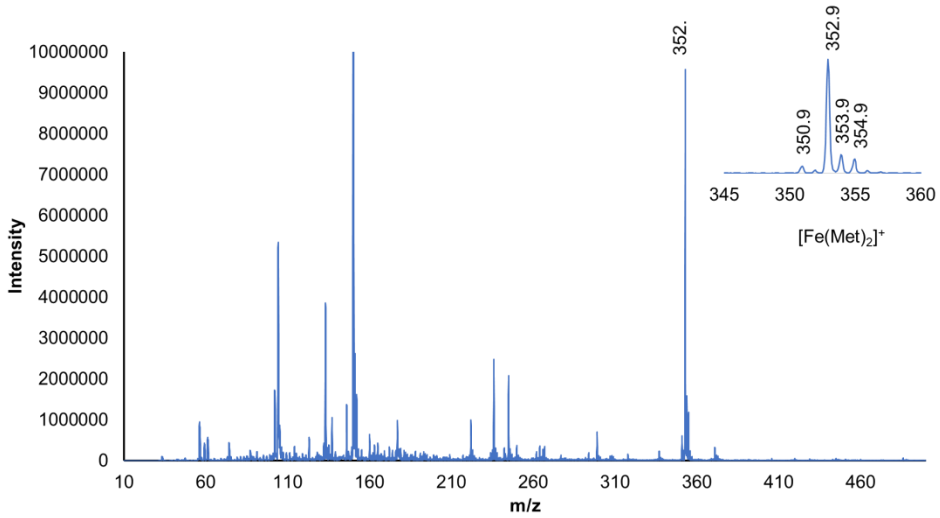

Figure 2.12 ESI-MS of $FeSO_4$ (2 mM) and methionine (4 mM) in 0.01 M $NaClO_4$ in methanol/water at pH 5. The inset shows the isotopic distribution that confirms the identity of the $[Fe(Met)_2]^+$ species.

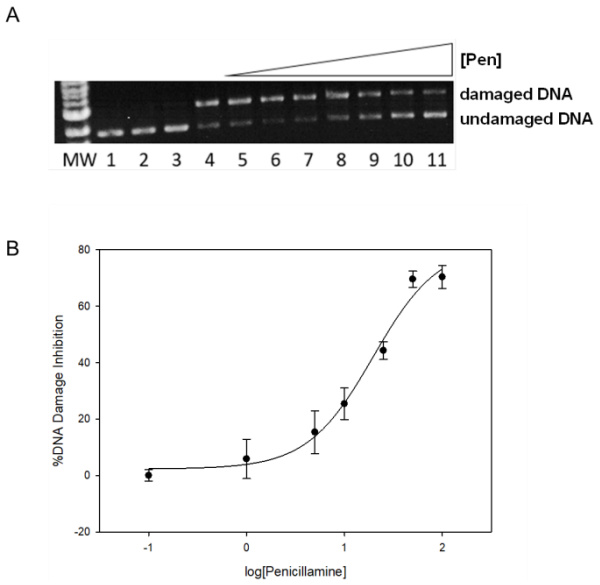

Figure 2.13 A) Gel electrophoresis image showing copper-mediated DNA damage inhibition by penicillamine. MW: 1 kb molecular weight marker; lane 1: plasmid DNA (p); lane 2: p + H_2O_2. lane 3: p + penicillamine (100 μM) + H_2O_2; lane 4: p + $CuSO_4$ (6 μM) + ascorbate (7.5 μM) H_2O_2; lanes 5-11: p + H_2O_2 + Cu(II) + AA + 0.1, 1, 5, 10, 25, 50, 100 μM, respectively. B) A graph of log penicillamine concentration vs. DNA damage inhibition showing the best-fit sigmoidal dose-response curve; IC_{50} value = 26.94 ± 0.07 μM).

Table 2.7 Gel electrophoresis results for DNA damage inhibition by penicillamine (Pen) with Cu(II), ascorbate, and H_2O_2.[a]

Gel lane	Contents	[Pen] (μM)	% Supercoiled DNA	% Nicked DNA	% DNA Damage Inhibition	*p* Value
1	plasmid DNA (p)	0	99.58 ± 0.73	0.42	-	-
2	p + H_2O_2 (50 μM)	0	100 ± 0	0.00	-	-
3	p + penicillamine + H_2O_2	100	99.86 ± 0.25	0.14	-	-
4	p + Cu(II) (6 μM) + ascorbate (7.5 μM) + H_2O_2	0	11.37 ± 4.91	88.63	-	-
5	p + Cu(II) + AA + H_2O_2 + Pen	0.1	11.40 ± 2.03	88.60	0.03 ± 2.03	0.982
6		1	16.61 ± 6.97	83.39	5.90 ± 6.94	0.279
7		5	25.01 ± 7.55	74.99	15.38 ± 7.52	0.071
8		10	33.93 ± 5.55	66.07	25.42 ± 5.57	0.016
9		25	50.66 ± 3.13	49.34	44.30 ± 3.11	0.002
10		50	73.02 ± 2.84	26.98	69.57 ± 2.84	<0.001
11		100	73.71 ± 4.11	26.29	70.33 ± 4.13	<0.001

[a]Data are reported as the average of three trials with calculated standard deviations shown.

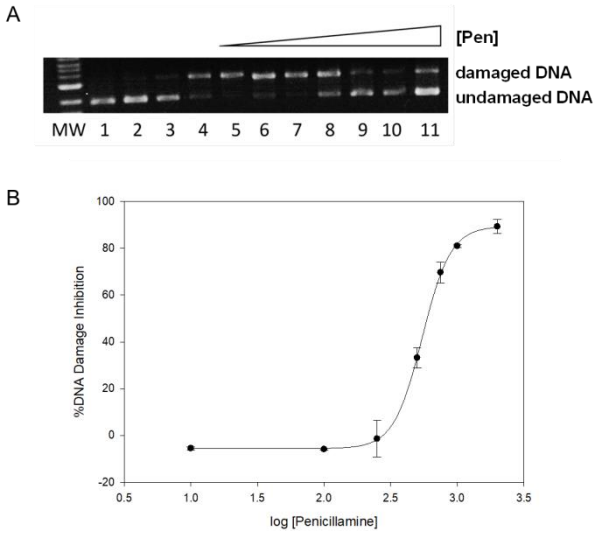

Figure 2.14 Gel electrophoresis image showing iron-mediated DNA damage inhibition by penicillamine. MW: 1 kb molecular weight marker; lane 1: plasmid DNA (p); lane 2: p + H_2O_2. lane 3: p + penicillamine (2000 μM) + H_2O_2; lane 4: p + $FeSO_4$ (2 μM) + H_2O_2; lanes 5-11: p + H_2O_2 + Fe(II) + 10, 100, 250, 500, 750, 1000, 2000 μM, respectively. B) A graph of log penicillamine concentration vs. DNA damage inhibition showing the best-fit sigmoidal dose-response curve; IC_{50} value = 591 ± 1 μM).

Table 2.8 Gel electrophoresis results for DNA damage inhibition by penicillamine (Pen) with Fe(II), ascorbate, and H_2O_2.[a]

Gel lane	Contents	[Pen] (μM)	% Supercoiled DNA	% Nicked DNA	% DNA Damage Inhibition	*p* Value
1	plasmid	0	100.0 ± 0	0.0	-	-
2	p + H_2O_2 (50 μM)	0	100 ± 0	0.0	-	-
3	p + penicillamine + H_2O_2	2000	100 ± 0	0.0	-	-
4	p + Fe(II) (2 μM) + H_2O_2	0	5.85 ±	94.15	-	-
5	p + Fe(II) + H_2O_2 + penicillamine	10	0.70 ± 0.7	99.30	- 5.47 ± 0.70	0.005
6		100	0.35 ± 0.35	99.65	-5.84 ± 3.61	0.107
7		250	4.53 ± 7.77	95.47	-1.40 ± 7.77	0.785
8		500	37.10 ± 4.40	62.90	33.19 ± 4.40	0.006
9		750	71.45 ± 4.45	28.55	69.68 ± 4.45	0.001
10		1000	82.10 ± 0.60	17.90	80.99 ± 0.60	< 0.001
11		2000	89.90 ± 2.95	10.10	89.27 ± 2.95	< 0.001

[a]Data are reported as the average of three trials with calculated standard deviations shown.

2.6 References

(1) Hallman, P. S.; Perrin, D. D.; Watt, A. E. *Biochem. J.* **1971**, *121*, 549-555.

(2) Tran-Ho, L. C.; May, P. M.; Hefter, G. T. *J. Inorg. Biochem.* **1997**, *68*, 225-231.

(3) Berthon, G. *Pure Appl. Chem.* **1995**, *67*, 1117-1240.

(4) Berthon, G.; Blais, M. J.; Piktas, M.; Houngbossa, K. *J. Inorg. Biochem.* **1984**, *20*, 113-130.

(5) Harris, W. R.; Sammons, R. D.; Grabiak, R. C. *J. Inorg. Biochem.* **2012**, *116*, 140-150.

(6) White, M. C. *Plant Physiol.* **1981**, *67*, 301-310.

(7) Konigsberger, L.-C.; Konigsberger, E.; Hefter, G.; May, P. M. *Dalton Trans.* **2015**, *44*, 20413-20425.

(8) Bellingham, S. A.; Guo, B.; Hill, A. F. *Biol. Cell* **2015**, *107*, 389-418.

(9) Mital, M.; Wezynfeld, N. E.; Fraczyk, T.; Wiloch, M. Z.; Wawrzyniak, U. E.; Bonna, A.; Tumpach, C.; Barnham, K. J.; Haigh, C. L.; Bal, W.; Drew, S. C. *Angew. Chem. Int. Ed. Engl.* **2015**, *54*, 10460-10464.

(10) Kawahara, A.; Tsukada, J.; Yamaguchi, T.; Katsuragi, T.; Higashi, T. *Biomark. Res.* **2015**, *3*, 10.

(11) Jomova, K.; Valko, M. *Toxicology* **2011**, *283*, 65-87.

(12) Mates, J. M.; Segura, J. A.; Alonso, F. J.; Marquez *J. Arch. Toxicol.* **2012**, *86*, 1649-1665.

(13) Halliwell, B.; Gutteridge, J. M. *Methods Enzymol.* **1990**, *186*, 1-85.

(14) Robert, A.; Liu, Y.; Nguyen, M.; Meunier, B. *Acc. Chem. Res.* **2015**, *48*, 1332-1339.

(15) Brosnan, J. T.; Brosnan, M. E. *J. Nutr.* **2006**, *136*, 1636S-1640S.

(16) Guttormsen, A. B.; Schneede, J.; Fiskerstrand, T.; Ueland, P. M.; Refsum, H. M. *J. Nutr.* **1994**, *124*, 1934-1941.

(17) Bergstroem, J.; Fuerst, P.; Noree, L.; Vinnars, E. *J. Appl. Physiol.* **1974**, *36*, 693-697.

(18) Kuzminski, A. M.; Del Giacco, E. J.; Allen, R. H.; Stabler, S. P.; Lindenbaum, J. *Blood* **1998**, *92*, 1191-1198.

(19) Solomon, L. R. *Blood Rev.* **2007**, *21*, 113-130.

(20) Selhub, J. *Annu. Rev. Nutr.* **1999**, *19*, 217-246.

(21) Mandaviya, P. R.; Stolk, L.; Heil, S. G. *Mol. Genet. Metab.* **2014**, *113*, 243-252.

(22) Hoey, L.; McNulty, H.; Askin, N.; Dunne, A.; Ward, M.; Pentieva, K.; Strain, J.; Molloy, A. M.; Flynn, C. A.; Scott, J. M. *Am. J. Clin. Nutr.* **2007**, *86*, 1405-13.

(23) Selmer, T.; Kahnt, J.; Goubeaud, M.; Shima, S.; Grabarse, W.; Ermler, U.; Thauer, R. K. *J. Biol. Chem.* **2000**, *275*, 3755-3760.

(24) Rubino, F. M.; Pitton, M.; Di Fabio, D.; Meroni, G.; Santaniello, E.; Caneva, E.; Pappini, M.; Colombi, A. *Biomed. Chromatogr.* **2011**, *25*, 330-343.

(25) Brewer, G. J. *Drugs* **1995**, *50*, 240-249.

(26) Brewer, G. J.; Askari, F. K. *J. Hepatol.* **2005**, *42*, S13-S21.

(27) Muijsers, A. O.; van de Stadt, R. J.; Henrichs, A. M. A.; Ament, H. J. W.; van der Korst, J. K. *Arthritis Rheumatol.* **1984**, *27*, 1362-1369.

(28) Burk, R. F.; Norsworthy, B. K.; Hill, K. E.; Motley, A. K.; Byrne, D. W. *Cancer Epidemiol. Biomarkers Prev.* **2006**, *15*, 804-810.

(29) Reid, M. E.; Stratton, M. S.; Lillico, A. J.; Fakih, M.; Natarajan, R.; Clark, L. C.; Marshall, J. R. *J. Trace Elem. Med. Biol.* **2004**, *18*, 69-74.

(30) Takahashi, K.; Suzuki, N.; Ogra, Y. *Int. J. Mol. Sci.* **2017**, *18*, 506-517.

(31) Byun, B. J.; Kang, Y. K. *Biopolymers* **2011**, *95*, 345-53.

(32) Kotrebai, M.; Birringer, M.; Tyson, J. F.; Block, E.; Uden, P. C. *Analyst* **2000**, *125*, 71-78.

(33) Burk, R. F.; Hill, K. E. *Annu. Rev. Nutr.* **2005**, *25*, 215-235.

(34) Burk, R. F.; Hill, K. E. *Biochim. Biophys. Acta* **2009**, *1790*, 1441-1447.

(35) Fairweather-Tait, S. J.; Bao, Y.; Broadley, M. R.; Collings, R.; Ford, D.; Hesketh, J. E.; Hurst, R. *Antioxid. Redox Signal.* **2011**, *14*, 1337-1383.

(36) Papp, L. V.; Holmgren, A.; Khanna, K. K. *Antioxid. Redox Signal.* **2010**, *12*, 793-795.

(37) Battin, E. E.; Zimmerman, M. T.; Ramoutar, R. R.; Quarles, C. E.; Brumaghim, J. L. *Metallomics* **2011**, *3*, 503-512.

(38) Stohs, S. J.; Bagchi, D. *Free Radic. Biol. Med.* **1995**, *18*, 321-336.

(39) Woodmansee, A. N.; Imlay, J. A. *Methods Enzymol.* **2002**, *349*, 3-9.

(40) Jhurry, N. D.; Chakrabarti, M.; McCormick, S. P.; Holmes-Hampton, G. P.; Lindahl, P. A. *Biochemistry* **2012**, *51*, 5276-5284.

(41) Zecca, L.; Youdim, M. B.; Riederer, P.; Connor, J. R.; Crichton, R. R. *Nat. Rev. Neurosci.* **2004**, *5*, 863-873.

(42) Zecca, L.; Gallorini, M.; Schunemann, V.; Trautwein, A. X.; Gerlach, M.; Riederer, P.; Vezzoni, P.; Tampellini, D. *J. Neurochem.* **2001**, *76*, 1766-1773.

(43) Zecca, L.; Stroppolo, A.; Gatti, A.; Tampellini, D.; Toscani, M.; Gallorini, M.; Giaveri, G.; Arosio, P.; Santambrogio, P.; Fariello, R. G.; Karatekin, E.; Kleinman, M. H.; Turro, N.; Hornykiewicz, O.; Zucca, F. A. *Proc. Natl. Acad. Sci. U. S. A.* **2004**, *101*, 9843-9848.

(44) Berg, D.; Gerlach, M.; Youdim, M. B.; Double, K. L.; Zecca, L.; Riederer, P.; Becker, G. *J. Neurochem.* **2001**, *79*, 225-236.

(45) Ward, R. J.; Zucca, F. A.; Duyn, J. H.; Crichton, R. R.; Zecca, L. *Lancet Neurol.* **2014**, *13*, 1045-1060.

(46) Yang, L.; McRae, R.; Henary, M. M.; Patel, R.; Lai, B.; Vogt, S.; Fahrni, C. J. *Proc. Natl. Acad. Sci. U. S. A.* **2005**, *102*, 11179-11184.

(47) Fahrni, C. J. *Curr. Opin. Chem. Biol.* **2013**, *17*, 656-662.

(48) Garcia, C. R.; Angele-Martinez, C.; Wilkes, J. A.; Wang, H. C.; Battin, E. E.; Brumaghim, J. L. *Dalton Trans.* **2012**, *41*, 6458-6467.

(49) Gaggelli, E.; Kozlowski, H.; Valensin, D.; Valensin, G. *Chem. Rev.* **2006**, *106*, 1995-2044.

(50) Sen, C. K. *J. Appl. Physiol.* **1995**, *79*, 675-686.

(51) Colovic, M. B.; Vasic, V. M.; Djuric, D. M.; Krstic, D. Z. *Curr. Med. Chem.* **2018**, *25*, 324-335.

(52) Gonzalez-Benjumea, A.; Begines, P.; Lopez, O.; Maya, I.; Fernandez-Bolanos, J. G. *Adv. Chem. Res.* **2014**, *22*, 51-81.

(53) Metayer, S.; Seiliez, I.; Collin, A.; Duchene, S.; Mercier, Y.; Geraert, P. A.; Tesseraud, S. *J. Nutr. Biochem.* **2008**, *19*, 207-215.

(54) Rahmanto, A. S.; Davies, M. J. *IUBMB Life* **2012**, *64*, 863-871.

(55) Palioura, S.; Herkel, J.; Simonovic, M.; Lohse, A. W.; Soll, D. *Biol. Chem.* **2010**, *391*, 771-776.

(56) Liu, J.; Zhao, Y.; Zhang, R.; Shu, J.; Zhang, X. *Zhongguo Shipin Tianjiaji* **2011**, *2*, 152-156.

(57) Battin, E. E.; Brumaghim, J. L. *J. Inorg. Biochem.* **2008**, *102*, 3036-3042.

(58) Zimmerman, M. T.; Bayse, C. A.; Ramoutar, R.; Brumaghim, J. L. *J. Inorg. Biochem.* **2015**, *145*, 30-40.

(59) Stadelman, B. S.; Kimani, M. M.; Bayse, C. A.; McMillen, C. D.; Brumaghim, J. L. *Dalton Trans.* **2016**, *45*, 4697-4711.

(60) Basolo, F.; Chen, Y. T. *J. Am. Chem. Soc.* **1954**, *76*, 953-955.

(61) Sovago, I.; Kiss, T.; Gergely, A. *Pure Appl. Chem.* **1993**, *65*, 1029-1080.

(62) Zainal, H.; Wolf, W. *Transition Met. Chem.* **1995**, *20*, 225-227.

(63) Albert, A. *Biochem. J.* **1950**, *47*, 531-538.

(64) Li, N. C.; Doody, E. *J. Am. Chem. Soc.* **1954**, *76*, 221-225.

(65) Hawkins, C. J.; Perrin, D. D. *Inorg. Chem.* **1963**, *2*, 843-849.

(66) Jokl, V. *J. Chromatogr.* **1964**, *14*, 71-78.

(67) Lenz, G.; Martell, A. *Biochemistry* **1964**, *3*, 745-750.

(68) Pella, P. A.; Purdy, W. C. *J. Electroanal. Chem.* **1965**, *10*, 51-55.

(69) Brookes, G.; Pettit, L. D. *J. Chem. Soc. Dalton Trans.* **1977**, *19*, 1918-1924.

(70) Prasad, K.; Mohan, M. S. *J. Coord. Chem.* **1987**, *16*, 251-262.

(71) Masoud, M. S.; Abdel-Nabby, B. A.; Soliman, E. M.; Abdel-Hamid, O. H. *Thermochim. Acta* **1988**, *128*, 75-80.

(72) Anwar, Z. M.; Azab, H. A. *J. Chem. Eng. Data* **1999**, *44*, 1151-1157.

(73) Albert, A. *Biochem. J.* **1952**, *50*, 690-697.

(74) Knoblock, E. C.; Purdy, W. C. *J. Electroanal. Chem.* **1961**, *2*, 493-496.

(75) Deschamps, P.; Kulkarni, P. P.; Sarkar, B. *Inorg. Chem.* **2004**, *43*, 3338-3340.

(76) Antolini, L.; Battaglia, L. P.; Bonamartini, C. A.; Marcotrgiano, G.; Menabue, L.; Pellacani, G. C.; Saladini, M.; Sola, M. *Inorg. Chem.* **1986**, *26*, 2901-2904.

(77) Tomita, K. *Bull. Soc. Chim. Jpn.* **1961**, *34*, 297-300.

(78) Borghesani, G.; Pulidori, F.; Remelli, M.; Purrello, R.; Rizzarelli, E. *J. Chem. Soc., Dalton Trans.* **1990**, *7*, 2095-2100.

(79) Israeli, M.; Pettit, L. D. *J. Inorg. Nucl. Chem.* **1975**, *37*, 999-1003.

(80) Sovago, I.; Petocz, G. *J. Chem. Soc., Dalton Trans.* **1987**, *7*, 1717-1720.

(81) Pinto, L. D.; Puppin, P.; Behring, V. M.; Alves, O.; Rey, N.; Felcman, J. *Inorg. Chim. Acta* **2012**, *386*, 60-67.

(82) Kuchinkas, E. J.; Rosen, Y. *Arch. Biochem. Biophys.* **1962**, *97*, 370-372.

(83) Gergely, A. *Acta Chim. Acad. Sci. Hung.* **1969**, *59*, 309-318.

(84) Perrin, D. D. *J. Chem. Soc.* **1958**, 3125-3128.

(85) Doornbos, D. A.; Faber, J. S. *Pharm. Weekbl.* **1964**, *99*, 289-309.

(86) Ou, C.; Powers, D.; Thich, J.; Felthouse, T.; Hendrickson, D.; Potenza, J.; Schugar, H. *Inorg. Chem.* **1978**, *17*, 34-40.

(87) Dubler, E.; Cathomas, N.; Jameson, G. B. *Inorg. Chim. Acta* **1986**, *123*, 99-104.

(88) Masoud, M. S.; Amira, M. F.; Ramadan, A. M.; El-AShry, G. M. *Spectrochim. Acta* **2008**, *A69*, 230-238.

(89) Veidis, M.; Palenik, G. *J. Chem. Soc. D* **1969**, *21*, 1277-1278.

(90) Yoneyama, S.; Kodama, T.; Kikuchi, K.; Kawabata, Y.; Kikuchi, K.; Ono, T.; Hosokoshi, Y.; Fujita, W. *CrystEngComm* **2013**, *15*, 10193-10196.

(91) Prout, C. K.; Armstrong, R. A.; Carruthers, J. R.; Forrest, J. G.; Murray-Rust, P.; Rossotti, F. *J. Chem. Soc. A* **1968**, *11*, 2791-2813.

(92) Freeman, H. C.; Snow, M. R.; Nitta, I.; Tomita, K. *Acta Crystallogr.* **1964**, *17*, 1463-1470.

(93) Casari, B. M.; Mahmoudkhani, A. H.; Langer, V. *Acta Crystallogr.* **2004**, *E60*, m1949-m1951.

(94) Konar, S.; Gagnon, K.; Clearfield, A.; Thompson, C.; Hartle, J.; Ericson, C.; Nelson, C. *J. Coord. Chem.* **2010**, *63*, 3335-3347.

(95) Lamshoft, M.; Ivanova, B. *J. Coord. Chem.* **2011**, *64*, 2419-2442.

(96) Yoshinari, N.; Kakuya, A.; Lee, R.; Konno, T. *Bull. Chem. Soc. Jpn.* **2015**, *88*, 59-68.

(97) Perrin, D. D. *J. Chem. Soc.* **1959**, 290-296.

(98) Izatt, R. M.; Johnson, H. D.; Christensen, J. J. *J. Chem. Soc. Dalton Trans.* **1972**, *11*, 1152-1157.

(99) Micskei, K. *J. Chem. Soc., Dalton Trans.* **1987**, *1*, 255-257.

(100) Magill, C. P.; Floriani, C.; Chiesi-Villa, A.; Rizzoli, C. *Inorg. Chem.* **1994**, *33*, 1928-1933.

(101) Yang, L.; McRae, R.; Henary, M. M.; Patel, R.; Lai, B.; Vogt, S.; Fahrni, C. J. *Proc. Natl. Acad. Sci. USA* **2005**, *102*, 11179-11184.

(102) Shannon, M.; Graef, J.; Lovejoy, F. H., Jr. *J. Pediatr.* **1988**, *112*, 799-804.

(103) Battin, E. E.; Perron, N. R.; Brumaghim, J. L. *Inorg. Chem.* **2006**, *45*, 499-501.

(104) Gans, P.; Sabatini, A.; Vacca, A. *Talanta* **1996**, *43*, 1739-1753.

(105) Bruker AXS Inc.: Madison, WI, 2015.

(106) Sheldrick, G. M. *Acta Cyrstallogr.* **2015**, *C71*, 3-8.

(107) Lloyd, R. S.; Haidle, C. W.; Robberson, D. L. *Biochemistry* **1978**, *17*, 1890-1896.

(108) Hertzberg, R. P.; Dervan, P. B. *J. Am. Chem. Soc.* **1982**, *104*, 313-315.

CHAPTER THREE

COORDINATION COMPLEXES OF METHIMAZOLE WITH COPPER: CONTROLLING REDOX REACTIONS AND SULFUR EXTRUSION

3.1 Introduction

Immense diversity in stoichiometry and redox activity has been demonstrated for the coordination of *N*-heterocyclic thioamides with softer metal centers such as Cu(I) and Fe(II).[1-4] This remarkable flexibility in redox activity has led to the exploration of thioamides in catalysis,[5,6] radiopharmaceuticals,[7] energy production,[8] corrosion resistance,[9,10] sensors,[11] and organometallic and coordination chemistry.[12,13] Although thioether- and thiol-containing amino acids have attracted considerable attention as ligands due to their bioavailability, imidazole thiones are of recent interest due to their sigma donor bonding ability,[4,14] potential for multidentate binding, and redox activity.[15] Methimazole (MMI), is the most widely prescribed hyperthyroid treatment in the U.S.[16] and is believed to bind Fe(II) in the heme protein, thyroid peroxidase.[17] The exact mechanism of action for MMI is poorly understood, and its biological redox activity and metal coordination has not been investigated fully. MMI is also structurally similar to ergothioneine, a known biological antioxidant.[18] Upon oxidation, MMI forms the corresponding disulfide, MMI^{DS}, a reaction reminiscent of cysteine oxidation to cystine.

Under inert atmosphere conditions, Cu(I)-MMI coordination has been widely studied, and a wide variety of mono-,[19,20] di-,[21-24] tetra-,[25] and polynuclear[26,27] complexes are reported. The two mononuclear Cu(I) complexes $[Cu(MMI)_3][NO_3]$[28] and

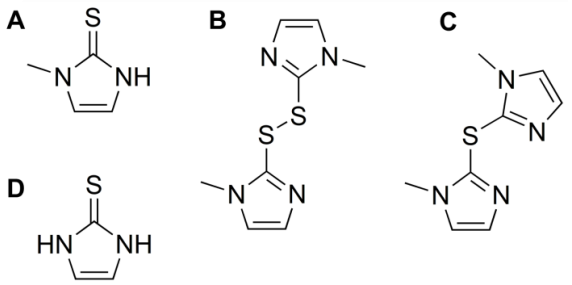

Figure 1.1. *N*-heterocyclic thione and disulfide compounds discussed in this study: A) methimazole (MMI), B) methimazole disulfide (MMI^{DS}), C) methimazole monosulfide (MMI^{MS}), and D) 2-mercaptoimidazole (HMI).

$[Cu(MMI_3)Cl]$[29] have monodentate coordination through the MMI sulfur atom and coordinate trigonal planar geometry. The multinuclear and polymeric complexes include *S*-bridging methimazole ligands bound to Cu(I) in trigonal planar or tetrahedral geometry. The dinuclear species form Cu_2S_2 rhombohedral cores, distorting the tetrahedral coordination around Cu(I). The relatively short Cu-S bond lengths (2.3-2.5 Å) in these dinuclear complexes are similar to the Cu-S(Cys) bond lengths observed in blue copper proteins, and indicate high π-covalency.[30]

In an unusual reaction illustrating the facile redox chemistry of methimazole and copper, copper promotes sulfur extrusion from methimazole disulfide (MMI^{DS}) to form a methimazole monosulfide ligand (MMI^{MS}; Figure 3.1). In the first step, Cu(II) oxidizes methimazole to its disulfide with and is reduced to Cu(I) (Scheme 3.1, reaction A).[15] In the presence of O_2 from air, Lobana and coworkers[31] established that Cu(I) was oxidized to Cu(II) and the disulfide was oxidized to a sulfone, resulting in sulfur elimination (Scheme 3.1, reaction B) and formation of MMI^{MS}, with mass spectroscopy data supporting the formation of the disulfide, the sulfone, and the monosulfide. The *in-situ*-generated

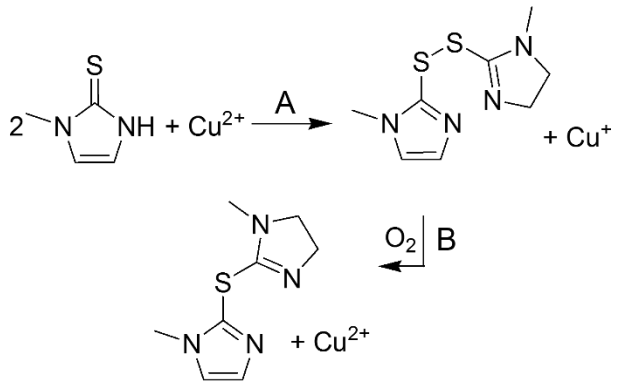

Scheme 3.1. Reduction of Cu(II) by methimazole (A) and subsequent oxidation of Cu(I) with sulfur extrusion (B) in air.

MMI^{MS} ligand coordinates Cu(II) in a bidentate fashion through an N atom on each of the heterocycles.[27,32-37] To date, no Cu(II) or Cu(I) complexes incorporating the intact MMI^{DS} ligand are reported.

To determine the effects of oxygen on the coordination chemistry of copper and methimazole, a series of reactions with Cu(II) or Cu(I) and MMI or MMI^{DS} were performed air-free and in air, yielding several novel dinuclear and polynuclear Cu(I)-MMI complexes. Under aerobic conditions, a series of novel Cu(II) complexes with the sulfur-extruded MMI^{MS} ligand were obtained, resulting in a greater mechanistic understanding of this unusual reaction. These goals were achieved through the contributions of Amanda Owen, for the development of the MMI^{DS} synthesis and crystallization, Sam Struder, for her part in the synthesis of the 2-mercaptoimidazole polymer, $\{[Cu^{I}_2(\mu\text{-HMI})_3](NO_3)_2\}_n$, and Colin D. McMillan for his expertise in X-ray crystallography.

3.2 Results and Discussion

Synthesis

The disulfide MMI^{DS} can be generated *in situ* by air oxidation of MMI to yield the $Zn(MMI^{DS})Cl_2$ complex,[38] and single crystal structures of the charged $[MMI^{DS}H_2][ClO_4]$ species,[39] where the imidazole nitrogen atoms are protonated or methylated,[39] have been isolated. However, direct synthesis of the neutral MMI^{DS} ligand has not been previously reported. By modifying a method for synthesis of the neutral *t*-butyl-substituted MMI^{DS}[40], MMI^{DS}(**1**) can be successfully synthesized in 49% yield.

Three variables were analyzed when exploring reactions between copper and methimazole: the oxidation state of the copper, the monomeric (MMI) or oxidized dimeric form of methimazole (MMI^{DS}), and the presence of oxygen. To determine the effect of copper oxidation state in the reaction, separate reactions of $[Cu(NCCH_3)_4][BF_4]$ or $Cu(BF_4)_2$ was treated with methimazole in acetonitrile were performed (Scheme 3.2A and 3.2B). After stirring both reactions for 18 h, the same dinuclear copper(I) complex $[Cu_2(\mu\text{-}MMI)_2(MMI)_4][BF_4]_2$ (**2**) is the primary product. With the $[Cu(NCCH_3)_4]^+$ starting material, **2** forms in 68% yield and is air stable in the solid state for several weeks, although sulfur extrusion is reported when the reaction is stirred for 3-4 days.[31] With $Cu(BF_4)_2$ as the copper source, the blue reaction solution becomes colorless, indicating reduction of Cu(II) to Cu(I), with concomitant formation of MMI^{DS} (Scheme 3.2B), and **2** was isolated as a colorless solid in 36% yield. Formation of MMI^{DS} in addition to **2** was verified by MALDI-MS of the reaction solution (*m*/*z* 229 for $[MMI^{DS}H]^+$), but no Cu(I)-coordinated MMI^{DS} product was isolated. Raper[23] previously synthesized complex **2**

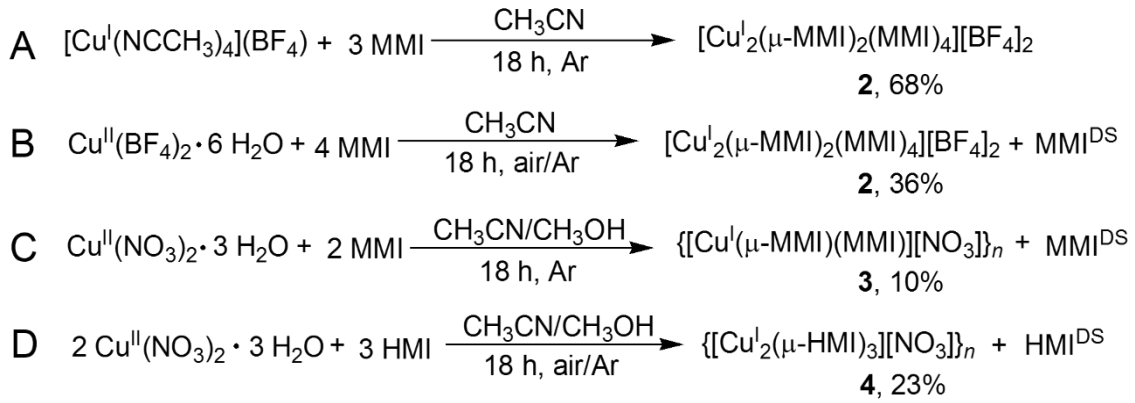

Scheme 3.2. Reaction conditions used to evaluate the effects of copper oxidation state and counterions on product formation.

from $Cu(BF_4)_2$ using similar methods, but MMI^{DS} formation during the reaction was not examined. Although O_2 was readily available during synthesis, there was no indication of sulfur elimination with acetonitrile as the solvent and tetrafluoroborate as the counterion, either in analysis of the reaction mixture by MALDI-MS or in the isolated products.

Sulfur extrusion to form copper-coordinated MMI^{MS} ligands is typically observed for reactions performed in air with $Cu(NO_3)_2$ as the copper source.[31,34-36,41] To examine the oxygen dependence of MMI^{MS} formation, $Cu(NO_3)_2$ and methimazole were combined under air-free conditions. Upon $Cu(NO_3)_2$ addition, the blue reaction mixture immediately becomes colorless, indicating Cu(II) reduction to Cu(I) by methimazole. MMI^{DS} formation was confirmed by mass spectrometry. The polymer, $\{[Cu^I(\mu\text{-MMI})(MMI)](NO_3)\}_n$ (**3**; 10% yield) was isolated under air-free conditions (Scheme 3.2C). Subsequent attempts to reproduce the synthesis of this product for further characterization were unsuccessful and resulted in isolation of the previously reported, mononuclear $[Cu(MMI)_3][NO_3]$ complex.[28]

A parallel, air-free reaction was also examined by combining $Cu(NO_3)_2$ with 2-mercaptoimidazole (HMI; Scheme 3.2D), the structurally similar but unmethylated

imidazole thione (Figure 3.1). This reaction also resulted in formation of a novel polymeric Cu(I) complex, $\{[Cu^{I}_2(\mu\text{-HMI})_3](NO_3)_2\}_n$ (**4**) in 21% yield. No evidence for sulfur extrusion was observed under air-free conditions, supporting the key role of oxygen in the elimination of the sulfur from the disulfide.

A similar reaction was performed under aerobic conditions (Scheme 3.2B). When MMI in acetonitrile is added to $Cu(NO_3)_2$ in methanol in a 4:1 ligand-to-metal ratio, the blue Cu(II) solution turns light yellow, indicating the reduction of the copper ion to Cu(I). After stirring for 12 hours, the solution turns back to light blue, due to oxidation of Cu(I) back to Cu(II) in air. After stirring for 3 days, products were isolated under a variety of conditions, using several different solvents (Scheme 3.3). One previously reported product, $[Cu^{II}(\eta^2\text{-MMI}^{MS})_2(H_2O)_2][NO_3]_2$ (**5**),[31] was obtained through ether diffusion into the reaction mixture, and previously reported, $Cu^{II}(\eta^2\text{-MMI}^{MS})_2(H_2O)_2][CH_3SO_4]_2$ (**6**) [42] as well as the novel $[Cu^{II}(\eta^2\text{-MMI}^{MS})_2(H_2O)][CH_3SO_4][HSO_4]\cdot H_2O$ (**7**) were obtained by solvent evaporation. $[Cu^{II}(\eta^2\text{-MMI}^{MS})_2(H_2O)][CH_3SO_4]_2$ (**8**) was obtained by slow evaporation after a reaction time of only 18 hours. The sulfate-bound $[Cu^{II}(\eta^2\text{-MMI}^{MS})(\eta^2\text{-}SO_4)(CH_3OH)]$ (**9**) and $[Cu(\eta^2\text{-MMI}^{MS})(\eta^2\text{-}SO_4)(DMSO)]\cdot 0.5$ DMSO (**10**) complexes were obtained when the ligand-to-metal ratio was reduced to 2:1. Mass spectrometry results of the reaction solutions confirm the presence of a number of Cu-MMI and Cu-MMI^{DS} fragments with no evidence of MMI^{MS} formation.

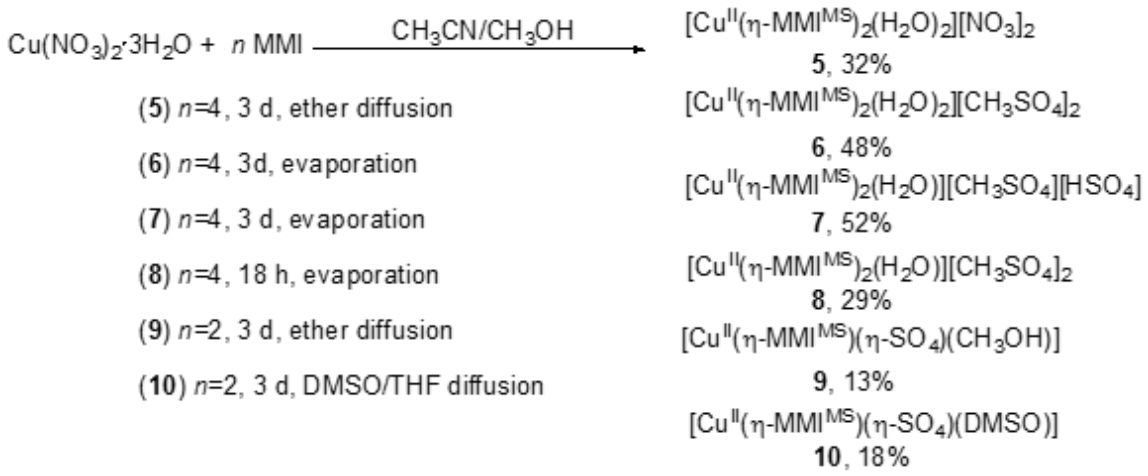

Scheme 3.3. Treating methimazole (MMI) with $Cu(NO_3)_2$ under aerobic conditions results in a variety of sulfur-extruded (MMI^{MS}) products **5**, **6**, **7**, **8**, **9**, and **10** that are dependent on MMI stoichiometry, reaction duration, and crystallization conditions.

Although sulfate or methylsulfate ions were not present in the starting materials of the reactions that yielded complexes **6-10**, sulfate and methylsulfate counterions are observed in the isolated products. This suggests that these counterions were formed from oxidation of the extruded sulfur during the course of the reaction. In cases where only two equivalents of MMI were used in this reaction, one of the two Cu(II)-coordinated MMI^{MS} ligands observed in complexes **5-8** is replaced with Cu(II)-coordinated sulfate in complexes **9** and **10**. In the reported synthesis of **6**, copper(II) sulfate was used as a reactant, so the source of the sulfate could not be positively identified.

To determine whether sulfur elimination to form complexes **5-10** is dependent on copper oxidation state, MMI^{DS} was treated with $[Cu(NCCH_3)_4]^+$ under air-free conditions (Scheme 3.4). After 3 h stirring, $[Cu^I_2(\mu\text{-}MMI^{DS})(MMI^{DS})_2](BF_4)_2$ (**11**) was isolated in 22% yield. In subsequent attempts to reproduce this synthesis, only the $[Cu(NCCH_3)_4][BF_4]$ starting material was recovered. This suggests that $[Cu(NCCH_3)_4][BF_4]$ may be more

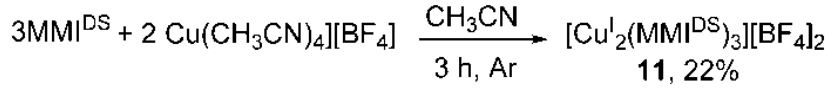

Scheme 3.4. Treating MMI^{DS} with Cu(I) under air-free conditions yields the novel, dinuclear Cu(I) complex $[Cu_2(MMI^{DS})_3][BF_4]_2$ (**11**).

stable than **11**, perhaps due to the strain on the disulfide bond induced in crystallization, as discussed in the *Structural analysis of Cu-methimazole complexes* section.

From the reactions shown in Schemes 3.1, 3.2, and 3.3, it is evident that oxygen availability, copper ionization state, and counter ion and solvent effects all influence the products formed with these relatively straightforward reactants. Cu(I) forms complexes with both the thione sulfur of MMI, as seen in complexes **1** and **2**, as well as the nitrogens of MMI^{DS}, as seen in complex **11**, but control of oxygen is crucial. Sulfur extrusion is only observed under aerobic conditions, as exemplified by complexes **5**-**10**. Although disulfide oxidation to sulfinates or sulfonates is fairly common,[43-46] sulfur elimination has only been reported for MMI reactions. The identity of the metal also plays a critical role. Complexes with imidazole disulfide ligands are reported with a variety of metals: Co(*t*-butyl-$MMI^{DS})_2Cl_2$,[47] Zn(*t*-butyl-$MMI^{DS})_2Cl_2$,[40] Fe(*t*-butyl-$MMI^{DS})_2Cl_2$,[40] Ni(*t*-butyl-$MMI^{DS})_2Cl_2$,[40] and $Zn(MMI^{DS})Cl_2$[38] All of these complexes are synthesized under aerobic conditions with no evidence of sulfur oxidation or elimination. Aside from the Cu(II) complexes mentioned above, no other metal complexes are reported with the MMI^{MS} ligand, although sulfur extrusion to form MMI^{MS} was observed when hydrotris(thioimdiazolyl) borate was treated with iodine.[48]

After MMI coordination to redox-active Cu(I) and subsequent oxidation to the MMI^{DS}, the formation of monosulfide methimazole-Cu(II) complexes were consistently

observed. Subsequent Cu(II) coordination of the monosulfide (MMI^{MS}) is favored in a bidentate fashion in the equatorial position, with a variety of solvents coordinating in the axial positions. Disulfide oxidation to sulfinate is common,[43,44,46] but this generally results in the breaking of the disulfide bond rather than complete oxidation and elimination of a sulfur atom. The presence of methylsulfate ions in **6**-**8** indicates that nucleophilic attack of methanol on a sulfur atom may occur prior to sulfur elimination.

NMR spectroscopy

^{1}H NMR spectra were obtained only for Cu(I) complexes **2**, **3**, and **4** due to Cu(II) paramagnetic effects in complexes **5**, **6**, **7**, **8**, **9**, and **10**. The ^{1}H NMR spectrum of **2** shows a small downfield shift for the MMI methyl resonance compared to unbound MMI (δ 3.53 vs. 3.42; Table 1), whereas the olefinic protons shift slightly upfield by an average of δ 0.1 compared to unbound methimazole. In contrast, similar dinuclear complexes, such as $[Cu_2(ebit)_2(MMI)_2][BF_4]$ (ebit = ethylene bis-imidazole thione),[49] show a downfield shift of the MMI olefinic protons upon copper coordination, indicating an increase in the electron density of the heterocycle.

For the Cu(I) polymeric complexes **3** and **4**, opposing shifts in the olefinic resonances are observed. The MMI olefinic resonance shifts downfield upon complexation, but the HMI olefinic responances shift slightly upfield. The imidazole –NH peak at δ 12.06 of the unbound methimazole is broad, indicating exchange. Upon complexation, this resonance is no longer observed for the polymeric **3**, and is shifted significantly upfield for the dinuclear **2**.

Table 3.1. ^{1}H NMR resonances (in CD_3CN) for ligands and their Cu(I) complexes.

Compound	^{1}H NMR Resonances		
	δ CH_3	δ CH	δ NH
MMI	3.42	6.87,7.05	12.06
2	3.54	6.83, 6.90	10.32
3	3.66	7.06, 7.13	-
HMI	-	7.10	12.56
4	-	6.85	11.98

Infrared spectroscopy

Compared to the C=S stretching band for unbound MMI in the infrared (IR) spectrum (1273 cm^{-1}), Cu(I) complex **2** has three separate C=S stretching bands at similar energies (1267, 1279, and 1267 cm^{-1}), consistent with IR data for **2** reported by Raper.[23] Although little change in energy of the δ C=S vibration is observed upon copper-MMI binding compared to MMI (674 vs, 673 cm^{-1}, respectively), the π C-S band shifts to lower energy (515 cm^{-1} for **2** and 529 cm^{-1} for MMI). This shift indicates that the double bond character of the thione in the polymer is increased, which one would not expect as the copper coordination occurs and is not indicated in the bond length of the complex, which is significantly longer for **2** as compared to methimazole. Broadening in the 1020-1100 cm^{-1} range typical of the tetrafluoroborate ion was observed in **2**.

Structural analysis of MMI^{DS} and Cu-methimazole complexes

N-heterocyclic disulfides with *t*-butyl and benzyl substituents on one nitrogen atom have been reported by Figueroa and coworkers,[40] and the ionic form of methimazole disulfide, with protons on one or both of the heterocyclic nitrogen atoms, has also been isolated. However, the structure of neutral MMI^{DS} (Figure 3.2 and Table 3.2), is reported

here for the first time. In contrast to $[H(MMI^{DS})]^{+}$ and $[H_2(MMI^{DS})]^{2+}$, **1** has no observable electron density around the unmethylated nitrogen of the imidazole ring, supporting the lack of protonation at N2 (Figure 3.2B). The MMI^{DS} molecules form layers along the *b*-axis with dihedral angles of 90.2˚ along the C-S-S-C bonds, as seen in the packing diagram in Figure 3.7.

Structures were also obtained for the Cu(I) complexes, $[Cu^{I}_2(\mu\text{-}MMI)_2(MMI)_4](BF_4)_2$ (**2**), $\{[Cu^{I}(\mu\text{-}MMI)(MMI)](NO_3)\}_n$ (**3**), and $\{[Cu^{I}_2(\mu\text{-}HMI)_3](NO_3)_2\}_n$ (**4**), (Figure 3.3 and Table 3.3). X-ray data for **2** is consistent with previous

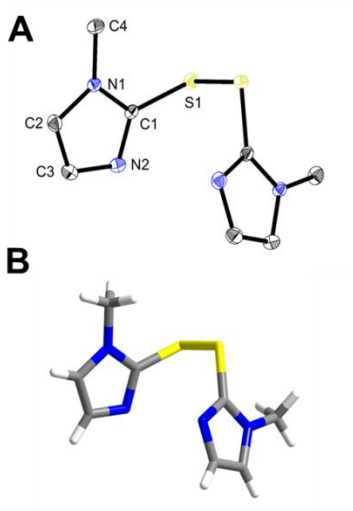

Figure 3.2. A) Crystal structure diagrams with 50% probability density ellipsoids for MMI^{DS} (**1**). Hydrogen atoms are omitted for clarity in A. B) Structure diagram showing hydrogen atoms, emphasizing the lack of protonation at the N2 atom.

Table 3.2. Selected bond lengths (Å) and angles (˚) for **1**.

	Bond length (Å)		**Bond Angle (˚)**
S1-S2	2.1010(4)	C1-S1-S1	101.72(3)
C1-S1	1.7413(8)	S1-C1-N2	123.81(6)
C1-N1	1.3678(10)		
C1-N2	1.3295(11)		

reports,[23] although our unit cell dimensions are slightly smaller (Table 3.7), likely due to structural determination at a lower temperature (100 K). Since all other structures in the present study were collected at low temperature, data from this low temperature structure of **1** will be used for comparisons.

The two polymeric methimazole complexes **2** and **3** have distorted tetrahedral geometry ($\tau = 0.895$) and trigonal planar geometry around Cu(I), respectively (Figure 3.3 and Table 3.3). Complex **2** exhibits an alternating Cu-S-Cu-S backbone incorporating one terminal and two bridging MMI ligands. Cu-S bond lengths (2.2243(4) Å and 2.2620(4) Å for terminal and bridging MMI, respectively) are shorter than the Cu-S bond lengths of **2** for both bridging (2.4394(4) Å) and terminal (2.3136(4) Å MMI ligands), due to the difference in Cu(I) coordination geometry. Similar to **3**, the polymeric structure of **4** with HMI ligands also has trigonal planar geometry around Cu(I), but a double S-Cu-S-Cu backbone is formed in which all of the S atoms are bridging (Figure 3.3B). The structures of copper-methimazole coordination polymers with bridging halides, $\{Cu_3Br_3(MMI)_3\}$ and $\{Cu_2I_2(MMI)_2\}_n$,[41] are reported, but this is the first homoleptic Cu-methimazole polymer. In the polymeric structures of **3** and **4**, π-π interactions resulting in alignment of the heterocyclic rings provides stability. Intermolecular and intramolecular π-π interactions are of particular interest in polymer research, and the

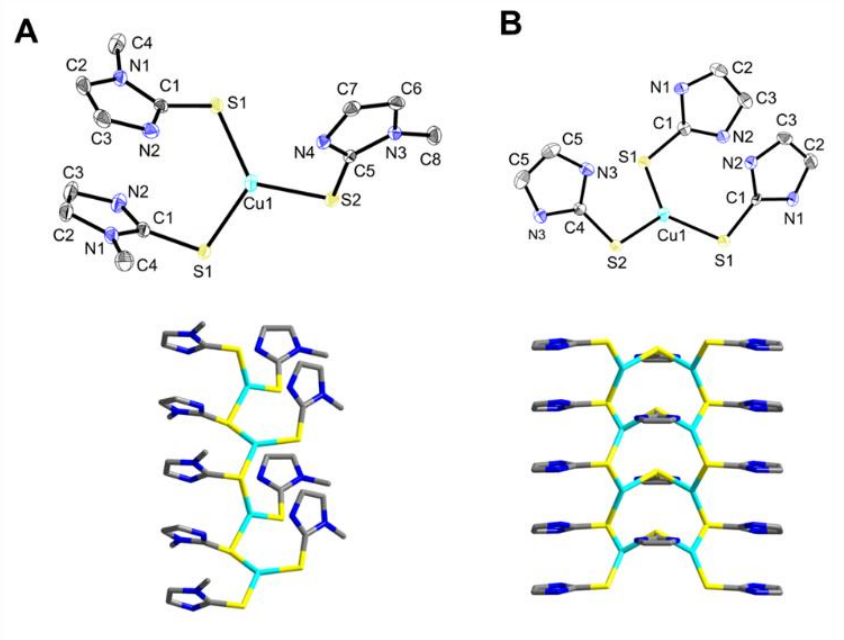

Figure 3.3. Crystal structure diagrams with 50% probability density ellipsoids for A) {[Cu^{I}(μ-MMI)(MMI)](NO_3)}$_n$ **3** (top) and B) {[Cu^{I}_2(μ-HMI)$_3$]$(NO_3)_2$}$_n$ **4** (top). Hydrogen atoms and counterions are omitted for clarity. Diagrams showing the extended structures for A) **3** with a single Cu-S-Cu-S backbone (bottom) and B) **4** with the bridging sulfurs creating a double Cu-S-Cu-S backbone (bottom.)

Table 3.3. Selected bond lengths (Å) and angles (˚) for **2**, **3**, and **4**. S_b denotes a bridging sulfur and S_t denotes a terminal sulfur.

	2	**3**	**4**
Cu-S_b	2.3475(4)	2.2620(4) 2.2739(4)	2.2374(12) 2.2534(12) 2.2773(11)
Cu-S_t	2.4394(4)	2.2243(4)	-
C-S_b	1.7157(11)	1.7243(16)	1.728(4) 1.731(6)
C-S_t	1.7055(11)	1.7143(15)	-
S_b-Cu-S_t	117.154(13)	125.94(2)	-
S_b-Cu-S_b	103.029(10)	118.79(2)	135.13(5) 118.45(5) 105.56(5)
C-S_b-Cu	99.40(4)	108.24(6) 104.11(5)	109.56(15) 103.49(14) 106.22(12)
C-S_t-Cu	107.75(4)	105.03(5)	-
Cu-S_b-Cu	76.972(10)	106.00(2)	93.28(4) 108.23(7)

incorporation of a redox active metal such as copper enhances both spectrochemical and electrochemical properties.[50-53]

Six differentstructures incorporate the sulfur-extruded MMI^{MS} ligand: $[Cu^{II}(\eta^2\text{-}MMI^{MS})_2(H_2O)_2][NO_3]_2$ (**5**), $([Cu^{II}(\eta^2\text{-}MMI^{MS})_2(H_2O)_2][CH_3SO_4]_2$ (**6**), $([Cu^{II}(\eta^2\text{-}MMI^{MS})_2(H_2O)][CH_3SO_4][HSO_4]\cdot H_2O$ (**7**), $([Cu^{II}(\eta^2\text{-}MMI^{MS})_2(H_2O)][CH_3SO_4]_2$ (**8**), $Cu^{II}(\eta^2\text{-}MMI^{MS})(\eta^2\text{-}SO_4)(CH_3OH)$ (**9**), and $Cu(\eta^2\text{-}MMI^{MS})(\eta^2\text{-}SO_4)(DMSO)\cdot 0.5$ DMSO (**10**). These Cu(II) complexes can be grouped into three categories based on cationic structure: 1) octahedral geometry with two MMI^{MS} ligands in the equatorial positions bound in a bidentate fashion through the nitrogen atoms and two waters in the axial positions (**5** and **6**, Figure 3.4B and Table 3.4), 2) distorted square pyramidal geometry with two MMI^{MS} ligands in the equatorial positions and one water in the axial position (**7** and **8**, Figure 3.4A and Table 3.4), and 3) distorted tetrahedral geometry with one MMI^{MS} ligand in the equatorial position, one bidentate sulfate in the equatorial position, and a solvent molecule (methanol or DMSO) in the axial position (**9** and **10**). Since the structure of **5** is published,[31] it will not be discussed in depth. Octahedral **6** is also reported,[42] but it will be used as a representative octahedral cation, to compare to **7** and **8**, and for general discussion of the fate of the extruded sulfur.

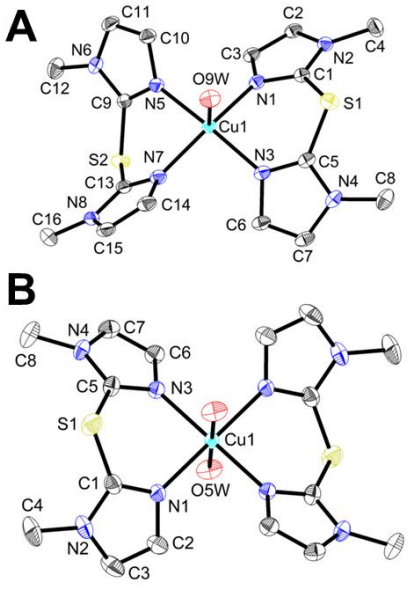

Figure 3.4. Crystal structure diagrams with 50% probability density ellipsoids for A) ([Cu^{II}(η^2-MMI^{MS})$_2$(H_2O)][CH_3SO_4][HSO_4]·H_2O **(7)**, showing the distorted square pyramidal geometry with an axial water molecule, and B) ([Cu^{II}(η^2-MMI^{MS})$_2$(H_2O)$_2$][CH_3SO_4]$_2$ **(6)**, showing octahedral geometry with two coordinated water molecules. Hydrogen atoms and counterions are omitted for clarity.

Table 3.4. Selected bond distances (Å) and angles (˚) for the [Cu(MMI^{MS})$_2$(H_2O)$_x$]$^{2+}$ complexes **5**, **6**, **7**, and **8**, with x = 2 for **5** and **6** and x = 1 for **7** and **8**.

	5	**6**	**7**	**8**
Cu-N1	2.0172(12)	2.000(2)	1.9969(17)	2.0034(18)
Cu-N3	2.0172(12)	2.002(2)	1.9998(17)	1.9943(18)
C1-S1	1.7474(15)	1.760(3)	1.746(2)	1.755(2)
C5-S1	1.7520(15)	1.768(3)	1.751(2)	1.756(2)
Cu-OW	2.4514(12)	2.4186(19)	2.1926(16)	2.1864(16)
N3-Cu-N5	180	180	169.86(7)	169.20(7)
N3-Cu-N7	91.58(5)	89.06(9)	91.97(7)	89.33(7)
N5-Cu-N7	88.42(5)	90.94(9)	87.16(7)	88.41(7)
N3-Cu-O1	88.61(5)	87.12(8)	100.09(7)	97.10(7)
N3-Cu-O2	91.39(5)	90.79(8)	--	--

Complexes **9** and **10** have distorted square pyramidal geometry about the copper ion and only one molecule of MMI^{MS} is coordinated in an equatorial position, (Figure 3.5 and Table 3.5). Equatorial coordination is completed by bidentate coordination of sulfate, although the equatorial plane is distorted due to the ring strain inherent in the 4-membered

chelate ring formed by the sulfate with copper. A solvent molecule coordinates in the axial position for both **9** (CH_3OH) and **10** (DMSO), varying depending on the solvent present during crystallization. All of these products are solvent dependent, since H_2O, CH_3OH, and DMSO stabilize the axial positions of the five-coordinate or six-coordinate complexes. The coordinated water molecules are likely from the waters of hydration of the $Cu(NO_3)_2 \cdot 3H_2O$ starting material, since dry solvents were used in all the reactions.

In the first copper structure with this ligand, the nitrogen atoms of one terminal, bidentate MMI^{DS} ligand in $[Cu^{I}_2(\mu\text{-}MMI^{DS})(MMI^{DS})_2][BF_4]_2$ (**11**) and one nitrogen atom of a bridging MMI^{DS} ligand coordinate each Cu(I) center, resulting in trigonal planar

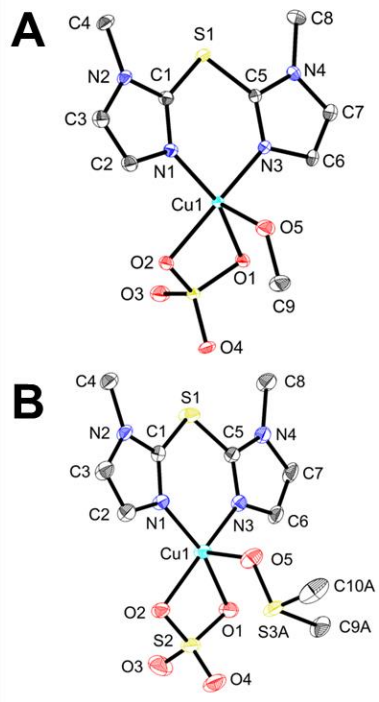

Figure 3.5. Crystal structure diagrams with 50% probability density ellipsoids for A) **9** and B) **10**. Both structures exhibit bidentate coordination of Cu(I) with *in situ*-generated sulfate and methanol (**9**) or DMSO (**10**) coordination. Hydrogen atoms and counter ions are omitted for clarity.

Table 3.5. Selected bond distances (Å) and angles (˚) for $[Cu(MMI^{MS})(SO_4)(L)]^{2+}$ complexes. For **9**, L = CH_3OH and for **10**, L = DMSO).

	9	**10**
Cu-N1	1.9547(16)	1.959(3)
Cu-N3	1.9587(16)	1.957(3)
C1-S1	1.7473(19)	1.744(4)
C5-S1	1.7493(18)	1.746(4)
Cu-OW	2.2186(15)	2.259(3)
Cu-O1	2.0083(13)	1.992(3)
N3-Cu-O2	160.84(7)	160.00(12)
N3-Cu-O1	95.41(6)	94.65(12)
N1-Cu-N3	93.40(6)	93.95(13)
N3-Cu-O5	100.82(6)	101.05(12)
O2-Cu-O1	71.29(6)	71.73(11)

geometry (Figure 3.6 and Table 3.6). Complex **11** is folded over with the bend in the molecule occurring through the C-S-S-C bond of the bridging molecule. The terminal MMI^{DS} ligands form a 7-membered ring with each Cu(I). The Cu(I) trigonal planar geometry is distorted, with bond angles of 110.81(11)˚, 119.53(11)˚, and 129.64(12)˚. The N-Cu-N angle closest to 120˚ (119.53(11) of the N4-Cu1-N1) is the ring-incorporated angle, indicating that the distortion of the other two angles is due to the strain of the bridging MMI^{DS}. The C-S-S angle (101.25˚) of the terminal MMI^{DS} ligands does not change from unbound MMI^{DS} (101.72(3)˚). However, the bridging MMI^{DS} bond angle is slightly broadened to 105.55(12)˚, indicating strain on the disulfide bond. The intramolecular Cu-Cu distance is 3.521 Å in **11**, and the intermolecular distance between Cu(I) of adjacent molecules is 3.705 Å (Figure 3.8).

The S-S bond length for all three MMI^{DS} ligands in **11** (2.0659(12)-2.0813(14) Å) is slightly smaller than that of unbound MMI^{DS} (2.1010(4) Å), but the C-S bonds do not significantly change (1.7413(8) Å in unbound MMI^{DS} (**1**) and 1.748(3) Å in **11**). The C1-N1 bond in the imidazole ring is 1.327(4) Å, compared to 1.470(4) Å for the N2-C4 bond

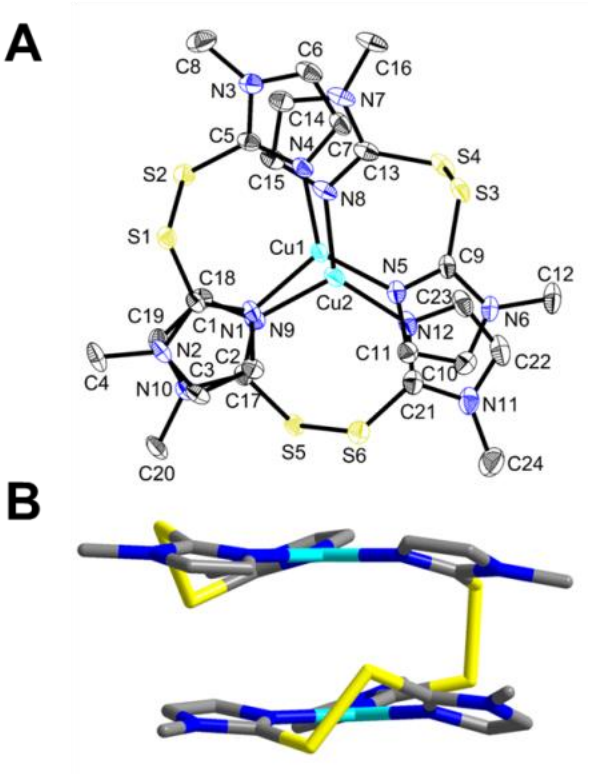

Figure 3.6. Crystal structure diagram with 50% probability density ellipsoids for **11**. Hydrogen atoms and counterions are omitted for clarity. The side view of **11** is shown in B, showing the intramolecular stacking and the disulfide ligand bridging the Cu(I) ions.

Table 3.6. Selected bond distances (Å) and angles (˚) for **11**.

	Bond length (Å)		**Bond Angle (˚)**
Cu1-N4	1.960(3)	N4-Cu1-N1	119.53(11)
Cu1-N1	2.021(3)	N4-Cu1-N5	129.64(12)
Cu1-N5	1.976(3)	N5-Cu1-N1	110.81(11)
S1-S2	2.0659(12)	C5-S2-S1	101.65(12)
C5-S2	1.748(3)	C1-S1-S2	101.25(11)
Cu-Cu	3.705	C9-S3-S4 (br)	105.55(12)
C1-N1	1.327(4)		
C4-N2	1.470(4)		

to the methyl group. The shorter bond length is consistent with the aromaticity of the imidazole ring and is consistent with the imidazole C-N of the unbound ligand (1.3295(11) Å).

For all of the structures, little change is observed in the C-S bond length (1.75 Å), whether the methimazole S is terminal, bridging, or in the monosulfide or disulfide ligands. This bond length is significantly longer than the C=S bond in uncoordinated methimazole (1.686 Å[54]) or dimethylimidazole thione (1.698 Å[55]), and is shorter than the C-S single bonds of thiols (1.86 Å). This suggests that the C-S bond is an extension of the electron delocalization exhibited in the heterocycle. In addition, the bond length of the non-methylated nitrogen of the imidazole ring and sulfur-bound carbon shortens upon complexation compared to the protonated, unbound ligands. This shortening in bond length suggests that electron density is shifted to the ring upon coordination for all complexes.

The thione exhibits a remarkable capacity to bridge copper ions, as seen in complexes **1**, **2**, and **3**. Even when MMI^{DS} is formed in the reduction of Cu(II) (Scheme 3.2B and 3.2C), the resulting Cu(I) ion shows preference for coordination of the thione of MMI over the imidazole nitrogen atoms in MMI^{DS}. As seen in the Cu(I) polymers, the imidazole moiety also increases stability to the three-dimensional structure through π-stacking.

Revising the sulfur extrusion mechanism

Sulfur extrusion is observed for all reactions performed in air with the $Cu(NO_3)_2$ starting material (Scheme 3.3). MMI^{DS} initially forms as Cu(II) is reduced by MMI

(Scheme 3.1); however, in the reaction and/or crystallization process, a sulfur atom is eliminated from the disulfide, and the resulting MMI^{MS} coordinates Cu(II). Previous groups have attributed oxidation of the disulfide bond to either water[44] or dioxygen exposure.[31] Subsequent sulfur elimination is only observed in the presence of strong oxidizers such as nitrate,[56,57] or in the presence of electron-rich transition metals, such as copper.[31,33-36,58,59] The most detailed mechanism for sulfur extrusion from MMI^{DS} to form MMI^{MS} is proposed by Lobana and coworkers,[31] but this mechanism fails to 1) incorporate the critical role of copper coordination, 2) does not address stoichiometry in the oxidation of the sulfur, and 3) does not address the role of the solvent in formation of the methyl sulfate counterion.

A revised mechanism for this sulfur extrusion reaction is proposed in Scheme 3.5. As in the mechanism proposed by Lobana and coworkers,[31] oxidation of MMI to MMI^{DS} is facilitated by Cu(II) reduction to Cu(I). Cu(I) coordinates MMI^{DS}, similar to the coordination we observe in complex **11**. In the presence of oxygen, one of the MMI^{DS} sulfur atoms is then oxidized to the sulfone, with concomitant oxidation of Cu(I) to Cu(II). Nucleophilic attack by water or methanol on the sulfone sulfur then initiates cleavage of the S-S bond to form an imidazole thiolate. Cu(II) coordination is likely vital to keep the nucleophilic imidazole thiolate in proximity to the now-separated, second imidazole ring. Nucleophilic attack by the imidazole thiolate on the C=S carbon of the second imidazole ring eliminates the extruded sulfur as sulfite or methylsulfite. Sulfite oxidation to sulfate catalyzed by transition metals, including copper, is well known,[60,61] and in this case, possible formation of superoxide from the oxidation of Cu(I) to Cu(II) by oxygen may also

contribute to sulfite oxidation.[61] Incorporation of water or methanol to generate sulfate or methylsulfate ions from the extruded sulfur is consistent with the sulfate and methylsulfate ions present in complexes **6-10**. Overall, this nucleophilic aromatic substitution mechanism is similar to that observed for thiolate deprotection of nitrobenzenesulfonyl.

Oxidation of disulfide bonds has been extensively studied under a variety of conditions,[62-66] and Cu(II) can oxidatively cleave disulfide bonds to form sulfinates.[43,44] Oxygen from air participates in the oxidation of the disulfide bond, but Cu(II) is shown to be crucial to disulfide oxidation, as opposed to other transition metals, such as Zn^{2+}.[37] Only aromatic, heterocyclic thiones have demonstrated the ability to eliminate one of the disulfide sulfur atoms by oxidation,[31,33-36,59] giving support to the proposed nucleophilic aromatic substitution mechanism as well as the importance of copper coordination to keep the nucleophilic thiolate in proximity to the site of nucleophilic attack.

3.3 Conclusions

Control of Cu(I) and Cu(II) reactions with methimazole was explored utilizing a variety of counterions, solvents, and the presence or absence of oxygen. In the absence of oxygen, Cu(I) reacts with MMI to form multinuclear complexes stabilized by bridging thiones and π-stacking, indicating an environment rich in electrons. In the presence of oxygen with tetrafluoroborate counterion, the dinuclear $[Cu_2(MMI)_6][BF_4]_2$ complex is the favored product with both Cu(I) and Cu(II) starting materials. In the presence of oxygen and nitrate, sulfur extrusion by oxidation of the MMI^{DS} ligand results in the formation of a variety of Cu(II)-MMI^{MS} complexes, with variation introduced by the solvent system and molar ratios of ligand available. To form MMI^{MS}, sulfur oxidation and elimination of

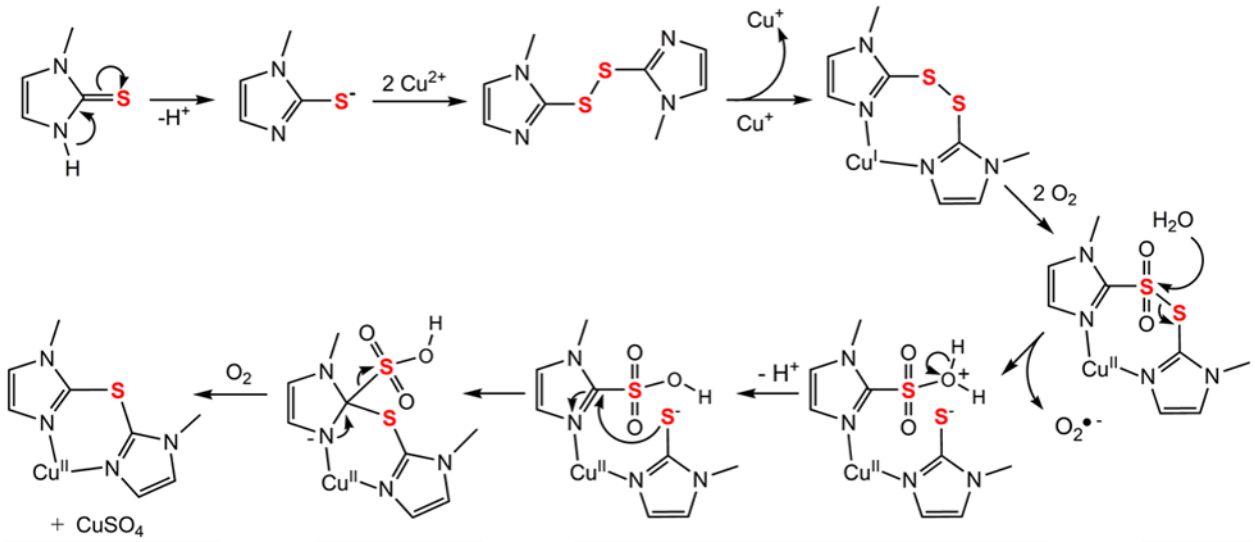

Scheme 3.5. New proposed mechanism for formation of MMI^{DS} by Cu(II) reduction, formation of the sulfone by reaction with dioxygen, and eventual sulfur extrusion via nucleophilic aromatic substitution.

sulfite or methylsulfite likely occurs to generate sulfate and methylsulfate ions, catalytically oxidized by the available copper. Cu(II) coordination likely imposes entropic control to align the resulting thiolate for nucleophilic aromatic substitution.

MMI^{DS} is a bridging ligand in the dinuclear Cu(I) complex $[Cu_2(MMI^{DS})_3][BF_4]$, but poor reaction yields and high recovery of the starting material suggest that this is not a particularly stable complex. Based on the reaction conditions and complexes obtained, Cu(I) coordination favors the thione of MMI, whereas Cu(II) favors bidentate coordination of the MMI^{MS} to form five-membered, almost planar, rings in the equatorial position.

The complexity of redox reactions between methimazole, copper, and other oxidative sources such as solvents and oxygen indicates a wide range of potential interactions within the cellular system. The propensity to coordinate copper ions in both the oxidized and reduced state, along with the sensitivity to oxidative species, has potential implications for biological MMI reactivity and catalysis with redox systems incorporating copper.

3.4 Experimental Methods

General Methods

1-Methylimidazole thione (methimazole, MMI), copper(II) nitrate heptahydrate, and copper(II) tetrafluoroborate were purchased commercially. Tetrakis(acetonitrile)copper(I) tetrafluoroborate was prepared according to published procedures.[67] Reactions were performed air-free where indicated, utilizing standard

Schlenk techniques under argon. IR spectra of the ligands and complexes were acquired in the range 4000-450 cm^{-1} as Nujol mulls on KBr plates or as KBr pressed pellets, as indicated, on a Magna 550 IR spectrometer. IR absorption abbreviations are vs, very strong; s, strong; m, medium; w, weak; b, broad; sh, shoulder. ^{1}H and $^{13}C\{^{1}H\}$ NMR spectra were obtained using Bruker-AVANCE 300 and 500 MHz NMR spectrometers. Chemical shifts are reported in δ relative to tetramethylsilane (δ 0) and referenced to solvent. MALDI mass spectrometry experiments were performed using a Bruker Microflex MALDI-TOF mass spectrometer with *trans*-2-3-(4-tert-butylphenyl)-2-methyl-2-propenyldiene (*m*/*z* 250.3) as the matrix. All peak envelopes matched calculated values.

*Synthesis of bis(1-methylimidazol)-2-yl-disulfide, MMI^{DS} (**1**)*

Synthesis of **1** was performed by adapting the published synthesis of the *t*-butyl-methimazole disulfide.[40] I_2 (1.62 g, 6.4 mmol) was added in portions to a solution of 1-methylimidazole thione (MMI; 1.46 g, 12.8 mmol) and NEt_3 (1.86 mL, 13.4 mmol) in CH_2Cl_2 (100 mL). The resulting orange mixture was stirred for 30 min and H_2O (100 mL) was added. The resulting layers were separated, and the CH_2Cl_2 layer was washed with H_2O (2 × 50 mL), dried over Na_2SO_4 for an additional 45 min, and filtered. After filtration, the solvent was removed *in vacuo* to give MMI^{DS} as a yellow powder (671 mg, 46 %). Crystals suitable for X-ray diffraction were grown from chloroform in diethyl ether. ^{1}H NMR (300 MHz, d_6-DMSO): δ 3.43 (s, 6H, CH_3), 7.09 (s, 1H, CH), 7.46 (s, 1H, CH). $^{13}C\{^{1}H\}$ NMR (d_6-DMSO):δ 33.4 (CH_3), 126.0 (CH), 130.3 (CH), 138.1 (C=S). IR (Nujol,

cm^{-1}): 3902 w, 2725 w, 1313 w, 1283 s, 1159 w, 1128 s,b, 919 s, 794 s, 724 s, 683 s, 500 s.

Synthesis of $[Cu_2(MMI)_4(\mu\text{-}MMI)_2](BF_4)_2$ ***(2)***

Method 1. Under air-free conditions, a solution of (MMI; 137 mg, 1.20 mmol) in acetonitrile (10 mL) was transferred by cannula to a solution of $Cu(BF_4)_2{\cdot}6H_2O$ (104 mg, 0.30 mmol) in acetonitrile (5 mL). As MMI was added a light green precipitate formed that turned yellow-white upon filtration and drying under vacuum. The precipitate was washed with diethyl ether (10 mL). Crystals of **2** were obtained by ether diffusion into an acetonitrile solution. Yield: 566 mg, 57 %. IR (Nujol mull, cm^{-1}): 3161 w, 3116 w, 2727 s, 1577 vs, 1517 w, 1462 vs, 1401 vs, 1350 s, 1289 s, 1279 s, 1267 s, 1246 w, 1160 s, 1108 b, 1063 b, 992 b, 918 w, 850 w, 763 s, 728 vs, 695 w, 673 s, 599 w, 515 s. ^{1}H NMR (500 MHz, CD_3CN): δ 3.54 (s, 18H, CH_3), 6.83 and 6.90, (each, d, 6H, C-H), 10.32 (br s, 5.5 H, N-H). $^{13}C\{^1H\}$ NMR (CD_3CN): 34.1 (CH_3), 115.1 (CH), 120.9 (CH), 156.5 (C=S). Anal. Calc. for $C_{24}H_{36}B_2Cu_2F_8N_{12}S_6$: C, 29.24; H, 3.68; N, 17.05. Found: C, 29.03; H, 3.66; N, 16.86.

Method 2. Complex **2** was also synthesized using the procedure outlined in method 1, except that $[Cu(CH_3CN)_4]BF_4$ (94 mg, 0.30 mmol) was used in place of $Cu(BF_4)_2{\cdot}6H_2O$. Yield: 566 mg, 57 %.

Method 3. A solution of MMI (137 mg, 1.20 mmol) in acetonitrile (10 mL) was transferred *via* cannula into a solution of $[Cu(CH_3CN)_4]BF_4$ (94 mg, 0.30 mmol) in acetonitrile (10 mL) under argon. The solvent volume was reduced by half *in vacuo*, and

then diethyl ether was added to precipitate out the product. The resulting white precipitate was filtered, washed with diethyl ether, and dried *in vacuo*. This reaction was also performed in air, affording the same product with a similar yield. Yield: 663 mg, 67%.

*Synthesis of {[Cu(μ-MMI)(MMI)](NO$_3$)}$_n$ (**3**)*

Under argon, a solution of MMI (137 mg, 1.20 mmol) in acetonitrile (10 mL) was transferred *via* cannula into a solution of Cu(NO$_3$)$_2$·3H$_2$O (73 mg, 0.30 mmol) in acetonitrile (5 mL). The solution was stirred for 3 hours and an oil formed upon solvent removal *in vacuo*. Methanol (5 mL) was added to dissolve the oil, and diethyl ether was diffused into the solution to afford needle-like, colorless crystals. Yield: 39 mg, 10.%. ^{1}H NMR (500 MHz, CD$_3$CN): 3.66 (s, 6 H, CH$_3$), 7.06 (s, 2H, CH), 7.13 (s, 2H, CH). ^{13}C{^{1}H} NMR (CD$_3$CN): 34.3 (CH$_3$), 120.2 (CH), 122.6 (CH), 150.6 (C=S).

*Synthesis of {[Cu$_2$(μ-HMI)$_3$](NO$_3$)$_2$}$_n$ (**4**)*

Under argon, a solution of HMI (120 mg, 1.20 mmol) in methanol (10 mL) was transferred *via* cannula into a solution of Cu(NO$_3$)$_2$·3H$_2$O (73 mg, 0.30 mmol) in methanol (10 mL). After stirring for 3 h, the blue solution became colorless, and a white precipitate formed. The precipitate was filtered, washed with diethyl ether (10 mL), and dried *in vacuo*. X-ray quality crystals were obtained by diffusion of diethyl ether into a methanolic solution of **4**. Yield: 118 mg, 21%. MALDI-MS (*m*/*z*): [Cu(C$_3$H$_4$N$_2$S)$_2$]$^+$ 262.3, [Cu(C$_3$H$_4$N$_2$S)]$^+$ 163.9. ^{1}H NMR (500 MHz, CD$_3$CN): 6.85 (s, 6H, CH), 11.98 (br s, 6H, NH). IR (Nujol mull, cm^{-1}): 3095 b,s, 2974 b,s, 2862 b,s, 2683 b,s, 1595 s, 1583 vs, 1459

s, 1319 vs, 1288 s, 1251 w, 1231 w, 1223 w, 1084 w, 1041 w, 912 s, 873 b, 761 s, 727 s, 680 s, 498 w. Anal. Calc. for $C_9H_{12}Cu_2N_8O_6S_3$: C, 19.60; H, 2.19; N, 20.32. Found: C, 19.93; H, 2.25; N, 19.33.

*Synthesis of [Cu(η^2-MMI^{MS})$_2$(H$_2$O)$_2$](NO$_3$)$_2$ (**5**)*

A solution of MMI (137 mg, 1.20 mmol) in acetonitrile (6 mL) was slowly added to a solution of $Cu(NO_3)_2 \cdot 3H_2O$ (73 mg, 0.30 mmol) in acetonitrile (5 mL), and the reaction mixture slowly turned light green. After stirring in air for 3 d, the solution became bright blue. The reaction mixture was allowed to slowly evaporate over a week to form blue crystals of **5**. Lighter blue crystals were also isolated and identified as $CuSO_4 \cdot 5H_2O$. The product obtained was consistent with that reported by Lobana and coworkers. Yield of **5**: 110 mg, 18%. Anal. Calc. for $C_9H_{12}Cu_2N_8O_6S_3$: C, 19.60; H, 2.19; N, 20.32. Found: C, 19.93; H, 2.25; N, 19.33.

*Synthesis of [Cu(η^2-MMI^{MS})$_2$(H$_2$O)$_2$](CH$_3$SO$_4$)$_2$ (**6**)*

A solution of MMI (228 mg, 2.00 mmol) in acetonitrile (10 mL) was added to a solution of $Cu(NO_3)_2 \cdot 3H_2O$ (120 mg, 0.50 mmol) in acetonitrile (10 mL). The colorless reaction mixture became blue after 1 h stirring, and a white precipitate formed. The precipitate was filtered and dried *in vacuo*. Methanol (5 mL) was added to dissolve the oil, and deep blue crystals of **6** formed upon solvent evaporation in air. The product obtained was consistent with the reported complex by Baldwin and coworkers. Yield: 369 mg, 52%. IR (Nujol mull, cm^{-1}): 3435 b, 3139 w, 2728 w, 1634 s, 1588 sh, 1532 w, 1487 sh, 1254 s,

1218 s, 1062 w, 1032 w, 1007 w, 960 w, 760 b, 710 sh, 655 w, 619 s, 576 w, 561 sh. Anal. Calc. for $C_{18}H_{38}CuN_8O_{10}S_4$: C, 30.10; H, 5.33; N, 15.60. Found: C, 29.32; H, 5.81; N, 15.53.

*Synthesis of [Cu(η^2-MMI^{MS})$_2$(H_2O)][CH_3SO_4][HSO_4][H_2O] (**7**)*

A solution of MMI (137 mg, 1.20 mmol) in 10 mL of acetonitrile was slowly added to a solution of $Cu(NO_3)_2 \cdot 3H_2O$ (73 mg, 0.30 mmol) in acetonitrile (10 mL), and the reaction mixture initially turned a light green. Upon stirring for 7 d, the solution turned blue, and the solvent was removed *in vacuo* to yield a dark-blue oil. Methanol (5 mL) was added to dissolve the oil, and blue crystals of **7** formed upon evaporation in air. Yield: 334 mg, 48%. IR, (Nujol mull, cm^{-1}): 3430 b, 3152 w, 3130 w, 2725 w, 2669 w, 1634 s, 1530 s, 1517 w, 1418 w, 1348 sh, 1307 w, 1286 w, 1234 s, 1147 b, 1059 s, 957 s, 867 sh, 849 s, 755 s, 708 w, 694 w, 687 w, 617 w, 581 s, 599 s, 521 w, 508 w, 460 w, 442 w. Anal. Calc. for $C_{17}H_{28}CuN_8O_{10}S_4$: C, 29.33; H, 4.05; N, 16.09. Found: C, 27.31; H, 3.82; N, 15.83.

*Synthesis of [Cu(η^2-MMI^{MS})$_2$(H_2O)](CH_3SO_4)$_2$ (**8**)*

A solution of MMI (137 mg, 1.20 mmol) in acetonitrile (6 mL) was slowly added to a solution of $Cu(NO_3)_2 \cdot 3H_2O$ (73 mg, 0.30 mmol) in dichloromethane (2 mL). As the MMI was added, a dark precipitate formed immediately and then redissolved with stirring, and the reaction mixture then turned light green. After stirring in air for 3 d, the reaction mixture turned bright blue, and a blue precipitate formed. The solution was filtered, and the isolated blue precipitate was highly hygroscopic, so the precipitate was quickly

dissolved in methanol (5 mL). Diethyl ether diffusion into the methanolic solution over the period of a week yielded crystals of **8**. Yield: 123 mg, 32%. MALDI-MS (*m*/*z*): $[Cu(C_3H_4N_2S)_2]^+$ 262.3, $[Cu(C_3H_4N_2S)]^+$ 163.9. IR (Nujol, cm^{-1}) 3430 b, 2727 w, 1577 s, 1517 w, 1481 w, 1401 sh, 1246 s, 1160 w, 1108 w, 885 sh, 850 s, 768 s, 728 w, 516 w.

*Synthesis of [Cu(η^2-MMI^{MS})(SO_4)(CH_3OH)] (**9**)*

A solution of MMI (137 mg, 1.20 mmol) in acetonitrile (6 mL) was slowly added to a solution of $Cu(NO_3)_2 \cdot 3H_2O$ (146 mg, 0.60 mmol) in acetonitrile (5 mL). As MMI was added, the reaction mixture slowly turned light green. After stirring in air for 3 d, the solution turned a light blue, and the solvent was removed *in vacuo*. Methanol (5 mL) was added to dissolve the resulting oil, and crystals were obtained by slow evaporation of the methanolic solution in air. Yield: 90 mg, 13%.

*Synthesis of [Cu(η^2-MMI^{MS})(SO_4)(DMSO)]· 0.5 DMSO (**10**)*

A solution of MMI (137 mg, 1.20 mmol) in acetonitrile (6 mL) was slowly added to a solution of $Cu(NO_3)_2 \cdot 3H_2O$ (73 mg, 0.30 mmol) in acetonitrile (5 mL). As MMI was added, the reaction mixture slowly turned light green. After stirring in air for 3 d, the solution turned a light green, and the solvent was removed *in vacuo*. Dimethylsulfoxide (5 mL) was added to dissolve the resulting oil, and crystals were obtained by tetrahydrofuran diffusion into the DMSO mixture. Yield: 76 mg, 16%.

*Synthesis of $[Cu_2(\eta^2\text{-}MMI^{DS})_2(\mu\text{-}MMI^{DS})](BF_4)_2$ (**11**)*

Under argon, a solution of bis(1-methylimidazol)-2-yl-disulfide (198 mg, 0.986 mmol) in methanol (6 mL) was slowly added to a solution of $[Cu(CH_3CN)_4](BF_4)_2$ (173 mg, 0.550 mmol) in dichloromethane (2 mL), and the resulting reaction mixture was allowed to stir for 3 h. The solvent volume was then reduced to ~3 mL *in vacuo*, and crystals of **11** were grown by ether diffusion. Yield: 223 mg, 22.3%.

X-ray crystallography

Single crystal X-ray diffraction measurements were performed at 100 K using Mo Kα (λ = 0.71073 Å radiation on a Bruker D8 Venture diffractometer with an Incoatec microfocus source and a Photon 100 CMOS detector. The Apex3 software suite was used for data collection, processing, and scaling corrections.[68,69] A summary of crystallographic data for **1**-**4** is available in Table 3.7, data for **5**-**7** are in Table 3.8, and data for **8**-**11** are in Table 3.9. Space group assignments were made based on systematic absences. Structures were solved by intrinsic phasing (SHELXT), and refined to convergence by full-matrix least squares using the SHELXTL software suite.[70] All non-hydrogen atoms were refined anisotropically. Hydrogen atoms attached to carbon atoms were placed geometrically and treated using appropriate riding models. Positions of hydrogen atoms attached to nitrogen and oxygen atoms were first verified using the difference electron density maps, and then placed in geometrically optimized positions using riding models. The final positions of these hydrogen atoms did not differ significantly from where their position was first indicated on the difference electron density map.

Several structures in the present study required somewhat special treatment during the refinement process. In the case of **3**, the nitrate counterion and methanol solvent molecule were found to be disordered in several different orientations. Thus, their electron density was best modeled using the SQUEEZE algorithm in the PLATON software package.[71] For **7**, the methyl sulfate counterion was modeled in two disordered orientations. In **10**, the coordinated DMSO molecule was found to be disordered, with the sulfur and carbon atoms modeled over split positions and the occupancy values for the two disordered orientations refined as free variables.

3.5 Supplementary Information

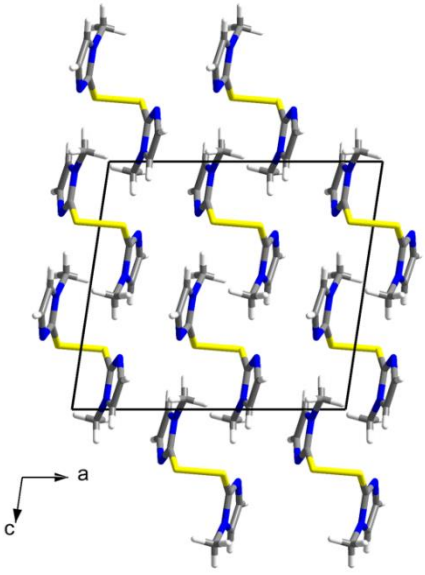

Figure 3.7 Packing diagram along the *b*-axis for MMI^{DS} (**1**). Yellow atoms: sulfur; blue atoms: nitrogen; grey atoms: carbon; white atoms: hydrogen.

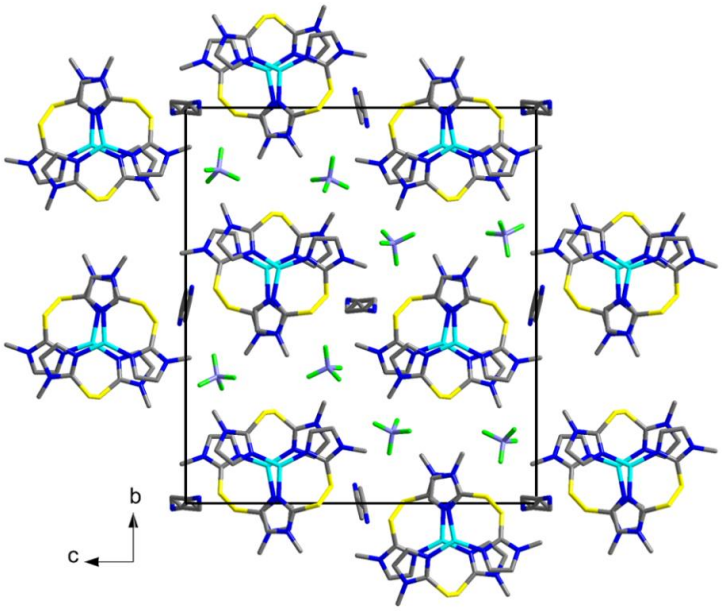

Figure 3.8. Packing diagram for $[Cu_2(MMI^{DS})_3][BF_4]_2$. Yellow atoms: sulfur; dark blue atoms: nitrogen; grey atoms: carbon; white atoms: hydrogen; light blue atoms: copper; green atoms: fluorine; and dark grey atoms: boron.

Table 3.7. Summary of crystallographic data for MMI^{DS} (**1**) and Cu(I) complexes **2**, **3**, and **4**.

	1	**2**	**3**	**4**
Chemical formula	$C_8H_{10}N_4S_2$	$C_{24}H_{36}B_2Cu_2F_8N_{12}S_6$	$C_9H_{16}CuN_5O_4S_2$	$C_9H_{12}Cu_2N_8O_6S_3$
F.W. (g mol^{-1})	226.32	985.71	385.93	551.53
Temperature, K	100(2)	100(2)	100(2)	100(2)
Wavelength, Å	0.71073	0.71073	0.7103	0.71073
Crystal system	Monoclinic	Monoclinic	Monoclinic	Orthorhombic
Space group	*C2/c*	*P*2/*c*	*P*2/*c*	*Pnma*
a, Å	12.2875(8)	14.4704(17)	16.3614(8)	6.4334(4)
b, Å	7.3836(5)	15.7849(17)	13.9033(7)	30.109(2)
c, Å	11.2422(7)	8.3677(10)	6.9472(3)	9.1569(7)
α, ˚	90	90	90	90
β, ˚	98.514 (2)	94.269(3)	98.539(2)	90
γ, ˚	90	90	90	90
V, $Å^3$	1008.72(11)	1906.0(4)	1562.81(13)	1773.7(2)
Z	4	2	4	4
D, g cm^{-3}	1.490	1.718	1.640	2.065
Absorption coefficient, mm^{-1}	0.492	1.523	1.686	2.801
Crystal size, mm^3	0.204×0.209×0.311	0.02×0.401×0.416	0.167×0.174×0.566	0.033×0.178×0.335
F(000)	472	1000	792	1104
2θ range, ˚	3.23 to 33.23	2.76 to 31.00	2.52 to 29.99	2.33 to 26.00
Collected reflections	13154	58706	45916	13711
Unique reflections	1919	6050	4546	1770
Final *R* (obs. Data)[α], R_1	0.0256	0.0216	0.0282	0.0395
wR_2	0.0696	0.0593	0.0696	0.1140

Table 3.8. Summary of crystallographic data for complexes **5**, **6**, and **7**.

	5	**6**	**7**
Chemical formula	$C_{16}H_{24}CuN_{10}O_8S_2$	$C_{38}H_{30}CuN_8O_{10}S_4$	$C_{17}H_{28}CuN_8O_{10}S_4$
F.W. (g mol^{-1})	612.11	710.28	696.25
Temperature, K	100(2)	140(2)	140(2)
Wavelength, Å	0.71073	0.71073	0.71073
Crystal system	Monoclinic	Monoclinic	Triclinic
Space group	*P* 2/*n*	*P* 2/*n*	P_{-1}
a, Å	8.6291(9)	8.3452(4)	8.6675(13)
b, Å	13.5838(16)	8.4167(5)	12.442(2)
c, Å	10.3684(11)	20.3354(12)	13.658(2)
α, °	90	90	70.800(5)
β, °	100.436(4)	99.568(2)	79.904(5)
γ, °	90	90	78.593(5)
V, Å^3	1195.2(2)	1408.47(14)	1353.8(4)
Z	2	2	2
D, g cm^{-3}	1.701	1.675	1.708
Absorption coefficient, mm^{-1}	1.154	1.138	1.182
Crystal size, mm^3	0.056×0.064×0.122	0.044×0.112×0.176	0.087×0.168×0.204
F(000)	630	734	718
2θ range, °	2.83 to 27.50	2.62 to 25.50	2.70 to 26.50
Collected reflections	26649	33742	57400
Unique reflections	2734	2613	5596
Final *R* (obs. Data)$^{\alpha}$, R_1	0.0253	0.0346	0.0289
wR_2	0.0592	0.0825	0.0706

Table 3.9 Summary of crystallographic data for complexes **8**, **9**, **10** and **11**.

	8	**9**	**10**	**11**
Chemical formula	$C_9H_{14}CuN_4O_5S_2$	$C_{18}H_{28}CuN_8O_9S_4$	$C_{11}H_{19}CuN_4O_{5.56}S_{3.50}$	$C_{25}H_{31.}50B_2Cu_2F_8N_{12.50}S_6$
F.W. (g mol^{-1})	385.90	692.26	471.05	1000.19
Temperature, K	100(2)	100(2)	100(2)	100(2)
Wavelength, Å	0.71073	0.71073	0.71073	0.7103
Crystal system	Triclinic	Triclinic	Monoclinic	Monoclinic
Space group	*P*1	*P*1	*P* 2/*c*	*P* 2/*c*
a, Å	7.2792(7)	9.0467(8)	12.4725(4)	7.0458(4)
b, Å	9.7671(9)	12.2650(11)	9.4873(3)	24.9693(16)
c, Å	10.1282(9)	13.2201(2)	15.3776(5)	22.3144(15)
α, ˚	95.449(3)	72.176(3)	90	90
β, ˚	104.276(3)	81.140(3)	96.3480(10)	96.468(2)
γ, ˚	96.167(3)	74.176(3)	90	90
V, Å^3	688.27(11)	1341.492)	1808.48(10)	3900.8(4)
Z	2	2	4	4
D, g cm^{-3}	1.862	1.714	1.730	1.703
Absorption coefficient, mm^{-1}	1.917	1.645	1.645	1.490
Crystal size, mm^3	0.082×0.086×0.088	0.031×0.133×0.461	0.031×0.133×0.461	0.048×0.112×0.387
F(000)	394	968	968	2020
2θ range, ˚	2.09 to 30.57	2.67 to 25.25	2.67 to 25.25	2.46 to 25.50
Collected reflections	33902	22581	22581	70149
Unique reflections	4212	3276	3276	7276
Final *R* (obs. Data) R_1	0.0266	0.0427	0.0427	0.0418
wR_2	0.0886	0.0850	0.0850	0.0941

3.6 References

(1) Raper, E. S. *Coord. Chem. Rev.* **1994**, *129*, 91-156.

(2) Lobana, T. S.; Sultana, R.; Hundal, G. *Polyhedron* **2008**, *27*, 1008-1016.

(3) Suzuki, T.; Matsumoto, J.; Kajita, Y.; Inomata, T.; Ozawa, T.; Masuda, H. *Dalton Trans.* **2015**, *44*, 1017-1022.

(4) Stadelman, B. S.; Kimani, M. M.; Bayse, C. A.; McMillen, C. D.; Brumaghim, J. L. *Dalton Trans.* **2016**, *45*, 4697-4711.

(5) Jia, W.-G. Lin, Y.-J.; Jin, G.-X. *Dalton Trans.* **2008**, 5612-5620.

(6) Kim, H. R.; Jung, I. G.; Yoo, K.; Jang, K.; Lee, E. S.; Yun, J.; Son, S. U. *Chem. Commun.* **2010**, *46*, 758-760.

(7) Maria, L. M., C.; Paulo, A.; Santos, I. C.; Santos, I. *J. Organomet. Chem.* **2006**, *691*, 4773-4778.

(8) Peng, Y.; Shang, L.; Cao, Y.; Waterhouse, G. I.; Zhou, C.; Bian, T.; Wu, L. Z.; Tung, C. H.; Zhang, T. *Chem. Commun.* **2015**, *51*, 12556-12559.

(9) Pan, Y.-C. W., Y.; Xue, L.-Y.; Guo, X.-Y.; Yang, H.-F. *J. Phys. Chem. C* **2012**, *116*, 3532-3538.

(10) Ateya, B. G., El-Anadouli, B. E., El-Nizamy, F. M. A. *Bull. Chem. Soc. Jpn.* **1981**, *54*, 3157-3161.

(11) O'Connor, N., Lopez, G. E., Cruz, A. *Curr. Chem. Lett.* **2014**, *3*, 189-194.

(12) Roy, G. Y., P. N.; Mugesh, G. *Chem. Asian J.* **2013**, *8*, 1910-1921.

(13) Parkin, G. *New J. Chem.* **2007**, *31*, 1996-2014.

(14) Kimani, M. M.; Bayse, C. A.; Brumaghim, J. L. *Dalton Trans.* **2011**, *40*, 3711-3723.

(15) Ainscough, E. W.; Brodie, A. M. *Coord. Chem. Rev.* **1978**, *27*, 59-86.

(16) Kravets, I. *Am. Fam. Physician* **2016**, *93*, 363-370.

(17) Manna, D.; Roy, G.; Mugesh, G. *Acc. Chem. Res.* **2013**, *46*, 2706-2715.

(18) Cheah, I. K.; Tang, R. M.; Yew, T. S.; Lim, K. H.; Halliwell, B. *Antioxid. Redox Signal.* **2017**, *26*, 193-206.

(19) Atkinson, E. R.; Jackson, A. R. W.; Raper, E. S. *Inorg. Chim. Acta* **1985**, *98*, 35-41.

(20) Karagiannidis, P. A.; Papastefanou, S.; Mentzafos, D.; Hountas, A.; Terzis, A. *Polyhedron* **1990**, *9*, 981-986.

(21) Creighton, J. R.; Gorvin, A. C.; Gutteridge, C.; Jackson, A. R.; Raper, E. S.; Sherwood, P. M. A. *Inorg. Chim. Acta* **1985**, *103*, 195-205.

(22) Raper, E. S. *Inorg. Chim. Acta* **1991**, *180*, 239-244.

(23) Raper, E. S.; Robson, D.; Wilson, J. D.; Clegg, W.; Milne, A. *Inorg. Chim. Acta* **1988**, *143*, 98-100.

(24) Atkinson, E. R.; Raper, E. S.; Gardiner, D. J.; Dawes, H. M.; Walker, N. P. C.; Jackson, A. R. W. *Inorg. Chim. Acta* **1985**, *100*, 285-291.

(25) Raper, E. S.; Clegg, W. *Inorg. Chim. Acta* **1991**, *183*, 179-187.

(26) Raper, E. S.; Wilson, J. D.; Clegg, W.; Milne, A. *Inorg. Chim. Acta* **1989**, *155*, 77-83.

(27) Lobana, T. S.; Hundal, G.; Butcher, R. J. *Polyhedron* **2009**, *28*, 1573-1577.

(28) Atkinson, E. R.; Jackson, A. R.; Raper, E. S. *Inorg. Chim. Acta* **1985**, *92*, 35-41.

(29) Creighton, J. R.; Gorvin, A. C.; Getteridge, C.; Jackson, A. R.; Raper, E. S.; Sherwood, P. M. *Inorg. Chim. Acta* **1985**, *103*, 195-205.

(30) Warren, J. J.; Lancaster, K. M.; Richards, J. H.; Gray, H. B. *J. Inorg. Biochem.* **2012**, *115*, 119-126.

(31) Lobana, T. S.; Sultana, R.; Butcher, R. J.; Casieneiras, A.; Akitsu, T.; Fernandez, F. J.; Vega, M. C. *Eur. J. Inorg. Chem.* **2013**, 5161-5170.

(32) Lobana, T. S. B., R. J.; Casineiras, A.; Akitsu, T.; Fernandez, F.J.; Vega, M. C. *Eur. J. Inorg. Chem.* **2013**, 5161-5170.

(33) Ainscough, E.; Baker, E. N.; Bingham, A. G.; Brader, M. L.; Brodie, A. M.; Gainsford, G.J. *Inorg. Chim. Acta* **1985**, *105*, L5-L7.

(34) Ainscough, E.; Brodie, A. M.; Gainsford, G. J. *Inorg. Chim. Acta* **1991**, *180*, 81-83.

(35) Baldwin, D. A.; Copperthwaite, R. G.; Loubser, J. H. N.; Markwell, A. J. *J. Crystallogr. Spectrosc. Res.* **1984**, *14*, 157-167.

(36) Baldwin, D.; Denner, L.; Markwell, A. J. *J. Crystallogr. Spectrosc. Res.* **1986**, *16*, 763-768.

(37) Kimura, K. K.; Kinoshita, I.; Nakashima, N.; Kitano, K.; Nichioka, T.; Isobe, K. *Chem. Commun.* **1999**, 497-498.

(38) Matsunaga, Y.; Fujisawa, K.; Amir, N.; Miyashita, Y.; Okamoto, K. *Appl. Organomet. Chem.* **2005**, *19*, 208.

(39) Isaia, F.; Aragoni, M. C.; Arca, M.; Demartin, F.; Devillanova, F. A.; Floris, G.; Garau, A.; Hursthouse, M. B.; Lippolis, V.; Medda, R.; Oppo, F.; Pira, M.; Verani, G. *J. Med. Chem.* **2008**, *51*, 4050-4053.

(40) Figueroa, J. S.; Yurkerwich, K.; Melnick, J.; Buccella, D.; Parkin, G. *Inorg. Chem.* **2007**, *46*, 9234-9244.

(41) Lobana, T. S.; Sultana, R.; Hundal, G.; Butcher, R. J. *Polyhedron* **2009**, *28*, 1573-1577.

(42) Baldwin, D. A.; Denner, L.; Marwell, A. J. *J. Crystallogr. Spectrosc. Res.* **1984**, *14*, 157-167.

(43) Odani, A.; Maruyama, T.; Yamauchi, O.; Fujiwara, T.; Tomita, K. *J. Chem. Soc., Chem. Commun.* **1982**, 646-647.

(44) Higashi, L. S.; Lundeen, M.; Hilti, E.; Seff, K. *Inorg. Chem.* **1977**, *16*, 310-313.

(45) Yamauchi, O.; Odani, A. *Pure Appl. Chem.* **1996**, *68*, 469-496.

(46) Kimura, K. K.; Kinoshit, I.; Nakashima, N.; Kitano, K.; Nichioka, T.; Isobe, K. *Chem. Commun.* **1999**, 497-498.

(47) Aggarwal, V.; Ram Kumar, V.; Signh, U. P. *J. Chem. Cryst.* **2011**, *41*, 121-1126.

(48) Rajasekharan-Nair, R.; Marckwordt, A.; Lutta, S. T.; Schwalbe, M.; Biernat, A.; Armstrong, D. R.; Watson, A. J.; Kennedy, A. R.; Reglinski, J.; Spicer, M. D. *Chemistry* **2013**, *19*, 13561-13568.

(49) Kimani, M. M.; Watts, D.; Graham, L. A.; Rabinovich, D.; Yap, G. P.; Brumaghim, J. L. *Dalton Trans.* **2011**, *44*, 16313-16324.

(50) Burattini, S.; Greenland, B. W.; Merino, D. H.; Weng, W.; Seppala, J.; Colquhoun, H. M.; Hayes, W.; Mackay, M. E.; Hamley, I. W.; Rowan, S. J. *J. Am. Chem. Soc.* **2010**, *132*, 12051-12058.

(51) Basak, S.; Nanda, J.; Banerjee, A. *Chem. Commun.* **2013**, *49*, 6891-6893.

(52) Demirel, G. B.; Daglar, B.; Bayindir, M. *Chem. Commun.* **2013**, *49*, 6140-2.

(53) Lee, W. E.; Jin, Y. J.; Kim, S. I.; Kwak, G.; Kim, J. H.; Sakaguchi, T.; Lee, C. L. *Chem. Commun.* **2013**, *49*, 9857-9859.

(54) Vampa, G. B.; Sever, F.; Malmusi, L.; Antolini, L. *J. Heterocycl. Chem.* **1995**, *32*, 227-234.

(55) Ansell, G. B. *J. Chem. Soc., Perkin Trans. 2* **1972**, *7*, 841-843.

(56) Trost, M.; Schinski, W. L.; Chen, F.; Mantz, I. B. *J. Am. Chem. Soc.* **1971**, *93*, 676-684.

(57) Corey, J.; Winter, R. A. E. *J. Am. Chem. Soc.* **1963**, *85*, 2077-2078.

(58) Chambers, J. Q.; Moses, P. R.; Shelton, R. N. *J. Electroanal. Chem.* **1972**, 245-248.

(59) Lobana, T. S.; Sultrana, R.; Hundal, G.; Butcher, R. J. *Dalton Trans.* **2010**, *39*, 7870-7872.

(60) Abel, E. *Monatsh. Chem.* **1951**, *82*.

(61) Brandt, C.; van Eldik, R. *Chem. Rev.* **1995**, *95*, 119-190.

(62) Natarajan, P. *Tetrahedron Lett.* **2015**, *56*, 4131-4134.

(63) Wandini, T.; Einaga, Y. *Chem. Sens.* **2005**, *21*, 10-12.

(64) Mukawa, T.; Goto, T.; Takeuchi, T. *Analyst* **2002**, *127*, 1407-1409.

(65) Kice, J. L.; Puls, A. R. *J. Am. Chem. Soc.* **1977**, *99*, 3455-3460.

(66) Maclaren, J. A.; Leach, S. J.; O'Donnell, I. J. *Biochim. Biophys. Acta* **1959**, *35*, 280-281.

(67) Merrill, C. L., Wilson, L. J., Thamann, T. J., Thomas, J., Loehr, T. M., Ferris, N. S., Woodruff, W. H. *J. Chem. Soc., Dalton Trans.* **1984**, *10*, 2207-2221.

(68) Bruker Axis, Inc.: Madison, WI, 2015.

(69) Rigaku and Molecular Structure Corporation: The Woodlands, TX, 2006.

(70) Sheldrick, G. *Acta Crystallogr.* **2008**, *A64*, 112-122.

(71) Spek, A. *Acta Crystallogr*. **2015**, *C71*, 9-18.

CHAPTER FOUR

REACTIVITY OF NON-INNOCENT IMIDAZOLE DISULFIDE AND DISELENIDE LIGANDS WITH COPPER

4.1 Introduction

Disulfide bonds play crucial roles in the structure, function, and catalytic activity of many proteins,[1,2] and metal complexes with ligands that incorporate disulfide bonds have been used in polymers,[3-8] switches,[9,10] and photodetectors.[11] Their high bond-dissociation energies contribute stability, and their redox properties can be tuned by steric strain, the nature of the local environment, and oxygen availability.[12,13] In thioredoxin enzymes, thiol-disulfide exchange reactions involve electron transfer from a higher-potential disulfide bond to redox-ready thiols, enabling a domino-effect of electron transfer using sulfur-sulfur bonds.[9] Disregulation of disulfide bond formation is implicated in development of Creutzfeldt-Jakob disease, amyotrophic lateral sclerosis (ALS), Parkinson's disease, and various cancers.[14-19]

Diselenide bonds are not as prevalent in biological systems or in biomimetic materials, although the diselenide bond has been identified in proteins[20,21] and non-native diselenides have been used to drive oxidative folding of proteins.[22] Selenocysteine is an essential component in a number of redox enzymes, including glutathione peroxidase, iodothyronine diodinases, and thioredoxin reductases,[23] but the redox mechanism in these enzymes does not involve diselenide bond formation. Lower reduction potentials and broader reactivity limit the stability of diselenide bonds in biological systems,[24,25] but

diselenides are promising antioxidants due to their ability to react with thiol groups in a glutathione peroxidase-like manner.[26]

Metals such as copper and iron serve as electron sinks for catalyzing disulfide-to-thiol reductions in metalloproteins.[9,27] Recently, heterocyclic thiones have attracted attention for the similarity of their redox properties to thiols, their ability to bond softer metals such as Cu(I) and Fe(II),[28-30] and their ability to form disulfide bonds.[31] Under anaerobic conditions, a wide variety of mono-,[32,33] di-,[32,34-36] tetra-,[35] and polynuclear[37,38] complexes have been reported as products of reactions between Cu(I) and methimazole (MMI; Figure 4.1). With the exception of two mononuclear complexes $[Cu(MMI)_3][NO_3]$[32] and $[Cu(MMI_3)Cl]$,[34] the products are typically multinuclear complexes that include bridging MMI ligands. Reactions of Cu(I) and the oxidized form of methimazole, methimazole disulfide (MMI^{DS}; Figure 4.1), have not been explored in depth. Only two metal complexes with coordinated MMI^{DS} are reported, $[Cu(MMI^{DS})_3][BF_4]$[39] and $Zn(MMI^{DS})Cl_2$,[40] although Figueroa and coworkers[41] synthesized complexes of Zn^{2+}, Fe(II), Cu(I), Co^{2+}, and Ni^{2+} with *t*-butyl (^{t}Bu-MMI^{DS}) and Co^{2+} with phenyl (Ph-MMI^{DS}) substituents in place of the methyl group. Structures with Cu(II), Cd^{2+}, Hg^{2+}, and Zn^{2+} coordinated to the selenium-containing methimazole diselenide (MMI^{DSe}; Figure 4.1) are also reported.[42,43]

In reactions of MMI with Cu(II), MMI is typically oxidized to MMI^{DS} and copper is reduced to Cu(I).[31] It is believed that a similar reaction of MMI^{Se} with Cu(II) results in formation of MMI^{DSe}, but upon treating $Cu(ClO_4)_2$ with MMI^{Se} in air, a selenium atom is eliminated from MMI^{DSe} and the monoselenide complex $[Cu(MMI^{MSe})_2(H_2O)_2][ClO_4]_2$ is

isolated.[44] In these studies, reactions were performed with Cu(I) and MMI^{DS} or MMI^{DSe} under air-free conditions to explore the possibility of reversible disulfide/thione and diselenide/selone formation. A similar reaction of Cu(I) with MMI^{DSe} was performed in air, resulting in three separate products isolated from the same reaction mixture and demonstrating the variable chemistry that can occur when combining a redox-active metal with a non-innocent ligand. The work in this chapter was performed in collaboration with Dr. Colin McMillen, Managing Director of the Molecular Structure Center at Clemson University.

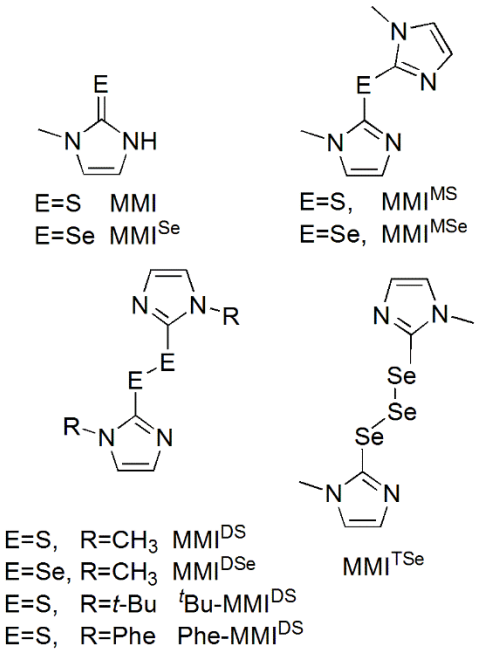

Figure 4.1. Sulfur- and selenium-containing imidazole ligands discussed in this work.

4.2 Results and Discussion

Synthesis

Transition metal complexes with heterocyclic thiones have been extensively examined, but few complexes of the disulfide forms of these heterocycles exist.[40,41,45] Formation of MMI^{DS} in $Zn(MMI^{DS})Cl_2$ was generated by air oxidation of MMI. Figueroa and coworkers demonstrated that electron-rich Ni^0 reduces the structurally-similar, ^{t}Bu-MMI^{DS} (Figure 4.1) to the corresponding thione.[41] Cu(II) oxidizes MMI to MMI^{DS} with concomitant reduction to Cu(I),[31] but the reversibility of this redox reaction has never been examined.

To investigate the reaction between Cu(I) and MMI^{DS}, $[Cu(CH_3CN)_4][BF_4]$ and MMI^{DS} were combined under air-free conditions (Scheme 4.1). As MMI^{DS} was added to the Cu(I) solution, the reaction mixture initially turned blue, indicating Cu(II) formation. Upon stirring for 1 hour, the reaction solution returned to a light yellow color, suggesting Cu(II) reduction to Cu(I).Red-orange crystals of the $[Cu_2(MMI)_2(MMI^{DS})_2][BF_4]_2$ (**1**) product were collected, but yield of **1** was extremely low and attempts to re-isolate this compound yielded crystals of the $[Cu(CH_3CN)_4][BF_4]$ starting material and a dark yellow oil.

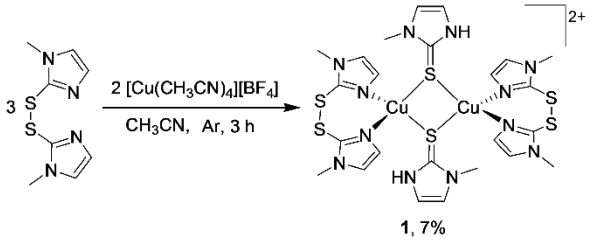

Scheme 4.1. Treating Cu(I) with MMI^{DS} under air-free conditions affords the dimeric complex $[Cu_2(MMI)_2(MMI^{DS})_2][BF_4]_2$ (**1**).

The analogous air-free treatment of $[Cu(CH_3CN)_4][BF_4]$ with MMI^{DSe} was performed under similar conditions (Scheme 4.2). Again, the reaction mixture turned blue upon MMI^{DSe} addition, but slowly became light red. Orange-red crystals of $[Cu_2(MMI)_2(MMI^{DS})_2][BF_4]_2$ (**2**) were obtained, but yield of **2** was also low, and efforts to re-isolate this product were unsuccessful. In both complexes **1** and **2**, the MMI or MMI^{Se} ligands are protonated, as confirmed in the crystal structure (*vide infra*), but the origin of these protons is not clear. The reduction of an imidazole disulfide to the monosulfide has been observed in a reaction with ^{t}Bu-MMI^{DS} and Ni^0, as described by Figueroa and coworkers, however, the Ni^0 bonded directly with the imidazole nitrogen, not the thione. In this case, a Cu(I)-thione bond is observed, and the imidazole nitrogen is protonated. The low yield and irreproducibility may be due to a limited proton source, such as adventitious water present in the reaction. There is no obvious source of protons to contribute to the protonation of the imidazole, but the most obvious source may be water contamination in the solvent.

The formation of MMI^{DS} or MMI^{DSe} with Cu(I) from the reaction of MMI and SeMMI with Cu(II), respectively, has been previously discussed in Chapter 3:Coordination Complexes of Methimazole with Copper: Controlling Redox Reactions and Sulfur Extrustion. The reactions that form complexes **1** and **2** involve cleavage of the disulfide/diselenide bond to yield copper-coordinated MMI or MMI^{Se}. Formation of the disulfide-containing MMI^{DS} in the presence of copper also has been reported, demonstrating the potential reversibility of thione/disulfide and selone/diselenide formation in the presence of copper. Such reactivity is a result of the redox activity of

copper in combination with the non-innocent character of the thione/selone ligands. Cu(I) can donate electrons to cleave S-S or Se-Se bonds in MMI^{DS} or MMI^{DSe}, and Cu(II) can accept electrons to oxidize MMI or MMI^{Se} to the corresponding disulfide/diselenide. While the solid-state structure suggests that the bridging disulfide ligand (MMI^{DS}) in $[Cu_2(N,N\text{-}\mu\text{-}MMI^{DS})(MMI^{DS})_2][BF_4]_2$ is strained, it is likely that disulfide cleavage is due to electron transfer of the Cu(I), with the metal ion playing a role by ligand association. The same reversibility was observed in the Cu(I)-MMI^{DSe} reaction, once again resulting in a mixed ligand, dinuclear complex.

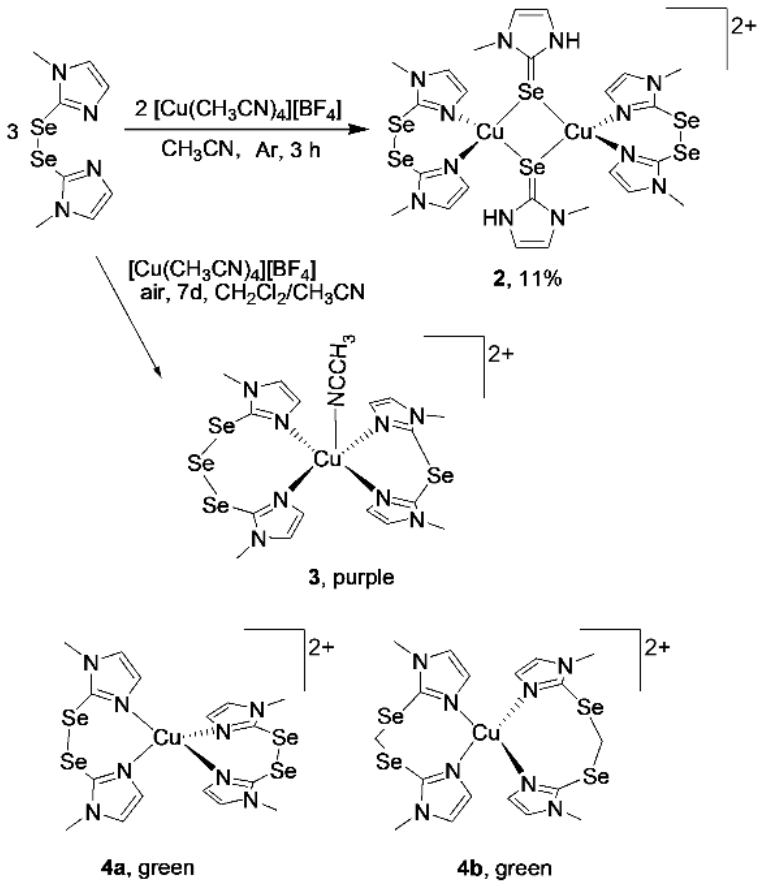

Scheme 4.2. Copper coordination complexes formed by treating Cu(I) with MMI^{DSe}.

Upon treatment of $Cu(NO_3)_2$ with MMI in air, the resulting Cu(II)-containing products are coordinated to methimazole monosulfide (MMI^{MS}) ligands that form by sulfur elimination from MMI^{DS}.[31,46-50] The only comparable reaction of MMI^{DSe} and $Cu(ClO_4)_2$ in air similarly yields $[Cu(MMI^{MSe})_2(H_2O)_2][ClO_4]_2$ with a monoselenide ligand.[44] Treating $Cu(BF_4)_2$ with MMI does not lead to sulfur elimination products, since it contains the non-oxidizing BF_4^- ion,[39]so using $Cu(BF_4)_2$ in place of $Cu(NO_3)_2$ as a starting material is useful for examining the coordination chemistry of MMI^{DS} and MMI^{DSe} without chalcogen extrusion.

To determine whether selenium elimination from MMI^{DSe} occurs when starting with Cu(I) rather than Cu(II), $[Cu(CH_3CN)_4][BF_4]$ was treated with MMI^{DSe} in air (Scheme 4.2). Initial formation of a blue solution upon MMI^{DSe} addition indicates Cu(I) oxidation to Cu(II), but upon stirring for 1 h in air, the reaction mixture became the same orange-red color as described for the synthesis of **2**. Upon stirring for 24 h in air, the reaction mixture slowly turned green, and four different types of crystals were obtained from slow evaporation of the dichloromethane/acetonitrile solution: colorless crystals of the $[Cu(NCCH_3)_4][BF_4]$ starting material, purple crystals of $[Cu(MMI^{MSe})(MMI^{TSe})(CH_3CN)][BF_4]_2$ (**3**), green crystals incorporating two mononuclear cations in one asymmetric unit, $[Cu(MMI^{DSe})_2][Cu(MMI^{Se}\text{-}CH_2\text{-}MMI^{Se})_2][BF_4]_4$ (**4a** and **4b**, respectively), and yellow-green columns of $[Cu(MMI^{Se}\text{-}CH_2\text{-}MMI^{Se})_2][BF_4]_2$.

The mixed ligand Cu(II) complex $[Cu(MMI^{MSe})(MMI^{TSe})(CH_3CN)][BF_4]_2$ (**3**) forms by oxidation of Cu(I) to Cu(II) in air, with concomitant selenium elimination from one copper-coordinated MMI^{DSe} ligand and selenium addition to a second coordinated

MMI^{DSe} ligand. It is the first complex where Cu(II) coordinates both a monoselenide (MMI^{MSe}) and a triselenide (MMI^{TSe}) ligand. Roy and coworkers[44] observed selenide elimination from MMI^{DSe} in the formation of $[Cu(MMI^{MSe})_2(H_2O)_2][ClO_4]_2$, but the eliminated selenium was recovered as a $CuSeO_3$ salt.

A small number of green crystals were also isolated from the Cu-MMI^{DSe} reaction mixture. This product crystallizes with two different, mononuclear, Cu(II) cationic structures per unit cell, $[Cu(MMI^{DSe})_2]^{2+}$ (**4a**) and $[Cu(MMI^{Se}\text{-}CH_2\text{-}MMI^{Se})_2]$ (**4b**; Scheme 4.2). In the $MMI^{Se}\text{-}CH_2\text{-}MMI^{Se}$ ligands of **4b**, a $-CH_2$ group bridges between selenium atoms of the original MMI^{DSe} ligand. It is postulated that this ligand forms upon two consecutive substitution reactions of MMI^{Se} with the dichloromethane solvent. The yellow-green columns were identified as $[Cu(MMI^{Se}\text{-}CH_2\text{-}MMI^{Se})_2][BF_4]_2$, with the same cationic structure as **4b**. The identity of the columns was confirmed, but the diffraction quality was poor, and the chemical aspects have already been discussed with **4b**.

Structural Analyses

Although yields were limited, the identity of products **1**-**4** are confirmed by X-ray crystallographic analysis. $[Cu_2(MMI^{DS})_2(MMI)_2][BF_4]_2$ (**1**) crystallizes in the *C*2/*c* space group. This mixed-ligand, dinuclear Cu(I) complex incorporates two sulfur-bridged methimazole ligands to create a rhombic Cu_2S_2 core (Figure 4.2, with selected bond lengths and angles in Table 4.1), similar to the homoleptic $[Cu_2(\mu\text{-}MMI)_2(MMI)_4][BF_4]_2$ complex reported by Raper and coworkers.[35] The terminal, bidentate MMI^{DS} ligands bind Cu(I) through the imidazole nitrogen atoms, creating a 7-membered chelate ring. The bridging

MMI ligand is protonated, as determined by 1) electron density near the nitrogen, 2) the long range H-F interactions between the hydrogen and the fluoride of the tetrafluoroborate, seen in the crystal packing structure (Figure 4.2A), and 3) the lengthened C1-N1 bond distance (1.349(3) Å) in the imidazole ring, compared to the C=N double bond seen in the MMI^{DS} ligand (1.328(3) Å[39]).

In **1**, each Cu(I) ion is coordinated by two N and two S atoms in a distorted tetrahedral geometry, with angles ranging from 101.5˚ to 117.2˚. Cu-N bond lengths are a consistent 2.013(2)-2.014(2) Å, but the Cu-S bond lengths are inequivalent at 2.3511(6) Å and 2.4461(6) Å. No significant change is observed in the C-S bond lengths for the MMI^{DS} ligand (1.746(2) Å and 1.750(2) Å) compared to unbound MMI^{DS} (1.7413(8) Å[39]) however, the bridging MMI ligand had a shorter C-S distance of 1.715(2) Å, consistent with the shift of electron density into the imidazole ring. Ring strain is reflected in the stretch of the N3-C5-S2 (126.23(18)˚) and N5-C9-S3 (126.09(18)˚) bond angles compared to 123.81(6)˚ observed in uncoordinated MMI^{DS}.

The disulfide S1-S2 bond length in **1** is 2.0676(10) Å, consistent with the terminal MMI^{DS} ligands (2.0659(12) Å and 2.06673(13) Å) in $[Cu_2(N,N\text{-}\mu\text{-}MMI^{DS})(MMI^{DS})_2][BF_4]_2$ but slightly shorter than the bridging MMI^{DS} (2.0813(14) Å) of the same molecule. The S-S bond length in **1** (2.0676(10) Å) is also slightly shorter than in unbound MMI^{DS} (2.1010(4) Å[39]), but is consistent with S-S bond lengths in disulfide the same molecule. The S-S bond length in **1** (2.0676(10) Å) is also slightly shorter than in unbound MMI^{DS} (2.1010(4) Å[39]), but is consistent with S-S bond lengths in disulfide

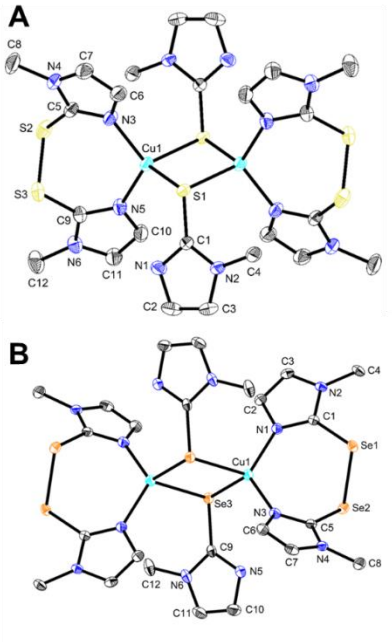

Figure 4.2. Crystal structure diagrams of A) $[Cu_2(MMI^{DS})_2(MMI)_2][BF_4]_2$ (**1**) and B) $[Cu_2(MMI^{DSe})_2(MMI^{Se})_2][BF_4]_2$ (**2**) with 50% probability density ellipsoids. Hydrogen atoms and counterions are omitted for clarity.

Table 4.1. Selected bond distances (Å) and angles (˚) for **1** and **2**.

	1		**2**
Cu1-N3	2.013(2)	Cu1-N1	2.0264(16)
C5-S2	1.746(2)	C1-Se1	1.8971(18)
S2-S3	2.068(1)	Se1-Se2	2.3361(3)
Cu1-S1	2.3511(6)	Cu1-Se3	2.4680(3)
S1-C1	1.715(2)	Se3-C9	1.862(2)
C1-N2	1.349(3)	C9-N5	
C5-N3	1.328(3)	C1-N1	
Cu-Cu	3.0368(6)	Cu-Cu	
N3-Cu1-N5	117.23(8)	N1-Cu1-N3	118.83(6)
C5-S2-S3	103.49(8)	C1-Se1-Se2	101.26(6)
S2-S3-C9	102.92(9)	Se1-Se2-C5	97.18(6)
S1-Cu1-S1	101.48(2)	Se3-Cu1-Se3	91.946(11)
Cu1-S1-Cu1	78.52(2)	Cu1-Se3-Cu	88.055(11)

complexes of other transition metals (Fe(II), Co^{2+}, Ni^{2+}, Zn^{2+}).[41] In a survey of structural data for disulfide bonds in extracellular globular proteins, the average S-S bond distance was found to be 2.02 Å,[2] significantly shorter than the disulfide bonds in coordinated imidazole disulfides. C-S-S bond angles of the terminal MMI^{DS} ligands of [Cu(*N*,*N*-μ-MMI^{DS})(MMI^{DS})$_2$[BF_4]$_2$ do not change from those of unbound MMI^{DS} (101.72(3)˚[39]), but there is a significant widening in the bridging MMI^{DS} C-S-S angles (105.55(12)˚-105.65(12˚). Complex **1** falls in the middle, with an average C-S-S bond angle of 103.2˚. Torsion angles (χ) for **1** are 92.33˚, 99.22˚ and 98.23˚ for the terminal MMI^{DS} ligands in [Cu(*N*,*N*-μ-MMI^{DS})(MMI^{DS})$_2$[BF_4]$_2$ and 86.36˚ for the bridging disulfide. In a study by Craig and coworkers,[51] ranges of 87˚ to 97˚ were measured for torsion angles of structural disulfides in a survey of proteins, and deviations from these angles can result in energy strain of several kcal/mol.[52,53]

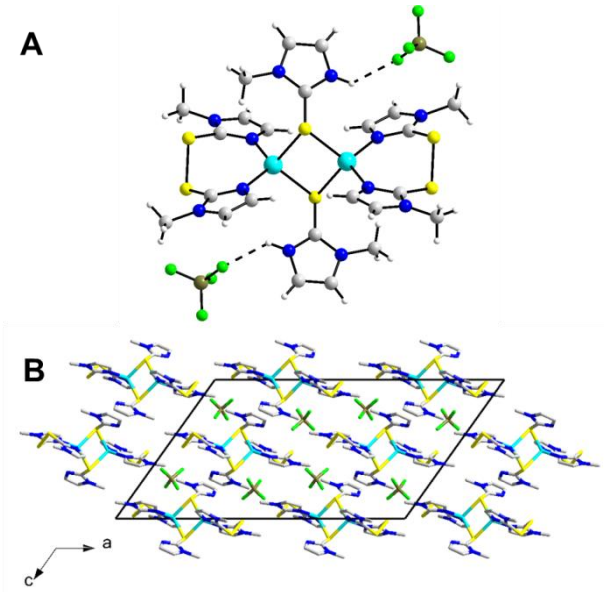

Figure 4.3. Packing diagrams for **1** showing A) the F-H interactions between the BF_4^- anions and the protons on the terminal MMI^{DS} and B) the layering of the BF_4^- ions along the *b*-axis. Color scheme: dark blue – nitrogen; yellow – sulfur; light blue – copper; grey – carbon; white – hydrogen; green – fluorine; and brown – boron.

$[Cu_2(MMI^{DSe})_2(MMI^{Se})_2][BF_4]_2$ (**2**) is the first reported Cu(I)-MMI^{DSe} complex. Similar to **1**, it also features a dinuclear Cu(I) core, with two MMI^{Se} ligands bridging through the Se atom (Figure 4.2, with selected bond lengths and angles in Table 4.1) and a rhombic Cu_2Se_2 core. The distorted tetrahedral geometry with a τ_4 of 0.921 around each Cu(I) atom is nearly identical tothat found in **1**. However, **2** crystalizes in space group *P*2/*n* as a result of the expansion of the cation structure due to the increased length of the Cu-Se, C-Se, and Se-Se bonds compared to **1**. Increased bond length is also observed in a longer Cu-Cu distance (3.492(4)) for **2** compared to **1** (3.0368(6)). Once again, the imidazole nitrogen of the selone is protonated, as indicated by the electron density around the imidazole nitrogen atom; the longer bond length of C12-N6 (1.460(3) Å) of the imidazole selone ring compared to the C1-N1 (1.329(2) Å) of the imidazole ring of the disulfide; and the H-F hydrogen bonding interactions with the BF_4^- counterion.

Structurally, MMI^{DSe} does not change to a large extent upon Cu(I) coordination. Strain on the diselenide bond is only detected through the slight opening of the N1-C1-Se1 angle (127.85(14)˚) compared to unbound MMI^{DSe} (122.8(3)˚).[54] Similar to the Cu(II) complex $[Tpm^{iPr}Cu(MMI^{DSe})][OTf]_2$,[43] the Se-Se bond is slightly shorter in **2** (2.3361(3) Å) compared to unbound MMI^{DSe} (2.3568(15).[54] The C-Se bond length of the bridging MMI^{Se} ligands are slightly shorter (1.862(2) Å) than the C-Se bond length of the MMI^{DSe} ligands (1.8971(18) and 1.8859(19) Å), consistent with greater double-bond character in the bridging MMI^{Se} ligand.

From the packing structures of **1** and **2** (Figures 3B and 4), the similarity between the cations can be seen. However, the crystal packing is slightly different for these two

complexes, since they crystalize in different in the space groups, *C*2/*c* (**1**) and P2/*n* (**2**). Although the bond angles and metal coordination geometry are similar for both structures, the packing effects of the longer Se-Se, Se-C, and Cu-Se bonds, as compared to the sulfur analogs, results in changes to the alignment of the BF_4^- counterion that changes the symmetry of crystal packing.

In the structure of $[Cu(MMI^{MSe})(MMI^{TSe})(CH_3CN)][BF_4]_2$ (**3**; Figure 4.5, with selected bond lengths and angles in Table 4.2), the MMI^{MSe} and MMI^{TSe} ligands both coordinate the Cu(II) center in a bidentate fashion through the imidazole nitrogen atoms. Cu(II) adopts near perfect square pyramidal geometry (τ_5 = 0.069), with an acetonitrile molecule in the axial position. The MMI^{MSe} ligand forms a 6-membered chelate ring with a N3-Cu1-N1 internal angle of 90.81(16)˚. The MMI^{TSe} ligand forms an 8-membered chelate ring with a similar N7-Cu1-N5 internal angle of 90.03(17)˚. Cu(II) coordination

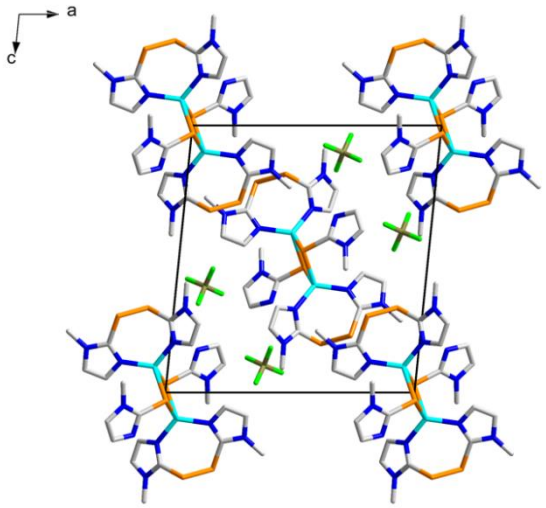

Figure 4.4. Packing diagram for **2** viewed along the *b*-axis. Color scheme: dark blue – nitrogen; orange – selenium; light blue – copper; grey – carbon; white – hydrogen; green – fluorine; and brown – boron.

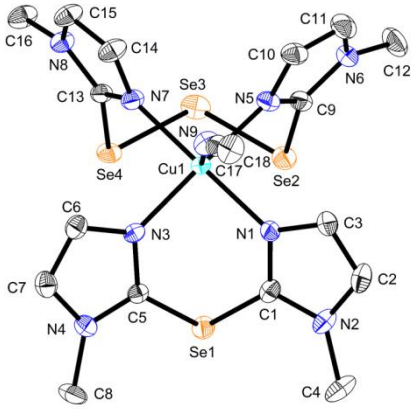

Figure 4.5. Crystal structure diagram of $[Cu(MMI^{MSe})(MMI^{TSe})(CH_3CN)][BF_4]_2$ (**3**) with 50% probability density ellipsoids. Hydrogen atoms and counter ions are omitted for clarity.

Table 4.2. Selected bond distances (Å) and angles (˚) for **3**.

Bond Length (Å)		**Bond Angle (˚)**	
Se4-Se3	2.3319(8)	C13-Se4-Se3	99.01(14)
Se3-Se2	2.3323(9)	Se4-Se3-Se2	103.46(3)
C13-Se4	1.902(5)	Se3-Se2-C9	99.61(15)
C9-Se2	1.908(5)	N7-Cu1-N3	90.03(17)
Cu1-N7	2.011(4)	N7-Cu1-N5	90.02(16)
Cu1-N5	2.007(4)	N3-Cu1-N1	90.81(16)
Cu1-N3	1.989(4)	N5-Cu1-N1	88.04(16)
Cu1-N1	1.998(4)	N7-Cu1-N9	92.80(16)
C5-Se1	1.893(5)	N1-Cu1-N9	93.27(16)
C1-Se1	1.895(5)	N3-Cu1-N9	96.56(16)
Cu1-N9	2.285(4)	N5-Cu1-N9	93.82(19)
		C5-Se1-C1	93.41(19)

in **3** shows a surprising rigidity, maintaining the 90˚ angle expected for equatorial ligands and resulting in observed ring buckling to incorporate the triselenide.

Although unbound MMI^{MSe} is not reported, Roy and coworkers[44] performed DFT calculations to predict the structure of this compound. C-Se bond lengths in the MMI^{MSe} ligands of **3** range from 1.893(5) to 1.908(5) Å, consistent with the DFT-calculated C-Se distance of 1.908 Å for unbound MMI^{MSe} and the C-Se distance of 1.897 Å for copper-coordinated MMI^{MSe} in $[Cu(MMI^{MSe})_2(H_2O)_2][ClO_4]_2$.[44] The MMI^{MSe} ligands in **3** have

longer C-Se bond lengths than the bridging MMI^{Se} ligands in **2** (1.862(5) Å), consistent with the greater double-bond character of the MMI^{Se} ligand. The C5-Se-C1 bond angle of 93.41(19)˚ in **3** is smaller than the DFT-calculated value of 97.1˚ for the C-Se-C angle in unbound MMI^{MSe}.

The MMI^{TSe} ligand features a triselenide moiety generated *in situ*. The chelate ring is buckled (Figure 4.2) to accommodate the additional Se atom in a ring with little flexibility afforded by the N-C bonds of the imidazole rings. The copper-coordinated MMI^{TSe} ligand in **3** is structurally similar to that in $Ru(MMI^{TSe})(PPh_3)Cl_2$,[55] although the triselenide buckle is inverted in the ruthenium complex, and a direct ruthenium-selenium bond to the central selenium creates two five-membered rings. Significant lengthening of the Se-Se bonds (2.4311(11) and 2.4161(11) Å) is observed in the ruthenium complex compared to Se-Se bond lengths of 2.3323(9) and 2.33191(8) Å in **3**.

The crystal packing diagram of **3** (Figure 4.6) clearly shows the nearly 90˚ dihedral angle observed for the triselenide along the C-Se-Se-Se angles. The orientation of the monoselenide and triselenide away from the coordination plane of the Cu(II), indicates relative proximity of the selenium atoms to the other diselenide. This spatial orientation is supportive of selenium migration from one ligand to the other. The BF_4^- counterions provide structural support for the bulky cation, with minimal interactions with the imidazole-carbon protons.

The co-crystallized product $[Cu(MMI^{DSe})_2][Cu(MMI^{Se}\text{-}CH_2\text{-}MMI^{Se})_2][BF_4]_4$ (**4**) formed in the same reaction as **3**. The unit cell contains three unique cations, $[Cu(MMI^{DSe})_2]^{2+}$ (**4a**) and two structural forms of $[Cu(MMI^{Se}\text{-}CH_2\text{-}MMI^{Se})_2]^{2+}$ that are

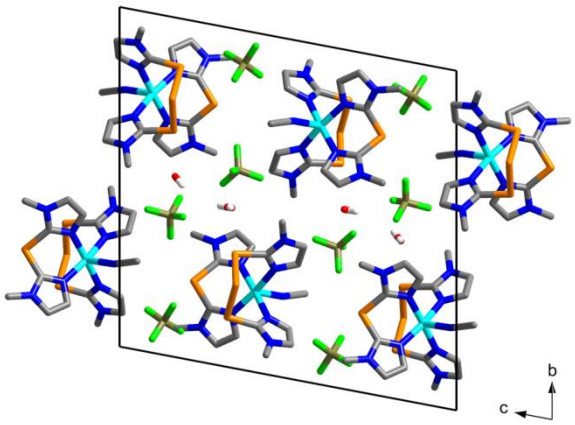

Figure 4.6. Packing diagram for **3** along the *a*-axis. Color scheme: dark blue – nitrogen; orange – selenium; light blue – copper; grey – carbon; white – hydrogen; green – fluorine; and brown – boron.

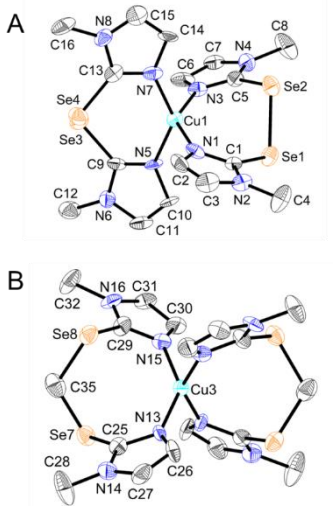

Figure 4.7. Crystal structure diagram of co-crystallized **4a** and **4b** with 50% probability density ellipsoids. Hydrogen atoms and counter ions are omitted for clarity.

very similar, such that the cation containing the Cu2 atom will be used for discussion purposes (**4b**; Figure 4.7 and Table 4.3). The packing diagram can be seen in Figure 4.8. Variable coordination geometries and oxidation states are notable features of copper. A

four-coordinate Cu(II) cation would typically be expected to be nearly square planar,[56] but **4a** exhibits significant shifts toward see-saw geometry with bond angles of 96.7(4)˚ – 99.7(4)˚ for the pseudo-equatorial bonds and a significant in-plane distortion of 137˚, resulting in a τ_4 value of 0.609. The bidentate MMI^{DSe} ligands are identical and coordinate the central Cu(II) through the imidazole nitrogen atoms. MMI^{DSe} coordination forms a 7-membered chelate ring with a 92˚ torsion angle, contributing to distortion of the Cu(II) equatorial plane.

In **4b**, the [Cu(MMI^{Se}-CH_2-MMI^{Se})$_2$] complex contains two unusual CH_2-bridged MMI^{DSe} ligands. These ligands coordinate the Cu(II) center, affording distorted square-planar geometry with bond angles of 94.5˚-98.9˚ and a planar distortion of 141.8(4)˚, similar to **4a** (τ_4 = 0.553). The Se-C-Se bond angles of 115.8(11) and 117.4(7)˚ in the MMI^{Se}-CH_2-MMI^{Se} ligand are significantly broader than the Se-Se-Se bond angle of 103.46(5)˚ in **3**.

The packing diagram of **4** (Figure 4.8) illustrates the complexity of the crystal structure and reaction products. Two unique molecules with the ligands containing the Se-C-Se bridge are located on the center of symmetry, so only half of each molecule is unique. The cations then alternate in sheets, with the tetrafluoroborate counterions and water molecules layering between the sheets. The hydrogen-bond interaction between the water and tetrafluoroborate ions can be seen in the packing diagram. The formation of multiple of Cu-selone complexes obtained from this two-reactant reaction emphasizes the varied and interesting nature of selone chemistry.

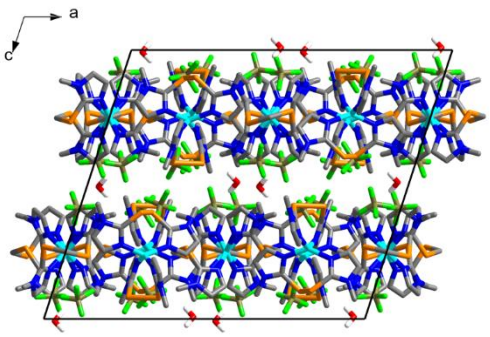

Figure 4.8 Packing diagram for **4** along the *b*-axis. Color scheme: dark blue – nitrogen; orange – selenium; light blue – copper; grey – carbon; white – hydrogen; green – fluorine; red – oxygen, and brown – boron.

4.3 Conclusions

Control of formation and cleavage of disulfide and diselenide bonds with electron-rich metals such as Cu(I) and Ni^0 has significant implications for catalysis and protein engineering. In this work, copper-mediated cleavage of the disulfide or diselenide bonds in MMI^{DS} or MMI^{DSe} was observed. This is essentially the reverse of the reaction that yields Cu(I) and MMI^{DS} from Cu(II) and MMI starting materials under airfree conditions. Comparable reactions with methimazole diselenide exhibit a greater diversity of ligand-rearranged products. In one reaction, products containing monoselenide diselenide, triselenide, and carbon-bridged selenide ligands coordinated to Cu(II) were obtained simultaneously. While true thione/disulfide and selone/diselenide reversibility may be obtainable, both these reactions and control over sulfur or selenium elimination and insertion reactions need further investigation. The role of copper in initiating the disulfide bond formation and/or cleavage with the thione and selone imidazole ligands highlights the potential for interaction of these non-innocent ligands within biological systems.

4.4 Experimental Methods

General Methods

All reactions were performed under an argon atmosphere of Ar using standard air-free procedures. Acetonitrile and dichloromethane were purified using standard procedures and were freshly distilled under an argon atmosphere prior to use. $[Cu(CH_3CN)_4][BF_4]$,[57] bis(1-methylimidazolyl)disulfide (MMI^{DS}),[41] and bis(1-methylimidazolyl)diselenide (MMI^{DSe})[54] were synthesized according to published procedures.

Synthesis of $[Cu_2(MMI^{DS})_2(MMI)_2][BF_4]_2$ (**1**)

A solution of MMI^{DS} (0.90 mmol, 133 mg) in acetonitrile (10 mL) was added *via* cannula to a solution of $[Cu(CH_3CN)_4][BF_4]$ (0.60 mmol, 189 mg) in acetonitrile (10 mL) under argon. Upon addition of the yellow MMI^{DS} solution, the reaction mixture immediately turned a green-blue color that slowly changed back to light yellow over the course of 1 h. The reaction mixture was stirred for an additional 3 h and diethyl ether (30 mL) was added. Orange-red crystals of **1** formed overnight and were filtered and dried. Yield: 20 mg, 6.8%.

Synthesis of $[Cu_2(MMI^{DSe})_2(MMI^{Se})_2][BF_4]_2$ (**2**)

A solution of MMI^{DSe} (0.90 mmol, 289 mg) was dissolved in dichloromethane (10 mL) and then added *via* cannula to a solution of $[Cu(CH_3CN)_4][BF_4]$ (0.60 mmol, 189 mg) in acetonitrile (10 mL) under argon. Upon addition of the orange MMI^{DSe} solution, the reaction mixture formed a green precipitate that immediately redissolved and then became

light green. After stirring for 1 h, the reaction became a light orange-red. After stirring for an additional 2 h, the solvent was reduced to approximately 5 mL *in vacuo,* and crystals were obtained from diethyl ether diffusion over the course of 3 d. After filtration, a few crystals of **2** suitable for X-ray diffraction analysis were isolated from a larger amount of crystallized $[Cu(CH_3CN)_4][BF_4]$ starting material. Yield: 42 mg, 11%.

Synthesis of $[Cu(MMI^{MSe})(MMI^{TSe})(CH_3CN)][BF_4]_2$ (**3**) *and* $[Cu(MMI^{DSe})_2][Cu(MMI^{Se}\text{-}CH_2\text{-}MMI^{Se})_2][BF_4]_4$ (**4**)

In air, a solution of MMI^{DSe} (1.0 mmol, 322 mg) in of dichloromethane (15 mL) was added to $[Cu(CH_3CN)_4][BF_4]$ (0.50 mmol, 315 mg) in acetonitrile (15 mL). Upon MMI^{DSe} addition, the reaction mixture became green. After stirring for 24 h, the reaction solution was slowly evaporated over 3 d to yield multiple crystaline products: colorless crystals of $[Cu(CH_3CN)_4][BF_4]$, purple crystals of **3**, green crystals of **4a** and **4b**, and yellow-green columns of **4b** identified but of poor resolution. Crystals of these different products were manually separated for analysis, and no overall yields were determined.

X-ray crystallography

Single crystal X-ray diffraction measurements were collected at 100-140 K with Mo Kα (λ = 0.71073 Å) radiation. A Bruker D8 Venture diffractometer with Incoatec microfocus source and a Photon 100 CMOS detector was utilized in the data collection. The Apex3 software suite was used for processing and scaling corrections.[58,59] Based on systematic absences, space group assignments were made. The structures were solved by

intrinsic phasing (SHELXT), and refined to convergence by full-matrix least squares using the SHELXTL software suite.[60] All non-hydrogen atoms were refined anisotropically. Hydrogen atoms attached to carbon atoms were placed geometrically and treated using appropriate riding models. Positions of hydrogen atoms attached to nitrogen and oxygen atoms were first verified using the difference electron density maps, and then placed in geometrically optimized positions using riding models. The final positions of these hydrogen atoms did not differ significantly from where their position was first indicated on the difference electron density map.

The tetrafluoroborate anion in **1** was found to be disordered, and the fluorine atom site occupancies were allowed to freely refine with appropriate similarity restraints placed on their anisotropic displacement parameters. In the case of **3**, some disorder was observed in the triselenide bridging units. In these cases the site occupancies of the disordered Se atoms were allowed to refine as free variables, with appropriate similarity restraints used for their anisotropic displacement parameters. All crystals of **4** tested proved to be non-merohedral twins, and the reflections of the twin components were distinguished using the program Cell_Now (Sheldrick, G. M. (2008). *CELL_NOW*. Version 2008/4. Georg-August-Universität Göttingen, Göttingen, Germany), and processed using the TWINABS algorithm of Apex3. The structure was refined as a two component twin with the minor twin component contribution refined as 33% according to the batch scale factor.

Table 4.3. Summary of crystallographic data for complexes **1** and **2**.

	1	**2**
Chemical formula	$C_{24}H_{32}B_2Cu_2F_8N_{12}S_6$	$C_{24}H_{32}B_2Cu_2F_8N_{12}Se_6$
F.W. (g mol^{-1})	981.67	1263.07
Temperature, K	100(2)	100(2)
Wavelength, Å	0.71073	0.71073
Crystal system	Monoclinic	Monoclinic
Space group	*C2/c*	*P2$_1$/n*
a, Å	26.164(2)	14.950(1)
b, Å	11.5872(8)	8.1531(6)
c, Å	15.383(1)	16.101(1)
α, ˚	90	90
β, ˚	125.60(2)	95.801(3)
γ, ˚	90	90
V, Å^3	1195.2(2)	1952.5(3)
Z	4	2
D, g cm^{-3}	1.721	2.148
Absorption coefficient, mm^{-1}	1.531	6.758
Crystal size, mm^3	0.046 × 0.136 × 0.157	0.116 × 0.120 × 0.289
F(000)	1984	1208
2θ range, ˚	2.00 to 26.50	2.54 to 26.50
Collected reflections	46086	64485
Unique reflections	3923	4050
Final *R* (obs. Data)$^{\alpha}$, R_1	0.0294	0.0169
wR_2	0.0830	0.0389

Table 4.4. Summary of crystallographic data for complexes **3** and **4**.

	3	**4**
Chemical formula	$C_{18}H_{24.43}B_2CuF_8N_9O_{0.72}Se_4$	$C_{32}H_{40}B_4Cu_2F_{16}N_{16}O_3Se_8$
F.W. (g mol^{-1})	931.38	1802.80
Temperature, K	140(2)	140(2)
Wavelength, Å	0.71073	0.71073
Crystal system	Triclinic	Monoclinic
Space group	*P*-1	*C2/c*
a, Å	8.1558(4)	23.8666(15)
b, Å	19.5369(8)	23.8404(15)
c, Å	19.7370(9)	21.1884(14)
α, ˚	79.287(2)	90
β, ˚	89.674(2)	107.908(2)
γ, ˚	88.918(2)	90
V, Å^3	1195.2(2)	11471.9(13)
Z	4	8
D, g cm^{-3}	2.002	2.088
Absorption coefficient, mm^{-1}	5.498	5.920
Crystal size, mm^3	0.156 × 0.177 × 0.302	0.087 × 0.145 × 0.151
F(000)	1793	6896
2θ range, ˚	2.19 to 26.50	2.12 to 25.50
Collected reflections	123328	18847
Unique reflections	12805	
Final *R* (obs. Data)$^{\alpha}$, R_1	0.0416	0.0694
wR_2	0.0936	0.1443

4.5 References

(1) Thornton, J. M. *J. Mol. Biol.* **1981**, *151*, 261-287.

(2) Petersen, M. T. *Protein Eng.* **1999**, *12*, 535-548.

(3) Canadell, J.; Goossens, H.; Klumperman, B. *Macromolecules* **2011**, *44*, 2536-2541.

(4) Braunova, A.; Pechar, M.; Laga, R.; Ulbrich, K. *Macromol. Chem. Phys.* **2007**, *208*, 2642-2653.

(5) Kohane, D. S.; Langer, R. *Chem. Sci.* **2010**, *1*, 441-446.

(6) Saito, G.; Swanson, J. A.; Lee, K. D. *Adv. Drug Deliv. Rev.* **2003**, *55*, 199-215.

(7) Zhang, S.; Zhao, Y. *J. Am. Chem. Soc.* **2010**, *132*, 10642-10644.

(8) Kroeze, R. J.; Hlder, M. N.; Govaert, L. E.; Smit, T. H. *Materials* **2009**, *2*, 833-856.

(9) Wouters, M. A.; Fan, S. W.; Haworth, N. L. *Antioxid. Redox Signal.* **2010**, *12*, 53-91.

(10) Hogg, P. J. *Trends Biochem. Sci.* **2003**, *28*, 210-214.

(11) Wang, H.; Zhang, C.; Chan, W.; Tiwari, S.; Rana, F. *Nat. Commun.* **2015**, *6*, 1-6.

(12) Sevier, C. S.; Kaiser, C. A. *Nat. Rev. Mol. Cell Biol.* **2002**, *3*, 836-847.

(13) Bechtel, T. J.; Weerapana, E. *Proteomics* **2017**, *17*.

(14) Parakh, S.; Atkin, J. D. *Front. Cell. Dev. Biol.* **2015**, *3*, 30.

(15) Xu, S.; Sankar, S.; Neamati, N. *Drug Discov Today* **2014**, *19*, 222-240.

(16) Mahmood, D. F.; Abderrazak, A.; El Hadri, K.; Simmet, T.; Rouis, M. *Antioxid. Redox Signal.* **2013**, *19*, 1266-1303.

(17) Mieyal, J. J.; Gallogly, M. M.; Qanungo, S.; Sabens, E. A.; Shelton, M. D. *Antioxid. Redox Signal.* **2008**, *10*, 1941-1988.

(18) Butera, D.; Cook, K. M.; Chiu, J.; Wong, J. W.; Hogg, P. J. *Blood* **2014**, *123*, 2000-2007.

(19) Dasuri, K.; Zhang, L.; Keller, J. N. *Free Radic. Biol. Med.* **2013**, *62*, 170-185.

(20) Shchedrina, V. A.; Novoselov, S. V.; Malinouski, M. Y.; Gladyshev, V. N. *Proc. Natl. Acad. Sci. U. S. A.* **2007**, *104*, 13919-13924.

(21) Ma, S.; Hill, K. E.; Burk, R. F.; Caprioli, R. M. *J. Mass. Spectrom.* **2005**, *40*, 400-404.

(22) Metanis, N.; Hilvert, D. *Angew. Chem. Int. Ed. Engl.* **2012**, *51*, 5585-5588.

(23) Johansson, L.; Gafvelin, G.; Arner, E. S. *Biochim. Biophys. Acta* **2005**, *1726*, 1-13.

(24) Jacob, C.; Giles, G. I.; Giles, N. M.; Sies, H. *Angew. Chem. Int. Ed. Engl.* **2003**, *42*, 4742-4758.

(25) Gromer, S.; Johansson, L.; Bauer, H.; Arscott, L. D.; Rauch, S.; Ballou, D. P.; Williams, C. H., Jr.; Schirmer, R. H.; Arner, E. S. *Proc. Natl. Acad. Sci. U. S. A.* **2003**, *100*, 12618-12623.

(26) Farina, M.; Barbosa, N. B.; Nogueira, C. W.; Folmer, V.; Zeni, G.; Andrade, L. H.; Braga, A. L.; Rocha, J. B. *Braz. J. Med. Biol. Res.* **2002**, *35*, 623-631.

(27) Sanchez, M.; Palacios, O.; Buchensky, C.; Sabio, L.; Gomez-Casati, D. F.; Pagani, M. A.; Capdevila, M.; Atrian, S.; Dominguez-Vera, J. M. *J. Inorg. Biochem.* **2018**, *180*, 135-140.

(28) Kimani, M. M.; Watts, D.; Graham, L. A.; Rabinovich, D.; Yap, G. P.; Brumaghim, J. L. *Dalton Trans.* **2016**, *44*, 16313-16324.

(29) Kimani, M. M.; Bayse, C. A.; Brumaghim, J. L. *Dalton Trans.* **2011**, *40*, 3711-3723.

(30) Stadelman, B. S.; Kimani, M. M.; Bayse, C. A.; McMillen, C. D.; Brumaghim, J. L. *Dalton Trans.* **2016**, *45*, 4697-4711.

(31) Ainscough, E. W.; Brodie, A. M. *Coord. Chem. Rev.* **1978**, *27*, 59-86.

(32) Atkinson, E. R.; Jackson, A. R.; Raper, E. S. *Inorg. Chim. Acta* **1985**, *92*, 35-41.

(33) Karagiannidis, P. A.; Papastefanou, S.; Mentzafos, D.; Hountas, A.; Terzis, A. *Polyhedron* **1990**, *9*, 981-986.

(34) Creighton, J. R.; Gorvin, A. C.; Getteridge, C.; Jackson, A. R.; Raper, E. S.; Sherwood, P. M. *Inorg. Chim. Acta* **1985**, *103*, 195-205.

(35) Raper, E. S.; Clegg, W. *Inorg. Chim. Acta* **1991**, *180*, 239-244.

(36) Raper, E. S.; Robson, D.; Wilson, J. D.; Glegg, W.; Milne, A. *Inorg. Chim. Acta* **1988**, *1432*, 98-100.

(37) Raper, E. S.; Creighton, J. R.; Wilson, J. D.; Clegg, W.; Milne, A. *Inorg. Chim. Acta* **1989**, *155*, 77-83.

(38) Lobana, T. S.; Sultana, R.; Hundal, G.; Butcher, R. J. *Polyhedron* **2009**, *28*, 1573-1577.

(39) Murphy, J. M., Clemson University, 2018, *Chapter 3*.

(40) Matsunaga, Y.; Fujisawa, K.; Amir, N.; Miyashita, Y.; Okamoto, K. *Appl. Organomet. Chem.* **2005**, *19*, 208.

(41) Figueroa, J. S.; Yurkerwich, K.; Melnick, J.; Buccella, D.; Parkin, G. *Inorg. Chem.* **2007**, *46*, 9234-9244.

(42) Kedarnath, G.; Kumbhare, L. B.; Jain, V. K.; Wadawale, A.; Dey, G. K.; Thinaharan, C.; Naveen, S.; Sridhar, M. A.; Prasad, J. S. *Bull. Chem. Soc. Jpn.* **2008**, *81*, 489-494.

(43) Kimani, M. M.; Wang, H. C.; Brumaghim, J. L. *Dalton Trans.* **2012**, *41*, 5248-5259.

(44) Roy, G.; Nethaji, M.; Mugesh, G. *Inorg. Chem. Comm.* **2006**, *9*, 571-574.

(45) Aggarwal, V.; Ram Kumar, V.; Signh, U. P. *J. Chem. Cryst.* **2011**, *41*, 121-1126.

(46) Lobana, T. S.; Sultana, R.; Butcher, R. J.; Casieneiras, A.; Akitsu, T.; Fernandez, F. J.; Vega, M. C. *Eur. J. Inorg. Chem.* **2013**, *2013*, 5161-5170.

(47) Ainscough, E. W.; Anderson, B. F.; Baker, E. N.; Bingham, A. G.; Brodie, A. M. *Inorg. Chim. Acta* **1985**, *105*, L5-L7.

(48) Baldwin, D. A.; Denner, L.; Marwell, A. J. *J. Crystallogr. Spectrosc. Res.* **1984**, *14*, 157-167.

(49) Baldwin, D. A.; Denner, L.; Markwell, A. J. *J. Crystallogr. Spectrosc. Res.* **1986**, *16*, 763-768.

(50) Lobana, T. S.; Sultrana, R.; Hundal, G.; Butcher, R. J. *Dalton Trans.* **2010**, *39*, 7870-7872.

(51) Craig, D. B.; Dombkowski, A. A. *BMC Bioinformatics* **2013**, *14*, 346.

(52) Qian, W.; Krimm, S. *Biopolymers* **1993**, *33*, 1591-1603.

(53) Creighton, T. E. *Protein structures and molecular properties*; W.H. Freeman and Company: New York, 1993.

(54) Roy, G.; Nethaji, M.; Mugesh, G. *J. Am. Chem. Soc.* **2004**, *126*, 2712-2713.

(55) Dewhurst, R. D.; Hansen, A. R.; Hill, A. F.; Smith, M. K. *Organometallics* **2006**, *25*, 5843-5846.

(56) Raithby, P. R.; Shields, G. P.; Allen, F. H.; Motherwell, W. D. *Acta Crystallogr.* **2000**, *B56*, 444-454.

(57) Kubas, G. J. *Inorg. Synth.* **1990**, *28*, 68-70.

(58) Bruker Axis, Inc.: Madison, WI, 2015.

(59) Rigaku and Molecular Structure Corporation: The Woodlands, TX, 2006.

(60) Sheldrick, G. *Acta Crystallogr.* **2008**, *A64*, 112-122.

CHAPTER FIVE

EFFECTS OF SULFUR- AND SELENIUM-CONTAINING LIGANDS ON COPPER AND IRON COORDINATION

5.1 Conclusions

Sulfur- and selenium-containing amino acids and other compounds play critical roles in the redox properties of metalloproteins[1] and control of cellular reactive oxygen species.[2] Metal-binding by these compounds is one mechanism by which generation of reactive oxygen species is controlled.[3-5] Redox-active metals such as copper and iron are two of the most abundant[6,7] and potentially damaging[8,9] transition metals in the cell, and loss of homeostasis for these metals that occurs with oxidative stress, protein dysfunction, and cell signaling in the brain has serious biological repercussions.[10] Production of hydroxyl radical via Fenton and Fenton-like reactions and redox-cycling of copper and iron can lead to oxidative damage that is an underlying cause of Parkinson's, Alzheimer's, and cardiovascular diseases.[9,11,12]

Due to their radical scavenging and metal binding abilities, sulfur and selenium amino acids as well as imidazole thiones and selones have been identified as potential antioxidants that prevent both copper- and iron-mediated oxidative damage,[3,13-15] but the mechanisms responsible for their antioxidant behavior are unclear and likely differ based on both the metal ion and the type of sulfur or selenium compound. Determination of thermodynamic parameters to predict the likelihood of complex formation and investigations into the redox reactions of copper with imidazole thiones can provide insight

into the cellular behavior of sulfur- and selenium-containing compounds and mechanisms for their prevention of oxidative damage.

Stability constants of Cu(II) with glycine, methionine, methylcysteine, selenomethionine, and methylselenocysteine were determined by potentiometric titration. (Chapter 2). Two species were identified in the best-fit models, $[CuL]^+$ and CuL_2, with stability constants of approximately 9 and 14, respectively. A novel crystal structure for $Cu(SeMet)_2$ was also reported, confirming bidentate coordination of the carboxylate and amine groups of selenomethioneine, with no coordination of the selenium atom. Based on similarities in IR results and the consistency of stability constants, it can be assumed that all the thio- and selenoether complexes bind Cu(II) in a similar fashion.

Under oxygen-free conditions, stability constants of Fe(II) with glycine, methionine, methylcysteine, selenomethionine, methylselenocysteine, and penicillamine were also determined by potentiometric titration. In contrast to Cu(II) titration results, the two identified Fe(II) species are $[FeL]^+$ and FeL(OH), highlighting the stability of Fe(II) hydrolysis products. Compared to Cu(II), these Fe(II) complexes have significantly lower stability constants with the thio- and selenoether-containing amino acids, approximately 3 and -5 for the $[FeL]^+$ and FeL(OH) species, respectively. IR analyses indicate bidentate binding through the carboxylate and amine groups, similar to binding in the Cu(II) complexes. The thiol-containing penicillamine has considerably higher Fe(II) stability constants than the thio- and selenoether amino acids: 7.48(7) and 13.91(7) for the Fe(Pen) and $[Fe(Pen)_2]^{2-}$ species, respectively. This considerable difference in stability is likely due

to direct coordination of the thiolate group, either in place of the carboxylate oxygen or in addition to amine and carboxylate coordination, resulting in tridentate coordination.

The stability constants determined in Chapter 2 can be combined with the projected speciation graphs in Chapter 1 (Figure 1.13) to predict percent complexation of Cu(II) and Fe(II) at biological pH by these amino acids. With stability constants of approximately 9 and 14 for the Cu(II)-thioether-amino-acid complexes and assumed concentrations of 10 μM Cu(II) and at least 10 μM of amino acid, 90-100% of available Cu(II) would be coordinated by these amino acids in a binary system. In a competitive environment such as the cell, other small molecules with higher stability constants, such as histidine or cysteine, would outcompete the bindentate-only binding in thio- or selenoamino acids, but labile metal ions would almost definitely interact with available, coordinating small molecules. Such binding correlates with *in vitro* inhibition of copper-mediated oxidative DNA damage (Figure 2.6).

When considering the Fe(II) stability constants of 3 and -5 for thio- and selenoether amino acid binding, it is unlikely that any Fe(II) would be coordinated at pH 7. However, Fe(II)-penicillamine stability constants are similar to those for Cu(II) binding to thio- and selenoether amino acids, so 90-100% of available Fe(II) would be bound by penicillamine at pH 7. The inability of thio- and selenoether amino acids to prevent Fe(II)-mediated oxidative damage in the biological pH range is consistent with this lack of amino acid coordination. When Fe(II) coordination is likely at pH 7, as seen for pencillamine, prevention of metal-mediated damage is observed (Table 2.5).

Copper exists both in the +2 and +1 oxidation state, and Cu(I) is more prevalent in the reducing cellular environment.[16] Cu(I) is also a softer Lewis acid than Cu(II), with greater affinity for binding the soft thio- and selenoether groups of amino acids, and it produces hydroxyl radical in the presence of hydrogen peroxide. Cu(I) is however, extremely difficult to work with in aqueous systems (Chapter 1). Sharma and cowokers[17] suggest sufficient chloride support (>1.0 M) can support the Cu(I) ion so that it does not disproportionate in solution. Strict avoidance of oxygen would still be needed if this method were to be pursued for stability constant determination. Other methods that have proven successful for Cu(I) stability constant determination include competition methods, such as the fluorimetric analysis developed for the determination of Cu(I) with cysteine and glutathione,[18] although weakly binding ligands may not effectively outcompete the fluormetric probes. Given the predominance of Cu(I) in cells, the body of knowledge needed to accurately predict interactions of transition metal ions with small biomolecules will not be complete, or particularly useful, until methods to determine Cu(I) stability constants are more fully developed and a more complete database of Cu(I) stability constants is available.

Methimazole (MMI) is a imidazole thione drug used to treat hyperthyroidism, with blood serum concentrations of 5-10 μM in treated patients.[19] Although this redox-active drug reduces Cu(II) to Cu(I),[20] it strongly inhibits Cu(I)-mediated DNA damage in *in vitro* antioxidant assays.[13] A variety of mononuclear,[21,22] dinuclear,[23-26] and polymeric[27,28] complexes of copper with methimazole are reported, and sulfur extrusion from methamidazole disulfide also occurs[29-33] upon methimazole oxidation in the presence of

Cu(II) and oxygen. Studies of copper-methimazole reactions were performed in an effort to more completely understand the role of oxygen, solvent, and copper oxidation state in the resulting products (Chapter 3).

With tetrafluoroborate as a counterion, both Cu(II) and Cu(I) reactions with methimazole(MMI) result in formation of the dinculear Cu(I) complex, $[Cu_2(MMI)_6][BF_4]_2$, with two bridging and four terminal methimazole ligands coordinated solely through the sulfur atoms (Chapter 3). This product was isolated in both air and air-free reactions and has been previously reported by Raper.[34] When the copper source was changed to $Cu(NO_3)_2$ and the same reaction was performed under air-free conditions, the polymeric $\{[Cu^{I}(MMI)_2](NO_3)\}_n$ was generated along with uncoordinated methimazole disulfide (MMI^{DS}). The same reaction in air resulted in Cu(I) oxidation to Cu(II) and extrusion of a sulfur atom, affording a variety of $[Cu^{II}(MMI^{MS})_2(H_2O)_x]^{2+}$ (x = 1 or 2) complexes with different counterions, including NO_3^-, $CH_3SO_4^-$, and HSO_4^-. When the molar ratio of the reaction was reduced to 2:1 methimazole-to-copper, only one MMI^{MS} ligand coordinated copper, and direct coordination of a bidentate SO_4^{2-} ligand was observed. Treatment of $[Cu^{I}(CH_3CN)_4][BF_4]$ with MMI^{DS} under air-free conditions resulted in no sulfur elimination products, instead yielding $[Cu_2(MMI^{DS})_3][BF_4]_2$, the first example of complex with copper coordination to this ligand.

From the results of these reactions, the mechanism for sulfur extrusion proposed by Lobana[29] was further developed (Chapter 3). The requirement for copper coordination to promote sulfur elimination and ligand rearrangement was incorporated. The central role of the solvent molecule, either water or methanol, in imidazole thiolate formation and

sulfate or methylsulfate generation is also indicated from the reaction products. Two areas in which the mechanism can be further developed include 1) proof of superoxide formation as Cu(I) is oxidized by O_2, which could be examined by EPR spectroscopy, and 2) determination of Cu(I) oxidation kinetics and the kinetics of subsequent sulfur elimination using UV-vis spectrophotometry.

In Chapter 4, the potential for reversibility in copper-disulfide and -diselenide reduction and oxidation was explored. The air-free reaction of $[Cu(CH_3CN)_4][BF_4]$ and MMI^{DS} and the parallel reaction with its selenium analog, MMI^{DSe}, afford $[Cu_2(MMI^{DS})_2(MMI)][BF_4]_2$ and $[Cu_2(MMI^{DSe})_2(Se\text{-}MMI)][BF_4]_2$ in low yields. These mixed-ligand products suggest that the reaction between electron-rich Cu(I) and the imidazole disulfide or diselenide may be reversible if protons are available to generate MMI and MMI^{Se}. Treatment of $[Cu(CH_3CN)_4][BF_4]$ with MMI^{DSe} in air yielded multiple products from the same reaction mixture, including a mixed tri- and monoselenide Cu(II) complex, and formation of a Cu(II) complex with an unusual dimeric methimazole selone-derived ligand containing a bridging CH_2 group between the selenium atoms of two methimazole selones. The diverse redox chemistry of both copper and Se likely aids in forming such product mixtures and highlights the difficulty in controlling the synthesis of specific selenium-containing species.

From the studies presented in this dissertation, thermodynamic interactions between sulfur- and selenium-containing amino acids and biologically relevant transition metals were determined and the biological consequences of these interactions were explored. Sulfur- and selenium-containing amino acids are much more likely to coordinate

Cu(II) over the Fe(II) in aqueous systems, which is likely related to the antioxidant properties of these amino acids. Thiol-containing amino acids show more stable copper and iron binding compared to those with thio- and selenoether side chains, but selenol-containing amino acid stability constants are still undetermined due to the instability and redox activity of these compounds.

Similar difficulties with redox reactions and complex stability are observed with the thione and selone imidazoles in their reactions with copper. In the presence of Cu(I), methimazole directly binds this soft metal ion through the thione sulfur, and Cu(I)-bridging thiones are observed in dinuclear complexes. Sulfur elimination from the methimazole disulfide ligand is observed and is dependent upon copper coordination, the presence of oxygen, and the availability of protic solvents, such as methanol and water. This sulfur extrusion is a phenomenon that seems unique to copper, since it is not observed with other transition metal ions under similar reaction conditions.[35,36] Finally, formation of methimazole disulfides and diselenides with concomitant Cu(II) reduction to Cu(I) may be reversible with a proton source and in an air-free environment. Better understanding these copper-methimazole and selenomethimazole reactions will shed light on the diversity of coordination chemistry in systems with redox-active metals and non-innocent ligands, knowledge that may lead to advances in catalysis and may have implications for the biological activity of methimazole.

5.1 References

(1) Jacob, C.; Giles, G. I.; Giles, N. M.; Sies, H. *Angew. Chem. Int. Ed. Engl.* **2003**, *42*, 4742-4758.

(2) Battin, E. E.; Brumaghim, J. L. *Cell. Biochem. Biophys.* **2009**, *55*, 1-23.

(3) Zimmerman, M. T.; Bayse, C. A.; Ramoutar, R.; Brumaghim, J. L. *J. Inorg. Biochem.* **2015**, *145*, 30-40.

(4) Weglicki, W. B.; Mak, I. T. *Mol. Cell. Biochem.* **1992**, *118*, 105-11.

(5) Lu, J. M.; Lin, P. H.; Yao, Q.; Chen, C. *J. Cell. Mol. Med.* **2010**, *14*, 840-860.

(6) Meneghini, R. *Free Radic. Biol. Med.* **1997**, *23*, 783-792.

(7) Mzhel'skaya, T. I. *Bull. Exp. Biol. Med.* **2000**, *130*, 719-727.

(8) Arredondo, M.; Nunez, M. T. *Mol. Aspects Med.* **2005**, *26*, 313-327.

(9) Dusek, P.; Roos, P. M.; Litwin, T.; Schneider, S. A.; Flaten, T. P.; Aaseth, J. *J. Trace Elem. Med. Biol.* **2015**, *31*, 193-203.

(10) Dodani, S. C.; Firl, A.; Chan, J.; Nam, C. I.; Aron, A. T.; Onak, C. S.; Ramos-Torres, K. M.; Paek, J.; Webster, C. M.; Feller, M. B.; Chang, C. J. *Proc. Natl. Acad. Sci. U. S. A.* **2014**, *111*, 16280-16285.

(11) Pohanka, M. *Curr. Med. Chem.* **2014**, *21*, 356-364.

(12) Cervantes Gracia, K.; Llanas-Cornejo, D.; Husi, H. *J. Clin. Med.* **2017**, *6*.

(13) Zimmerman, M. T., Clemson University, 2013.

(14) Battin, E. E.; Brumaghim, J. L. *J. Inorg. Biochem.* **2008**, *102*, 3036-3042.

(15) Battin, E. E.; Perron, N. R.; Brumaghim, J. L. *Inorg. Chem.* **2006**, *45*, 499-501.

(16) Festa, R. A.; Thiele, D. J. *Curr Biol* **2011**, *21*, R877-83.

(17) Sharma, V. K.; Millero, F. J. *J. Solution Chem.* **1990**, *19*, 375-390.

(18) Walsh, M. J.; Ahner, B. A. *J. Inorg. Biochem.* **2013**, *128*, 112-123.

(19) Skellern, G. G.; Stenlake, J. B.; Williams, W. D. *Br. J. Clin. Pharmac.* **1974**, *1*, 265-269.

(20) Ainscough, E. W.; Brodie, A. M. *Coord. Chem. Rev.* **1978**, *27*, 59-86.

(21) Atkinson, E. R.; Jackson, A. R.; Raper, E. S. *Inorg. Chim. Acta* **1985**, *92*, 35-41.

(22) Karaginannidis, P. A.; Papastefanou, S.; Mentzafos, D.; Hountas, A.; Terzis, A. *Polyhedron* **1990**, *9*, 981-986.

(23) Creighton, J. R.; Gorvin, A. C.; Getteridge, C.; Jackson, A. R.; Raper, E. S.; Sherwood, P. M. *Inorg. Chim. Acta* **1985**, *103*, 195-205.

(24) Raper, E. S.; Creighton, J. R.; Robson, D.; Wilson, J. D.; Clegg, W.; Milne, A. *Inorg. Chim. Acta* **1988**, *143*, 95-100.

(25) Raper, E. S.; Clegg, W. *Inorg. Chim. Acta* **1991**, *180*, 239-244.

(26) Atkinson, E. R.; Raper, E. S.; Gardiner, D. J.; Dawes, H. M.; Walker, N. P.; Jackson, A. R. *Inorg. Chim. Acta* **1985**, *100*.

(27) Raper, E. S.; Creighton, J. R.; Wilson, J. D.; Clegg, W.; Milne, A. *Inorg. Chim. Acta* **1989**, *155*, 77-83.

(28) Lobana, T. S.; Sultana, R.; Hundal, G.; Butcher, R. J. *Polyhedron* **2009**, *28*, 1573-1577.

(29) Lobana, T. S.; Sultana, R.; Butcher, R. J.; Casieneiras, A.; Akitsu, T.; Fernandez, F. J.; Vega, M. C. *Eur. J. Inorg. Chem.* **2013**, *2013*, 5161-5170.

(30) Ainscough, E. W.; Brodie, A. M.; Gainsford, G. J. *Inorg. Chim. Acta* **1991**, *180*, 81-83.

(31) Baldwin, D. A.; Boeyens, J.C.A. *J. Crystallogr. Spectrosc. Res.* **1984**, *14*, 157-167.

(32) Baldwin, D. A.; Denner, L.; Markwell, A. J. *J. Crystallogr. Spectrosc. Res.* **1986**, *16*, 763-768.

(33) Lobana, T. S.; Sultrana, R.; Hundal, G.; Butcher, R. J. *Dalton Trans.* **2010**, *39*, 7870-7872.

(34) Raper, E. S.; Brooks, J. L. *J. Inorg. Nucl. Chem.* **1977**, *39*, 2163.

(35) Figueroa, J. S.; Yurkerwich, K.; Melnick, J.; Buccella, D.; Parkin, G. *Inorg. Chem.* **2007**, *46*, 9234-9244.

(36) Matsunaga, Y.; Fujisawa, K.; Amir, N.; Miyashita, Y.; Okamoto, K. *Appl. Organomet. Chem.* **2005**, *19*, 208.